ISTANBUL TECHNICAL UNIVERSITY ★ GRADUATE SCHOOL OF SCIENCE ENGINEERING AND TECHNOLOGY

PRODUCTION OF COPPER – SILICON CARBIDE COMPOSITES FOR THERMAL MANAGEMENT APPLICATIONS BY ELECTROFORMING PROCESS

M.Sc. THESIS

Burak EVREN

Department of Materials Science and Engineering

Materials Science and Engineering Programme

Thesis Advisor: Prof. Dr. Mustafa ÜRGEN

JUNE 2019

ISTANBUL TECHNICAL UNIVERSITY ★ GRADUATE SCHOOL OF SCIENCE ENGINEERING AND TECHNOLOGY

PRODUCTION OF COPPER – SILICON CARBIDE COMPOSITES FOR THERMAL MANAGEMENT APPLICATIONS BY ELECTROFORMING PROCESS

M.Sc. THESIS

Burak EVREN
521171005

Department of Materials Science and Engineering

Materials Science and Engineering Programme

Thesis Advisor: Prof. Dr. Mustafa ÜRGEN

JUNE 2019

ISTANBUL TEKNİK ÜNİVERSİTESİ ★ FEN BİLİMLERİ ENSTİTÜSÜ

TERMAL YÖNETİM UYGULAMALARINDA KULLANILMAK ÜZERE BAKIR - SİLİSYUM KARBÜR KOMPOZİTİNİN ELEKTROŞEKİLLENDİRME YÖNTEMİ İLE ÜRETİMİ

YÜKSEK LİSANS TEZİ

Burak EVREN
521171005

Malzeme Bilimi ve Mühendisliği Ana Bilim Dalı

Malzeme Bilimi ve Mühendisliği Programı

Tez Danışmanı: Prof. Dr. Mustafa ÜRGEN

HAZİRAN 2019

Burak EVREN, a M.Sc. student of ITU Graduate School of Science Engineering and Technology student ID 521171005, successfully defended the thesis entitled "PRODUCTION OF COPPER – SILICON CARBIDE COMPOSITES FOR THERMAL MANAGEMENT APPLICATONS BY ELECTROFORMING PROCESS", which he prepared after fulfilling the requirements specified in the associated legislations, before the jury whose signatures are below.

Thesis Advisor :	**Prof. Dr. Mustafa ÜRGEN** Istanbul Technical University	.....
Jury Members :	**Asst. Prof. Dr. Nuri SOLAK** Istanbul Technical University	.....
	Asst. Prof. Dr. Fatma BAYATA Istanbul Bilgi University	.....

Date of Submission : 03 May 2019
Date of Defense : 11 June 2019

To infinity and beyond,

FOREWORD

I would particularly like to thank my advisor Prof. Mustafa Ürgen for his remarkable mind, tremendous wisdom and his patient guidance.

I also thank Asst. Prof. Nuri Solak, Prof. Hüseyin Çimenoğlu and their research groups for their contributions.

This study could not be conducted without the support of Res. Asst. Çağatay Yelkarası, Res. Asst. Erkan Kaçar and Res. Asst. Eyüp Metin to whom one can truely count on for anything.

Furthermore, I present my sincere graditudes to Res. Asst. Burçak Avcı, Seyhan Atik, Sevgin Türkeli, Orkun Serter Kurt and Pars Seyhan for their help.

I would like to express my deepest gratitude and my dearest appriciation to my beloved fiancé Res. Asst. Gökçe Mutlu for always standing by my side.

Most importantly, nothing would be achieved without the presence of my family.

May 2019

Burak EVREN
(Res. Asst.)

TABLE OF CONTENTS

Page

ABBREVIATIONS

BSE : Back-scattered electrons
CE : Counter electrode
CEP : Conventional electrodeposition
CD : Current density
CIP : Cold isostatic press
conc. : Concentration
CTAB : Cetyl trimethyl ammonium bromide
CTE : Coefficient of thermal expansion
EDS : Energy dispersion spectroscopy
GPI : Gas pressure infiltration
mag. : Magnification
MMC : Metal matrix composite
PM : Powder metallurgy
RE : Reference electrode
SCD : Sediment codeposition
SE : Secondary electrons
SEM : Scanning electron microscope
WE : Working electrode
XRD : X-ray diffraction

SYMBOLS

A	**:** Unit area
F	**:** Faraday constant
I_a	**:** Anodic current
I_c	**:** Cathodic current
i_a	**:** Anodic current density
i_c	**:** Cathodic current density
i_0	**:** Exchange current density
J	**:** Current density
K	**:** Thermal conductivity
l_0	**:** Initial length
l_f	**:** Final length
R	**:** Gas constant
t	**:** Time
T	**:** Temperature
Q	**:** Heat transfer rate
Z	**:** Number of electrons
α	**:** Linear thermal expansion coefficient
ρ	**:** Density
η	**:** Overpotential
η_a	**:** Anodic overpotential
η_c	**:** Cathodic overpotential
η_d	**:** Activation overpotential

LIST OF TABLES

Page

LIST OF FIGURES

Page

PRODUCTION OF COPPER – SILICON CARBIDE COMPOSITE FOR THERMAL MANAGEMENT APPLICATIONS BY ELECTROFORMING PROCESS

SUMMARY

Technology of an era is limited with advancement in materials science. Validity of this phrase is much more sensible in todays world where science and technology are developing with acceleration. This statement is also perceptible in electronics. Size of the electronic elements is getting smaller every day in conjunction with an increment in number. Thus, components reach higher surface area values. As a result, released heat exceeds critical points and leads to deficiency in material performance and may even lead to material failure. For this reason, thermal management applications require a further attention.

In this study, copper–silicon carbide composites are fabricated by electrochemical deposition method to serve as a thermal management material. Electrochemical deposition is conducted by using a modiefied version of Sediment-Codeposition (SCD) technique. A particular electrode system is designed for obtaining a self standing deposit. Acid copper sulfate electrolyte is selected as the electroforming bath.

Silicon carbide particles are initially wetted in a solution containing the electroforming bath, afterwards they are manually settled on substrate surface of designed system. Different sets of experiments are conducted for achieving a smooth copper deposit between silicon carbide particles by 6 hours of electroforming. Operating conditions are benchmarked through obtaining cathodic polarization curve. The cathode potential corresponding to the optimized current density (1 A/dm^2) is determined. Composite electroforming process is conducted potential controlled for keeping the current density stable because of continous area change of the cathode with the advancement of the coating process.

After achieving the desired copper morphology for reinforcing silicon carbide particles, deposition time is extended to 30 hours. A set of samples are produced by using SiC particle with sizes of 75 μm and 1 mm. Scanning Electron Microscopy (SEM) investigations revealed that under these conditions it became possible to produce composite with 500 μm average thickness and over 65% reinforcing particle volume. At the matrix-particle interfaces some void formations but strong particle incorporation are observed.

In order to enhance matrix-particle interface, as deposited samples are treated by annealing at 650 °C for 2 hours, cold isostatic pressing under 1500 kN for 10 minutes and cold isostatic pressing prior to annealing. SEM images of cold isostatic pressed samples reveal that copper is compressed from both surfaces and smooth copper morphology is converted to a needle-shaped, cornered form, while voids at the interfaces are diminished.

For investigating the structural changes, x-ray diffraction patterns of samples are plotted. Copper peaks of as deposited sample shift to smaller angles, showing that

compression stress forms during deposition. Annealing revokes compression stresses induced by deposition. Silicon carbide peaks are observed in diffraction pattern of cold isostatic pressed sample since copper gets compressed through harder silicon carbide particles, bringing these particles closer to composite surface. Wide peak broadening is seen for pressed samples as a result of induced compression strength and dislocations. Peaks are sharpened after annealing.

X-ray diffraction patterns also show that silicon carbide particles do not chemically react with copper. Composite can be annealed at 650 °C without any significant structural change.

Formability of the as deposited and annealed samples are measured by three point flexural test. Flexural strength of as deposited sample is 11.72 MPa while flexural strength of annealed sample is 4.67 MPa. Ductility is enhanced to composite by annealing.

The viability of process for desired application is evaluated and concluded through experimental findings. Copper – silicon carbide composite is produced in the desired form and desired reinforcement concentration by electroforming. Depending on the usage area, the fabricated material is suitable for directly using as product right after deposition, or it can be cold isostatic pressed and annealed before operation.

TERMAL YÖNETİM UYGULAMALARINDA KULLANILMAK ÜZERE BAKIR – SİLİSYUM KARBÜR KOMPOZİTİNİN ELEKTROŞEKİLLENDİRME YÖNTEMİ İLE ÜRETİMİ

ÖZET

Bir devrin teknolojisi o dönemin malzemesi ile sınırlıdır. Yüksek hızla gelişen günümüz teknolojisinde bu sözün geçerliliği elektronik alanında da hissedilir. Elektronik alanındaki gelişimi ivmelendirmek adına devre elemanları gün geçtikçe daha da küçülmekte, nanoboyutlara yaklaşıp kapasiteleri artmaktadır. Fakat, işlemci boyutu küçülüp sayısı arttıkça, yüzey alanı da artmaktadır. Bu durum yüksek kapasiteli işlemcilerin çok daha fazla ısı yaymasına sebep olur. Elektrik akımına karşı oluşan dirençten dolayı, elektronik cihazlar çalışma esnasında ısınır. Açığa çıkan ısı kontrol altına alınamazsa cihaz aşırı ısınma nedeniyle verimini kaybedebilir, hatta bozulabilir. Belirtilen nedenden ötürü günümüz teknolojisinde aşırı ısınma büyük önem arz etmektedir ve ısı kontrolü uygulamaları alanında çalışmalar sürmektedir.

Elektronik cihazların çalışma süresince açığa çıkardığı ısıyı kontrol edebilmek adına çeşitli yöntemler geliştirilmiştir. Bu yöntemlerden elektronik devrelerde en yaygın olarak kullanılanı ısıyı dağıtma prensibine dayanan ısı alıcılardır. Isı alıcı olarak kullanılacak malzeme, elektronik devrelerde aşırı ısınan transistör gibi devre elemanlarına tamamen temas edecek şekilde yapıştırılır veya monte edilir. Devre elemanından açığa çıkan ısı doğrudan ısı alıcıya iletilir, ısı alıcı da genellikle hava gibi bir dış ortam vasıtasıyla soğur, böylece devre elemanının sıcaklığı kritik çalışma sıcaklığına ulaşamadan soğumaktadır.

Isı alıcı malzemesi seçiminde dikkat edilmesi gereken iki önemli unsur mevcuttur; ısıl iletkenlik ve ısıl genleşme katsayısı. Malzemenin ısı iletkenliği ne kadar yüksekse malzeme aynı derecede hızlı ısınıp hızlı soğumaktadır. Yüksek ısı iletkenlikleri sayesinde bakır ve aluminyum metalleri en çok kullanılan ısı alıcı malzemeleridir. Fakat, bu metallerin ısıl genleşme katsayıları temas ettikleri devre elemanlarının ısıl genleşme katsayılarından yüksektir. Isıl genleşme katsayısı yüksek olan bakır ve aluminyum gibi metaller ısınma durumunda temas halinde oldukları düşük ısıl genleşme katsayısına sahip devre elemanından daha fazla genleşmektedir. Bu sebeple ısı alıcının devre elemanından yüksek sıcaklıkta ayrılması en sık yaşanan problemlerden biridir. Mevcut kullanılan ısı alıcı malzemelerinin termal genleşme katsayılarını düşürmek için farklı yöntemler uygulanmıştır. Bakır; tungsten ve molibden gibi genleşme katsayısı düşük metaller ile alaşımlandırılmış, genleşme katsayısı transistör gibi yarı iletkenlerinkine yaklaşmıştır. Fakat, bu durum bakırın ısıl iletkenliğini düşürmüş ve ısı alıcı olarak kullanılabilirliğini negatif etkilemiştir. Isıl iletkenliği azaltmadan ısıl genleşmeyi düşürebilmek için ise kompozit malzemeler tasarlanmıştır.

Bakır, termal genleşmesi düşük ve ısıl iletkenliği yüksek olan elmas, silisyum karbür gibi malzemeler ile kombine edilip bakır matrisli kompozit üretilmiştir. Teoride, ısıl iletkenlik azalmadan ısıl genleşme istenilen mertebeye düşürülürken, pratikte kompozitin ısıl iletkenliği beklenenin altında olmuştur.

Bu durumun sebebi kompozitin üretim yöntemi ile ilgilidir. Bakır - silisyum karbür kompozit üretiminde en gelişkin teknik olan basınçlı infiltrasyon yöntemi bakırın ergitilip silisyum karbür iskeletinindeki boşlukları doldurması mekanizmasına dayanır. Sıvı fazdaki bakır, silisyum karbür tanelerini istenilen şekilde ıslatamadığı için matris-takviye sınırlarında zayıf bir arayüzey oluşur ve ısıl iletkenlik azalır. Diğer kompozit üretim yöntemlerinde de metal genellikle ergitilir ve aynı problemle karşılaşılır. Başka bir sorun da, bakırın yüksek sıcaklıkta silisyum karbür partikülleri ile kimyasal reaksiyona girmesidir. Bu nedenle toz metalurjisiyle üretilen kompozitlerde de sinterleme sıcaklığında reaksiyon gerçekleşmekte, ısıl iletkenlik düşmektedir.

Bu çalışmada, ısı alıcı olarak kullanıma yönelik bakır – silisyum karbür kompoziti alternatif bir kompozit üretim yöntemi olarak elektrokimyasal şekillendirme ile üretilmiştir. Elektrokimyasal şekillendirme işlemi sediment biriktirme yöntemi ile yapılmıştır.

Silisyum karbür tozu, elektrolit çözeltisinde ıslatıldıktan sonra tasarlanan elektrot sisteminde katot yüzeyine yerleştirilmiştir. İlk aşamada, silisyum karbür partikülleri arasında düzgün morfolojide bakır biriktirebilmek için 6 saat süreli deneyler uygulanmıştır. Çalışma koşulları katodik polarizsyon eğrisinin oluşturulmasıyla belirlenmiştir. Optimize edilen akım yoğunluğu 1 A/dm^2 olup buna karşılık gelen katot ve referans elektrot arasındaki potansiyel fark 160 mV ölçülmüştür. Elektroşekillendirme işlemi akım yoğunluğunu sabit tutabilmek adına potansiyel kontrollü gerçekleştirilmiştir.

Partiküller arasında istenilen morfolojide bakır biriktirme işleminin sağlanmasının ardından yerleştirilen tozların tamemen bakır matris içerisinde sıkışması amacıyla optimize edilen parametreler ile 30 saatlik elektrokimyasal biriktirme işlemi yapılmıştır. Farklı partikül boyutunun etkisi denenmiştir. Sediment biriktirme işlemi 75 µm ve 1 mm çapında silisyum karbür partikülleri kullanılarak yapılmıştır. Yüzeyi saf bakır ile kaplı numuneler üretilmiştir. Üretilen malzeme herhangi bir ek işlem gerektirmeden altlık malzemeden ayrılabilmiştir. Numunelerin yüzeyi ve kesiti taramalı elektron mikroskobu ile incelenmiş, yapının istenilen morfolojide, ortalama 500 µm kalınlıkta olduğu ve hacimce yaklaşık %65 silisyum karbür takviyesi içerdiği görülmüştür. Matris-partikül arayüzeylerinin kısmen boşluk içermesine rağmen partiküllerin bakır ile istenilen formda sıkıştırıldığı gözlemlenmiştir.

Elde edilen numunelere matris-partikül arayüzeylerini güçlendirmek ve arayüzey boşluklarını gidermek adına ek işlemler yapılmıştır. Bir grup numune 1500 kN basınç altında 10 dakika soğuk izostatik preslenmiş, bir grup numune 650 °C' de 2 saat tavlanmış, bir grup numune ise aynı parametreler ile önce soğuk izostatik preslenip ardından tavlanmıştır. Preslenen numune grubunda bakırın iki yüzeyden baskılanıp morfolojisinin iğnesel ve köşeli bir yapıya dönüştüğü, arayüzeydeki boşlukların büyük ölçüde giderildiği, tavlanan numune grubunda da arayüzeyin iyileştirildiği taramalı elektron mikroskobu analizi ile görülmüştür.

Elektrokimyasal biriktirme işleminin ve ek işlemlerin malzemede oluşturduğu yapısal değişimler x-ışını difraktometresi örgüleri ile irdelenmiştir. Elektrokimyasal biriktirmenin bakır piklerinde küçük açılara doğru kaymaya sebep olduğu, yapıda basma gerilmesi oluşturduğu görülmüştür. Elektrokimyasal biriktirme ile oluşan iç gerilme, tavlama sonrası giderilmiş, piklerin büyük açılara doğru kaydığı gözlemlenmiştir. Soğuk izostatik preslenen numunenin örgüsünde silisyum karbür pikleri görülmüştür. Bu durum bakırın pres sırasında merkeze doğru kayması, sert silisyum karbür partiküllerinin ise pozisyonlarını koruyarak yüzeye yaklaşması ile açıklanmıştır. Ayrıca, bakır pik açıklıklarının geniş olduğu görülmüştür. Pres sırasında oluşan basma gerilmesi ve dislokasyonlar ile pik genişliğinin açık olması beklenmektedir. Bu durum tavlama sonrası düzelmiş, pik açıklıkları daralmıştır.

X-ışını difraktometresi örgülerinde bakırın silisyum karbürle kimyasal reaksiyona girmediği görülmüştür. Yapılan tavlama işleminin ardından da yapıda herhangi bir faz değişimi olmadığı belirlenmiştir.

Üretilen kompozit malzemenin mekanik özelliklerini değerlendirmek adına işlem yapılmamış numune ile tavlanmış numune üç nokta eğme testine tabi tutulmuştur. İşlem görmemiş numunenin eğme dayanımı 11,72 MPa, tavlanmış numunenin eğme dayanımı ise 4,57 MPa ölçülmüştür. Eğme testi neticesinde tavlanmanın sünekliliği yüksek ölçüde arttırdığı belirlenmiştir.

Bakır – silisyum karbür kompoziti, elektrokimyasal şekillendirme işleminin ardından istenilen formda üretilerek uygulama alanına göre doğrudan veya presleme, tavlama işleminin ardından ürün olarak kullanılabilir.

1. INTRODUCTION

Electronic circuits generate heat under operation. In case of overheating, performance of the semiconductor circuit elements drop drastically subsequent to material failure. Overheating is prevented by thermal management systems when circuits are deficient in cool down. Commonly, heat dissipaters, such as heat sinks are attached to electronic circuits as a passive thermal management material. As heat is generated through semiconductor, it is simultaneously transferred to the heat sink, while heat sink dissipates the heat to a fluid media [1].

For proper heat dissipation, heat exchanger material must have high thermal conductivity and its coefficient of thermal expansion (CTE) value must match the semiconductor.

Aluminum and copper heat sinks are widely used in electronic devices because of their high thermal conductivities. However, CTE of these metals are much higher than silicon semiconductor, hence the mismatch results in fracture [2,3].

Another problem with the current heat dissipaters is emerging with developing technology. The advancement in microelectronics require advanced heat sink materials. The technology of an era is limited by its materials. Here comes the role of materials engineers to satisfy the requirements of technology by either producing new or modifying existing materials [4].

Silicon carbide is a ceramic with a thermal conductivity higher than most metals and CTE constitutes less problems than copper or aluminum. Although the two important criteria's of a decent heat sink are met, compared to metals, silicon carbide is a very brittle material, therefore it cannot be used as a heat sink in its pure state and its properties must be enhanced [5,6].

Combination of a copper matrix with silicon carbide reinforcement with high amount of SiC incorporation is a proper solution for the mentioned problem and it is a suitable heat sink material. State of the art production method for Cu-SiC composites is Gas Pressure Infiltration (GPI), where copper is molten and poured into a skeleton made

up of SiC particles. Around temperatures where copper is at liquid state, it has a tendency of reacting with silicon, which causes a significant decrease in thermal conductivity [7].

Another drawback of GPI is the low wettability between liquid copper and silicon carbide. Poor wettability causes formation of weak interfaces which strongly inhibits thermal conduction.

With electrochemical composite plating, incorporation of a reinforcing phase to a metal matrix is also possible. The operation temperature is the room temperature, as a result, copper does not react with silicon, the wettability is handle able and operation costs are resolutely reduced [8].

Sediment codeposition (SCD) is a developing method of electrochemical composite plating, from which it is possible to obtain a concentration of reinforcing phase with more than 50 vol% particle incorporation [9,10].

The aim of this study is to produce Cu-SiC composite structures with a high percentage incorporation of silicon carbide particles using electrochemical deposition method. For achieving this aim SCD process is used. Effects of deposition variables, sedimentation settings, operation conditions, electrolyte, surface modifications to electroformed composite morphology and properties are investigated. Various systems for electrochemical composite plating cells are designed and built for serving optimum.

2. LITERATURE OVERVIEW

2.1 Heat Transfer Phenomena

Transfer of thermal energy from one place to other is called heat transfer. Heat flows between objects according to the principle of minimum energy, energy states approach towards equilibrium. Flow direction is determined by the second law of thermodynamics. Heat transfer occurs primarily under three different mechanisms:

I. Convection

II. Radiation

III. Conduction

Heat transfer by convection occurs through the movement of fluid. Natural convection takes place as a result of density variation within the material. When a material is heated, it becomes expanded, therefore its density is decreased. Presence of a density gradient within a material results in a motion between the regions. Expanded particles shift towards denser regions. In other words, heated particles move to cooler regions, switch positions with colder particles, the cycle continues till equilibrium is attained.

Radiation is another heat transfer mechanism in which there is no need for a presence of a substance, the heat is transferred through electromagnetic radiation. Every substance can absorb and emit radiation. In radiation mechanism, emitted wave from a hot substance is absorbed by the colder substance, till their temperatures are at equilibrium.

Conduction is the fundamental heat transfer mechanism, where a hotter substance transfers its thermal energy to a colder substance. Transfer takes place at molecular scale, where two neighboring atoms interact with each other. Heat transfer rate is shown with Fourier's law:

$$Q = -K.A.\frac{\Delta T}{\Delta x} \tag{2.1}$$

Where Q is heat transfer rate, in other words, Q is the transferred thermal energy through an area in a unit time. A is the area, $\Delta T/\Delta x$ is the temperature gradient and k is the thermal conductivity [11]. The mechanism does not investigate the atomic behavior of materials during heat transfer. Table 2.1 shows thermal conductivities of different materials. In order to understand why some materials conduct heat better, thermal conductivity mechanisms, explained in p.6, must be understood.

2.1.1 Thermal management

From everyday objects to complex materials, human lives rely on electronic items. Under operation, electric current passes through the electronic components. As current flows, because of the electrical resistance, components undergo massive heating. Especially with developing technology, electronic components get smaller and more efficient each day; micro-scale electronic component production causes an excessive rise in the quantity of generated heat per component volume. Elevated working temperature endangers the performance and consistency of components. Overheating of a component may even result in material failure. Moreover, even if the component can withstand high temperatures, solder conjunctions can be detached due to emerged thermal stresses and lead to failure [4].

In thermal management applications the main goal is preventing material failure by cooling the components via using methods such as conduction, radiation, forced-air, liquid and immersion cooling. The main principle of these methods is transferring the generated heat from the component to another media as it is explained in the previous page. Thermal management applications are conducted under two categories; passive thermal management and active thermal management. The latter relies on cooling by supplying energy from an external system. Forced air, forced liquid, solid state heat pumps are exemplary methods for active thermal management systems, in which an external system is connected to the material that needs to be cooled. Due to the high energy consumption of active thermal management systems, passive thermal management systems are more common. In addition to being cost efficient, passive systems are more practical to apply.

Heat sinks, heat pipes, heat spreaders and thermal interface materials are the main passive thermal management systems. Heat spreaders are usually made of metal foils or plates which have high thermal conductivity, they are connected with the material

that needs to be cooled. Heat spreaders have a similar function with heat sinks. Difference of heat spreaders and heat sinks is that heat spreaders consist of a flat surface while heat sinks usually have pins. Thermal interface materials are thermal pads, grease or gels which fill the irregularities or imperfections of the surface of a component, and it increases the surface area, thereby allowing elevated heat transfer. Heat pipes are consisted of a tube which contains a coolant or a liquid. One end of the pipe is in contact with the heat source and the other end is in contact with a heat sink. Liquid vaporizes on the heated area and travels through the cool end where vapor condenses and liquefies thereby a cycle is created.

Heat sinks are the most commonly used passive thermal management materials. A heat sink is a thermally conductive material attached to a heat generating component. The heat is transferred from component to heat sink by conduction and then the conducted heat is dissipated to a fluid media usually by convection of air.

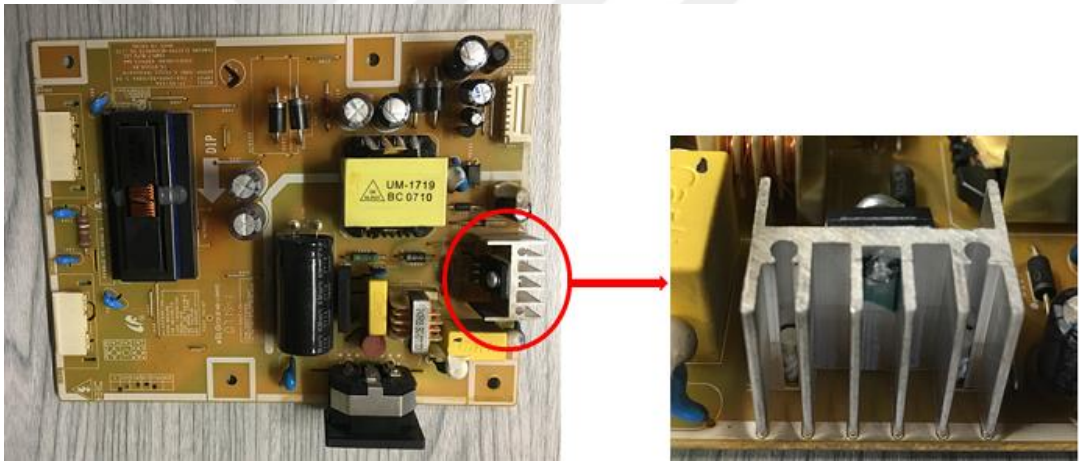

Figure 2.1 : Aluminum heat sink attached on a circuit board to cool the transistor.

Heat sinks are used in printed circuit boards to cool the electronic package, including transistors, regulators, and diodes. They usually have fins or pins to maximize its surface area. The more surface area it has, the more heat it can transfer. Therefore, design of a heat sink is an important parameter to achieve the highest efficiency. However, the crucial factor that affects the heat sink performance is the material selection. In order to produce a decent heat sink, material selection must match two important criteria's. Firstly, thermal conductivity of the heat sink material must be high enough to receive the generated heat and dissipate it at the same time while keeping the temperature of component at desired level. Second criteria is that the coefficient of

thermal expansion of heat sink must be similar to component that it is attached to. In printed circuit boards, where heat sinks are used the most, heat sinks are mounted on the semiconductors, which have a CTE value of 4 $10^{-6}.K^{-1}$. Owing to their superior thermal conductivities, copper and aluminum are the most widely used heat sinks. However, CTE values of these metals are 12 and 16 $10^{-6}.K^{-1}$ respectively. Due to that reason, once the package operates, heat sinks volume expansion becomes much higher than the semiconductor's, this mismatch leads to performance deficiency and in some cases to material failure. In order to manufacture heat sinks with lower CTE values, studies have been going, but while decreasing the CTE values thermal conductivity is also decreased. The motivation of this thesis is that it focuses on how the CTE value can be decreased but thermal conductivity is not sacrificed. The solution is proposed to be manufacturing a metal matrix composite, reinforced with thermally conductive ceramic particles [1].

2.1.2 Thermal conductivity

Thermal conductivity is the ability of a material to conduct heat. When an atom is energetically excited, it vibrates and transfers the energy in terms of kinetic energy to a neighboring atom. In thermally insulating materials, heat is transferred through phonons due to the lack of free electrons. In thermally conducting materials heat is transferred both by electrons and phonons. Thermal conductivity is calculated by the addition of electron and phonon contributions.

$$K = K_e + K_{ph} \tag{2.2}$$

Materials in which thermal conduction occurs through electrons, free electrons are in charge of conduction. Free electrons located in the heated part of material obtain kinetic energy. These electrons then flow to the colder parts of the material, where they collide with atoms or imperfections inside the crystal, resulting in conversion of energy from kinetic to atomic vibration.

In metals, due to the very high concentration of free electrons emerged from metallic bonding, contribution of electrons to conductivity is superior to the contribution of phonons, generally;

$$K_{ph} = 10^{-2}.K_e \tag{2.2}$$

Another reason for the superior contribution of electrons to phonons is that electrons are less scattered than phonons and electrons have higher velocity. Since metals have a high amount of free electrons, thermal conductivity of metals are very high, ranging usually between 20 – 400 W/m.K.

Non-metallic materials are usually thermally isolating due to the lack of free electrons. In ceramics, thermal conduction primarily occurs through phonons, K_e is much smaller than K_{ph}. Moreover, lattice defects cause a dramatic scattering in phonons, thereby decreasing the thermal conductivity [12]. Polymers have the lowest thermal conductivity, transfer of energy occurs through the vibration and rotation of chain molecules. Semi-crystalline polymers have higher thermal conductivity than amorphous polymers since polymer molecule chains present in a crystal structure can vibrate more regularly.

Thermal conductivity values k and Coefficient of Thermal Expansion (CTE) values α for different materials are given in Table 2.1 & 2.2. In terms of thermal conductivity, metals are superior to ceramics and polymers. Among metals; silver and copper are even better conductors with their thermal conductivity almost five times higher than metals such as iron and nickel. Silicon carbide however is an exceptional ceramic that thermal conductivity of a pure monocrystal SiC is 490 $W.m^{-1}.K^{-1}$ [5].

Table 2.1 : Thermal properties of various metals at 25 °C [13].

Material	k ($W.m^{-1}.K^{-1}$)	α ($10^{-6}.K^{-1}$)
Metals		
Silver	428	19.7
Copper	398	17
Gold	315	14.2
Aluminum	247	23.6
Tungsten	178	4.5
Nickel	90	13.3
Iron	80	11.8

Table 2.2 : Thermal properties of various materials at 25°C [13].

Material	k ($W.m^{-1}.K^{-1}$)	α ($10^{-6}.K^{-1}$)
Ceramics		
Alumina (Al_2O_3)	39	7.6
Magnesia (MgO)	37.7	13.5
Spinel (MgAlO)	15	7.6
Soda-lime glass	1.7	9
Fused silica (SiO_2)	1.4	0.4
Borosilicate glass	1.4	3.3
Polymers		
Polypropylene	0.12	145-180
Polystyrene	0.13	90-150
Nylon 6,6	0.14	144
Polyisoprene	0.14	220

2.1.3 Thermal expansion

Volume of most materials increase once they are heated, this is called thermal expansion. The change in length of a material upon thermal expansion is defined as;

$$\frac{l_f - l_0}{l_0} = \alpha(T_f - T_0) \tag{2.3}$$

Where l_0 is the initial length and l_f is the final length, T_0 is the initial temperature and T_f is the final temperature, α is the linear CTE value, which is characteristic for each material and shows how much increment there will be on material volume upon

heating. In atomic scale, thermal expansion is expressed as the increment of interatomic spacings. The weaker the interatomic bonding energy is, the more will be the volume difference, therefore a higher CTE value will exist [14].

Given in Table 2.1, CTE of metals vary between 5 x 10^{-6}.K^{-1} and 25 x 10^{-6}.K^{-1}. Thermal expansion values of metals are in between ceramics and polymers. Ceramics have very low thermal expansion values (0.5 x 10^{-6}.K^{-1} – 15 x 10^{-6}.K^{-1}) due to the strong interatomic bondings. Linear and branched polymer materials have the highest CTE values due to weak bondings between molecules.

2.1.4 Material selection for heat sinks

For proper heat dissipation, heat exchanger material must have high thermal conductivity and the Coefficient of Thermal Expansion (CTE) value must match the CTE of semiconductor that heat sink is attached to. While ideal CTE range for heat sinks is between 4-8 ppm/K, CTE of copper and aluminum are 17 and 23.6 respectively. In some applications, to reduce the CTE value of copper heat sinks, copper is alloyed with tungsten or molybdenum.

Table 2.3 : Thermal properties of alloy heat sinks [15].

Material	CTE ($10^{-6}K^{-1}$)	Thermal conductivity (W/mK)
Copper	17	401
Mo50Cu50	9.9	250
Mo70Cu30	7.5	195
W80Cu20	8	210
W85Cu15	7	200

Although alloying successfully brings the CTE value to desired range, thermal conductivity values drop drastically. As an alternative to alloying, copper is combined with thermally conductive ceramics with low CTE values such as diamond and silicon carbide. State-of-the-Art manufacturing techniques for copper matrix composites contain difficulties and disadvantages. The motivation of this thesis comes from the idea of producing copper-silicon carbide composites by a novel method while solving the emerged problems during conventional manufacturing techniques.

2.2 Composite Materials

Materials are generally divided into four groups: Metals, Ceramics, Polymers and Composites. Composite is a material class which consists of a combination from two or more material groups. The reason of combining different materials is benefiting from combination of various properties such strength, hardness, toughness, chemical resistance, weight and conductivity. The difference between a compound and a composite is that a compound has altered properties than the raw materials due to the occurring chemical reactions. However, when different materials are combined to produce a composite, there is not a chemical reaction present.

Composites can be macroscale or microscale. Steel-reinforced concrete is a macroscale composite, consisting of a concrete block which has a steel rode embedded in it. Compression strength of concrete is very high however tensile strength of it is very pure. For enhancing tensile strength of concrete, a steel bar is embedded in it, hereby a composite material is produced. In microscale composites, there are a matrix phase, a dispersed phase and an interface holding the phases together. The matrix phase is continuous, the dispersed phase, also referred as secondary phase or reinforcement, is less continuous.

Composites are also classified as particle-reinforced or fiber-reinforced according to the shape of the reinforcement. Another composite class is structural composites such as laminates or sandwich, where there are alternating layers of different materials.

In composites, properties and volume fractions of individual phases are important. Volume fraction of the secondary phase significantly affects the composite properties. Rule of mixture is the average considered value for the properties of composite such as density, ultimate tensile strength, and elastic modulus. The volume fraction determines the proportion of phase properties [16].

2.2.1 Metal-matrix composites (MMCs)

The term metal matrix indicates that the continuous phase is formed by a metallic material. The dispersoids of the second phase must have very low solubility in the matrix, matrix phase and secondary phase must not react with each other but they must build a strong physical bond along the interface.

2.2.2 Conventional MMC production methods

Metal-Matrix Composites are produced by various techniques, including powder metallurgy, internal oxidation, stir casting, spray deposition and vapor deposition. The most commonly applied production technique for manufacturing high thermally conductive MMC's has been powder metallurgy, along with State-of-the-Art manufacturing method Gas Pressure Infiltration (GPI).

2.2.2.1 Powder metallurgy

Powder metallurgy is a technology that permits the combination of a wide range of materials. Initially, the raw material must be pulverized. Powders can be produced by techniques including: Grinding, atomization, electrodeposition, reductions through chemical reactions. After obtaining the raw material in powder form, powder metallurgy involves three steps: Powder blending, die compaction and sintering. Many materials in powder form can be mixed to obtain composites. After mixing and compaction, the final shape is sintered under a controlled atmosphere to obtain a strong bonding between particles and reducing porosities. Powder metallurgy offers a near net shape production with dimensional accuracy, the end product may not even require machining.

Blending stage:

Composite materials with high thermal conductivity can be produced by powder metallurgy. During powder blending, powders of both the matrix material and reinforcing phase are mechanically mixed, the end product is a mixture of particles with desired chemical composition.

Compaction stage:

Compaction process starts after filling a die with particles and involves compression of powders in the die by applying high pressure. Commonly, die stands vertically, uniaxial pressure is applied from a punch by a hydraulic or mechanical press. Compacted powder has increased density due to the shrinkage in its volume. Compacted powder is called green compact. After compaction, green compact is ejected from the die to be sintered.

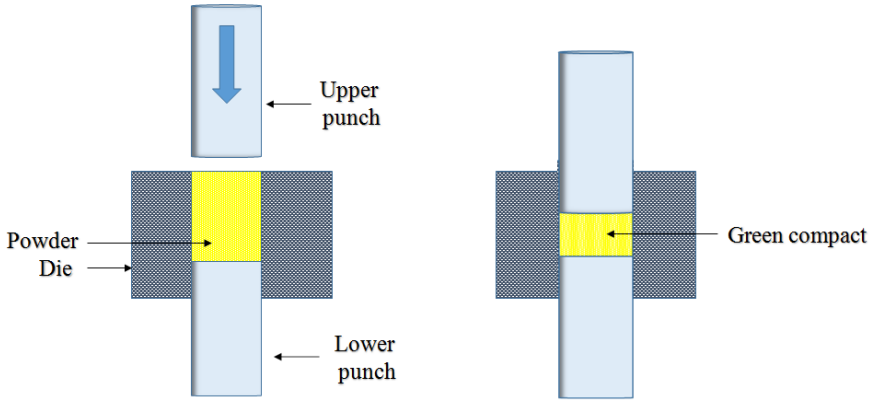

Figure 2.2 : Stages of powder compaction [17].

Sintering stage:

After compaction, the green compact is heated at its sintering temperature. The sintering temperature depends on various parameters including:

- Sintering duration
- Sintering type (Solid state sintering-Liquid state sintering)
- Furnace atmosphere
- Particle size.
- Component size

Sintering temperature is commonly above the half of the melting temperature of the material it can elevate up to 90% of the melting temperature of the material. With the effect of heat, particles bond to each other. Sintering is divided into three stages. In first stage, neck growth occurs between particles, but particles keep their distance. In second stage, pore sizes between the particles start to be reduced. Second stage is the stage where densification is at highest. In third stage, rate of densification is reduced. The particles diffuse into each other. Remaining pores are spherodized. In order to completely eliminate the porosity, sintering duration can be extended. However, extended sintering duration results in increased grains size, which can negatively affect the desired properties of the product [18].

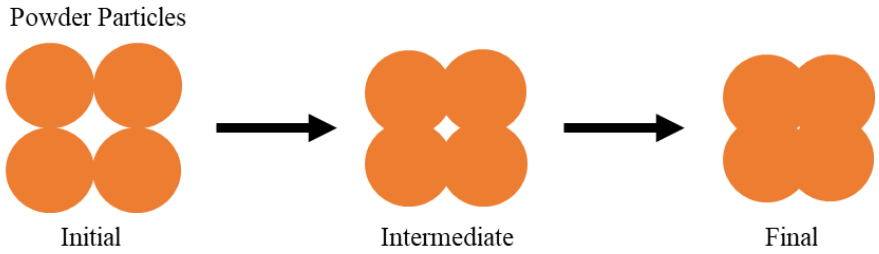

Figure 2.3 : Stages of sintering

2.2.2.2 Gas pressure infiltration

Another method for producing high thermal conductive composite materials, where the reinforcing material has very high melting temperature, is Gas Pressure Infiltration (GPI) process. In GPI, the reinforcement material with high melting temperature is obtained in powder form. After obtaining the reinforcement material of the composite in powder form, a graphite mold is filled with the powder with the desired concentration ratio. Afterwards, a metal ingot, which will be the matrix of the composite, is put above the powder. The mold, filled with reinforcement powder and ingot, is sealed and vacuumed to remove remaining air inside the mold. The mold is then heated in vacuum furnace above the melting temperature of the metal ingot, system is heated till the metal ingot liquidifies. After metal ingot liquidifies, gas pressure is applied to the mold. Since the reinforcing phase is in powder form and has high melting temperature, it keeps its solid state and functions as a skeleton. Gas pressure infiltrates the liquid metal to the powder, metal fills the powder particle interfaces, becomes the matrix of the composite. After the infiltration is completed, the mold is furnace cooled [8].

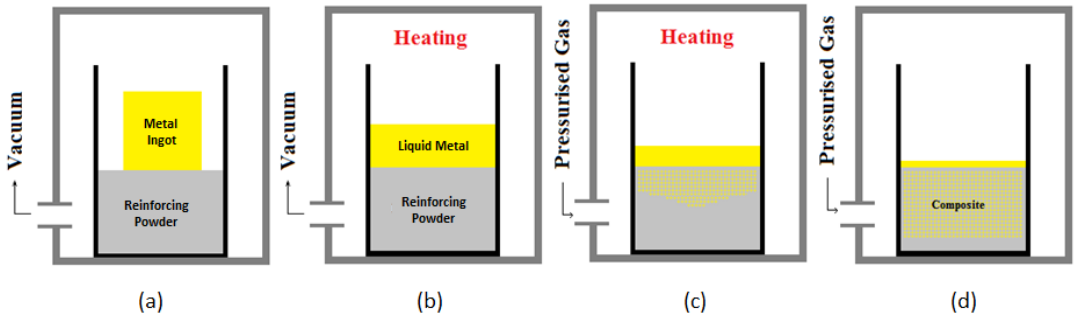

Figure 2.4 : Steps of Gas Pressure Infiltration Process [19].

2.2.2.3 Stir casting

In stir casting, reinforcing phase is added to molten metal. Mixture is stirred till the reinforcing particles homogeneously disperse in molten metal. Afterwards mixture is casted on a mold.

2.2.2.4 Spray deposition

In spray deposition technique, molten metal is sprayed on reinforcing phase, which is usually in fiber shape but process can also be applied for particle shaped reinforcements.

2.2.2.5 Vapor deposition

In vapor deposition technique, vaporized metal is condensed on the reinforcing phase. Vapor deposition process is usually applied for fiber-reinforcements.

2.2.3 Problems in conventional MMC production

Conventional MMC production techniques mentioned in previous chapter operate at very high temperature where metal is either at liquid phase or is very close to the smelting temperature. Therefore, energy consumptions of these systems are very high, processes are complicated and hazardous to practice. Moreover, when manufacturing MMC's, one of the most common problems is that; molten metal does not wet the reinforcing phase. In definition, wettability is the tendency of a solid surface to decrease the surface tension of a liquid, so that the liquid can completely cover the entire solid surface with a contact angle of 0°. Due to the poor wettability of metal, weak interfacial bonding occurs between matrix and dispersoids. As a result, product does not show the expected specifications [20].

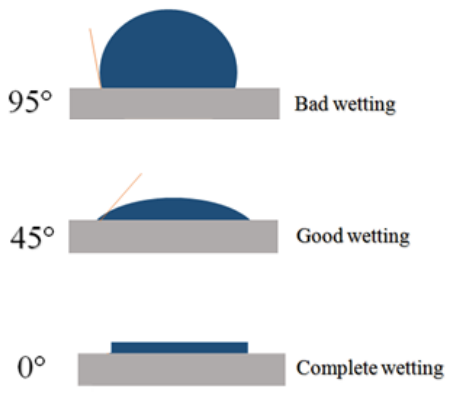

Figure 2.5 : Comparison of wettability of a surface by wetting angle.

2.3 Electrochemical Composite Production

Apart from the conventional MMC production techniques, production of composite materials is also possible by electrochemical processes [21]. Metal-matrix composite production by electrodeposition process is conducted around room temperature; hence, the energy consumption of the process is much lower than conventional production techniques. Additionally, since the used metal does not liquidify, wettability problem of molten metals does not occur.

Electrochemical composite plating technique is based on electrodeposition principles. Electrodes are immersed in an electrolyte containing dissolved metal salts and ions which carry out the flow of electricity. Direct current is supplied to the electrodes by an external power source to initiate oxidation reaction on anode surface, the dissolved metal ions in the bath are then forwarded to the cathode, where they are reduced at the cathode-electrolyte interface. During electrochemical composite production, reinforcing phase is either suspended in the electrolyte or settled on the cathodic electrode surface.

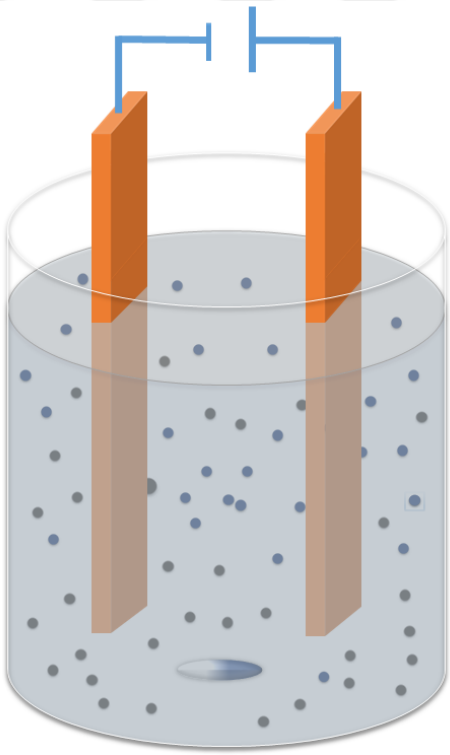

Figure 2.6 : Illustration of electrochemical composite plating setup.

While matrix metal is being deposited, reinforcement is incorporated in it. To understand the principles and mechanisms of electrochemical composite production, electrolytic metal deposition must be widely investigated.

2.3.1 Electrolytic metal deposition

Under certain conditions, metals tend to dissolve in an electrolyte containing metal salt once they are submerged in it. Surface atoms of the metal leave the lattice and form cations, in exchange, metal ions from the electrolyte may enter the metal lattice. After metal atoms leave the lattice they are converted into positively charged ions, subsequently pass to the electrolyte by migration. This incident is called anodic dissolution. After the transfer of positively charged ions from metal to electrolyte, formation of an equally negative charge on the metal takes place. The emerged charge diversity causes the negative loaded metal to pull back the released positively charged ions. Attracted ions then reduce at the cathode, resulting in cathodic deposition. If the rates of anodic dissolution and cathodic deposition are equal, this circumstance is defined as dynamic equilibrium and it is described as:

$$Me \leftrightharpoons Me^{z+} + z.e^{-} \tag{2.4}$$

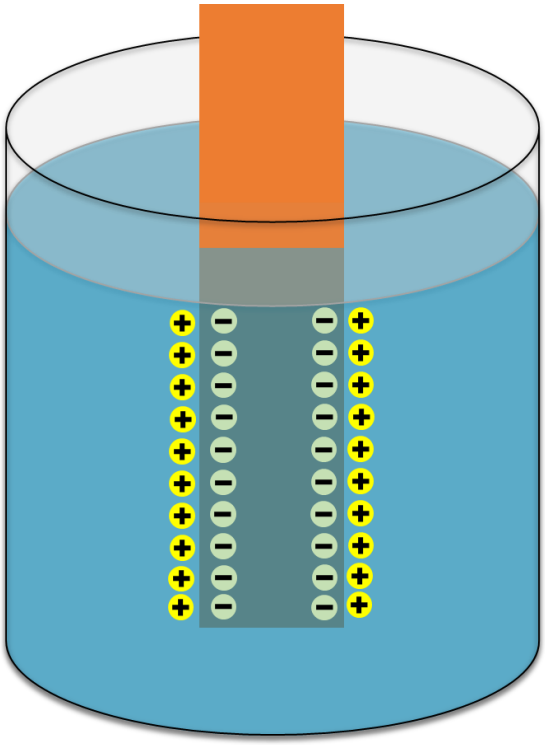

Figure 2.7 : Spontaneous charge distribution at metal surface immersed in an aqueous solution.

Z is the amount of electrons involved in reaction. The reaction is described by reversible arrow, which indicates that the reaction is in equilibrium, reduction rate of the metal atoms is equal to the pulling rate of the positive loaded metal. At equilibrium state, anodic current (I_a) and cathodic current (I_c) are equal, since anodic current is equal to the cathodic current, there is no net current flowing. This is shown as:

$$|I_c| = |I_a| = I^0 \tag{2.5}$$

Current density is the current passing through the cross-sectional area. Current density is usually referred j, while anodic CD and cathodic CD are referred as i_a and i_c respectively. i^0 is the exchange current density. Equation can be rewritten as:

$$|i_c| = |i_a| = i^0 \tag{2.6}$$

At equilibrium, no net reaction occurs. Equilibrium is broken once the metal deviates from the open circuit state. In order to trigger deviation from open state, metal must be connected to an electron source. Once an electron source is brought, electrons move to the metal, thereby making it more negative. As a result, metal is able to pull cations with a stronger force. If the metal is negatively charged and is able to attract cations, it is cathodic and electrodeposition process starts, cations in the electrolyte reduce on the cathodic metal surface. If the metal is attached to an electron sink, electrons of the metal will be transferred to the sink, thereby making the metal more positively charged, in other words, making the metal anodic. In this case, repulsion of positive ions takes place, metal atoms will be oxidized and dissolve. Briefly, if the equation 2.4 occurs from left to right, metal donates electrons and it is oxidation reaction, if reaction occurs from right to left, electrons are consumed and it is a reduction reaction.

Electrodeposition process is usually conducted by using direct current (DC). In DC electrodeposition, there are mainly two electrodes which are connected to an external DC power supply and an electrolyte in which electrodes are immersed. Electrodes consist of a cathode and an anode. Cathode is the negative electrode, metal deposits on the cathode surface. Cathode material can be metal or an electrical conductor such as graphite. It can even be a semiconductor. Anode materials are classified into two groups: Soluble Anodes and insoluble anodes. Soluble anodes are made of the material which is desired to be coated on cathode surface. Soluble anode metal dissolves into the electrolyte and migrates to the cathode surface where it is reduced at the cathode-

electrolyte interface. Insoluble anodes are made of metals or alloys, such as platinum coated titanium, which do not dissolve in the electrolyte. Reduced ions are supplied from the electrolyte. When using insoluble anodes, ion concentration of the electrolyte decreases, therefore the electrolyte must be replenished. However, when using soluble anodes, the same electrolyte can be used over and over if it is kept clean from impurities. It is therefore easier to control the process when using soluble anodes.

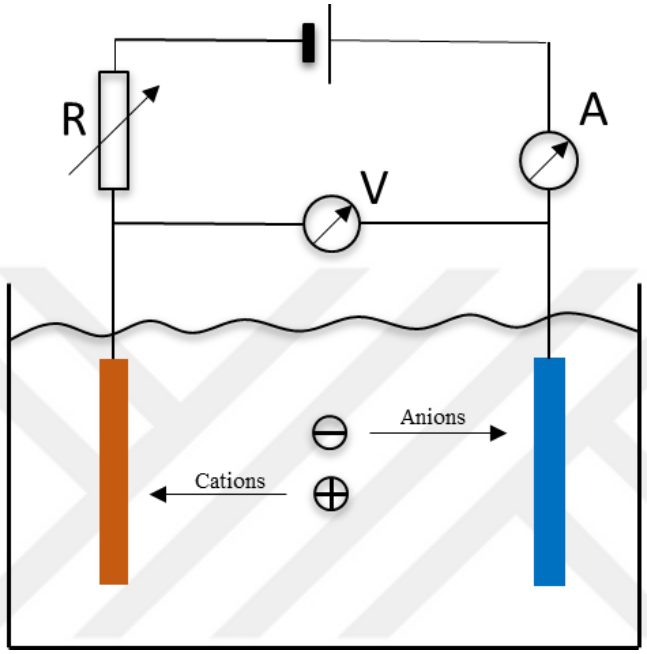

Figure 2.8 : Components of a direct current electroplating setup.

When an external potential is applied to a system at equilibrium, equilibrium is broken. Equation 2.4 will be shifted to left or right according to the connection polarity. When the applied voltage increases, rate of the reaction will increase. After the equilibrium state is broken, net electrochemical reaction can be analyzed. At equilibrium potential, there is no current flowing, current flow is present when the equilibrium is broken. Once equilibrium state is broken, reaction shifts towards left or right. This shifting is conducted by overpotential (η), it can be cathodic (η_c) or anodic (η_a). Overpotential is basically the subtraction of equilibrium potential from the electrode potential emerged from current flow, it is described as:

$$\eta = |\varepsilon - \varepsilon_{Me/Me^{z+}}| \qquad (2.7)$$

Overpotential can be defined as the required energy to exceed the reaction activation energy, equilibrium can only be upset if activation energy barrier is overcome. The higher the overpotential is, the higher will be the reaction rate. If only the charge transfer reaction at the double-layer is considered as the step that controls the rate during cathodic process, overpotential can be described as activation overpotential η_d. Activation overpotential is severely important in reduction-oxidation couples where i^0 is low. For couples where exchange current density is high, the reaction has the higher capability to be reversible. In electrodeposition, rates of anodic dissolution and cathodic deposition are described as following equations:

$$i_a = i^0 \, x \, e^{\alpha.z.F/RT)\eta_d} \tag{2.8}$$

$$i_c = -i^0 \, x \, e^{-[(1-\alpha).z.F/RT]\eta_d} \tag{2.9}$$

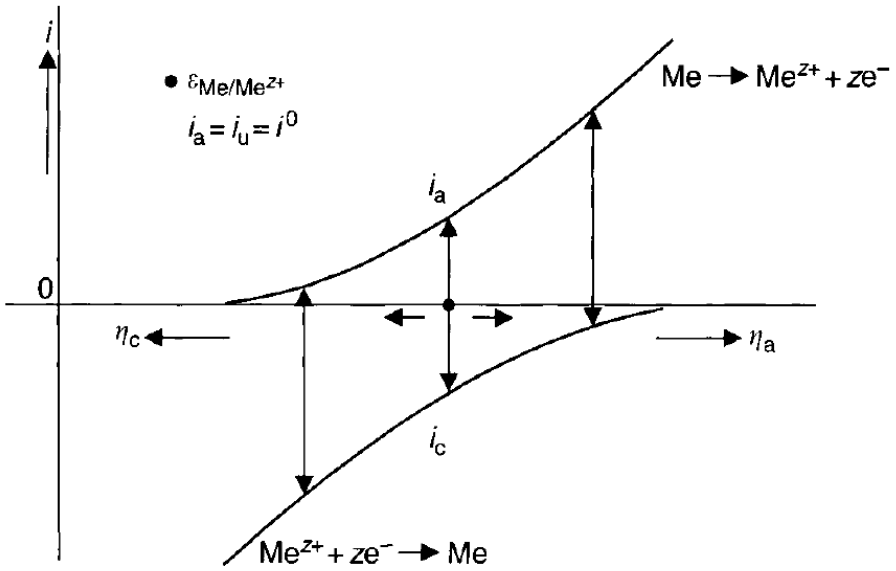

Figure 2.9 : Polarization curves indicating the rates of anodic dissolution and cathodic deposition [22].

In anodic and cathodic overpotential equations, α is the transfer coefficient, which is generally taken as 0.5, but can vary between 0-1. It designates the dependence of charge transfer to potential [22]. Leaving the activation overvoltage on the left hand side, it can be expressed as:

$$\eta_d = \frac{RT}{(1-\alpha.z.F)} \, x \ln\left(\frac{i^0}{i_c}\right) \tag{2.10}$$

2.3.2 Copper electrodeposition

Owing to its convenient process, copper is one of the most electrodeposited metals. Even the copper production process from ore involves copper electrolysis for refinement. In electronics, interconnection lines of circuit boards are made of electroplated copper on a plate.

Copper plating modifies the surface properties of materials since it is highly conductive in terms of electricity and heat. By electrodeposition, it is also possible to manufacture a self-standing purely electrolytic piece, this method is called electroforming.

A conventional electrodeposition cell consists of primarily two electrodes and an electrolyte containing metal salts. Electrodes are connected to positive and negative ends of an external power supply. Most commonly, Direct current is supplied from the source. Electrode that is connected to the positive end is called anode and electrode connected to the negative end is called cathode. However, to initiate anodic dissolution, enough potential must be supplied to shift the equation to right hand side.

In copper electrodeposition, the anode metal is either copper or an insoluble anode is used. As mentioned, when insoluble anodes are used, ion concentration in the electrolyte changes and bath control is necessary. Using copper anodes is therefore practical. Cathode is the part where copper is desired to be deposited.

Conductive metals such as copper, iron, nickel or conductors such as graphite can be selected as cathode. However, adhesion of copper and some metals such as iron is low, therefore the deposit cannot stick to the cathode. Electrolyte selection is also crucial for deposit properties. For copper electrodeposition, alkaline baths such as cyanide, pyrophosphate or acidic baths like sulfate, fluoborate can be used.

Cyanide containing copper plating baths are unviable to work with due to the toxicity of the salt and hardness of waste treatment. Fluoborate baths on the other hand need to be stabilized by acid addition, instantaneous electrolyte control is necessary, which makes the process inconvenient .

Due to the encountered difficulties in mentioned baths, sulfate containing acid copper plating electrolytes are the most commonly used baths in copper plating. Constituents of a conventional copper sulfate bath are given in Table 2.4.

Table 2.4 : Conventional copper sulfate bath [22].

Constituents	Concentration (g/L)
Copper sulfate	200
Sulfuric acid	30
Hydrochloric acid	0.1

Electroplating bath affects many properties of the deposit including mechanical properties, adhesion, microstructure, roughness and the deposition efficiency. Moreover every bath has a different capability of transferring ions through electrolyte. This feature is called macro throwing power. While cyanide baths have a high macro throwing power, it is relatively lower for copper sulfate bath [23]. For composite electroforming, the voids between reinforcing particles need to be filled with deposited metals. Since the size of voids are at micrometer scale, instead of macro throwing power, high micro throwing power is desired.

2.3.3 Electroforming method

Electroforming is a method based on electrolytic metal deposition. Principles of electroforming process is very similar to electroplating process, the only difference is the deposit thickness [24]. The goal in electroplating is to coat thin films for modifying the surface properties of a material, the coating thickness usually extend only to micrometers. In electroforming, a thick layer is deposited on a substrate which can later be separated from the substrate to be used as a product on its own. The thickness of electroformed layer can exceed milimeters.

3. STUDIES REGARDING COMPOSITE ELECTRODEPOSITION

3.1 Pioneering Studies

In the beginning of 20th century it was already discovered that suspended particles in electrolyte tend to co-deposit with reduced metal ions and by that way becoming incorporated in cathode. The general idea was that these suspended particles such as insoluble carbonates in hard water, contagious silicates, sand and dust cause surface roughness and nodular deposits and they were considered as impurites. Therefore producers avoided presence of these impurities by continuously filtering the electrolyte and by using anode bagging methods. However, years later it was observed that the so called impurities have a very strong adverse effect on the deposit properties. By intentionally adding inert particles to the electrolyte, composite coatings with a metal matrix and dispersed particles as reinforcement were produced, the process was named electro-codeposition. The first usage of electrodeposited composites is stated to be in navy to prevent slipping. Stairs of naval ships were coated by a nickel matrix incorporated with SiO_2 particles [25]. According to the collections from different reviews regarding composite electrodeposition history, in 1928, Fink and Prince studied self-lubricating Cu-Graphite composites manufactured by composite electroplating, to be used in car engines. After this invention, tendency of suspended particles to codeposit was not widely investigated for decades. At the beginning of 1960's, composite electroplating received interest again and profound investigations have started. In 1959, Grazen published a study where reinforcing hard particles were embedded in nickel, copper and silver matrixes for increasing the abrasion resistance of cutting tools. In 1962, Withers codeposited alumina and zirconia particles separately with nickel. It is reported that even 44 μm of particles can be imbedded in the coating, however recommended particle size range is between 1-3 μm for better properties. In the same year, Spencely studied Ni-SiC composites [23-27].

Sautter published in 1963 one of the first articles investigating the codeposition parameters [30]. Nickel-Al_2O_3 composite was produced by a Watt's bath consisting of chemicals given in Table 3.1.

Table 3.1 : Watt's bath for nickel electroplating [30].

Constituents	Concentration (g/L)
$NiSO_4.6H_2O$	300
$NiCl_2.6H_2O$	45
H_3BO_3	30

Additionally, electrolyte was fed with Al_2O_3 powder. Effect of particle size on deposit properties was investigated, particles with size variation of from 0.01 μm to 0.3 μm were used. 3 different methods were applied to feed the electrolyte with alumina particles. Firstly, powder was directly dispersed in the bath. Secondly, powder was dispersed in water and then put into the electrolyte. Lastly, powder was dispersed in water and then water was filled with electrolyte. All three methods resulted in the same suspension. The critical procedure of the experiment was keeping inert alumina particles suspended in the electrolyte. For that matter a laboratory type magnetic stirrer was used. As anode, 99.9% rolled nickel, as cathode, polished stainless steel was used. Selection of cathode material is based on the pure adhesion between nickel and steel. Nickel based deposit can easily be separated from the cathode surface. The operating conditions of the experiment are given in Table 3.2.

Table 3.2 : Operating conditions for Ni-Al_2O_3 composite electroplating [30].

Operating conditions	
Temperature	50 °C
pH	3.5
Current density	2 A/dm^2
Plating time	4 h

After 4 hours of plating, a coating thickness of 100 μm was obtained. For calculating the concentration of embedded alumina particles, the sample was dissolved in 50 vol% nitric acid solution. 50 vol. % nitric acid cannot solve aluminum oxide. The alumina is then separated from solution by centrifuging. By modifying parameters such as

temperature, current density, pH, concentration of alumina particles in electrolyte, final alumina concentration of the deposit was tried to be increased. Temperature and current density do not have a significant effect on concentration of the dispersed phase. Lower than pH levels of 2, incorporation falls to zero. Maximum Al_2O_3 incorporation (5 vol. %) is achieved when Al_2O_3 concentration of the electrolyte is increased to 150 g/L. However, increasing the concentration of suspended particles lead to particle agglomeration.

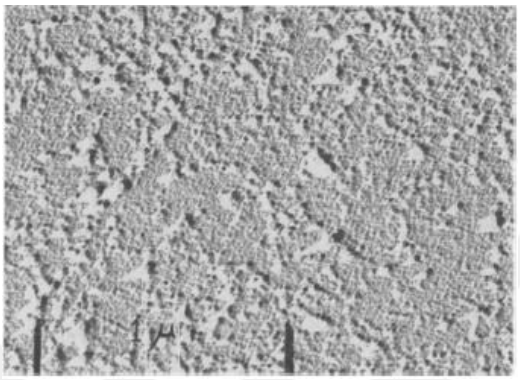

Figure 3.1 : SEM image of Ni-Al_2O_3 alloy with 50kX magnification [30].

Three months after the publication of Sautter, Williams and Martin conducted a wide research on composite electroplating by incorporated various materials to different metal matrixes [31]. Applied coatings regarding this study are given in Table 3.3.

The aim of the coatings were obtaining high hardness. All coatings were applied on steel sheet cathode. The cathode was first degreased, pickled and then washed with de-ionized water. Plating was done by suspending the reinforcing particles in the electrolyte. Another aim of the study was analyzing the effects of parameters such as bath agitation, current density, electrolyte concentration.

Electrolyte agitation is required for suspension of the inert particles, moreover, it is also necessary to prevent trapping hydrogen bubbles inside the deposits. Presence of hydrogen gas on the cathode surface leads to pitting. Agitation speed is determined qualitatively by observing the behavior of particles, agitation must be fast enough to keep the particles suspended but it cannot be too fast to inhibit codeposition. Unlike Sautter, current density is found to affect concentration of the deposit. Optimum current density for maximum reinforcement concentration was found to be 1 A/dm^2. Like Sautter, increased fiber concentration in the electrolyte greatly increases the reinforcement concentration of the deposit.

Table 3.3 : Composite coatings produced by Williams and Martin [31].

Matrix	Bath constituent	Conc. (g/l)	Reinforcement
Iron	Ferrous sulphate	240	Silica fibers Alumina powder
	Ammonium sulphate	120	
	Potassium chloride	10	
Copper	Copper cyanide	100	Silica fibers
	Sodium carbonate	12	
	Sodium hydroxide	25	
Copper	Phyrophosphate solution		Silicon carbide
Copper	Copper sulphate	200	Graphite
	Sulphuric acid	80	
Nickel	Nickel chloride	300	Alumina powder
	Boric acid	30	
Nickel	Nickel sulphate	200	Tungsten carbide
	Nickel chloride	180	
	Boric acid	40	

Although parameters affecting the deposit properties or incorporation concentration were analyzed, the mechanism of composite electrodeposition was not understood.

3.2 Codeposition Mechanism

Pioneering studies have shown the capability of inert particles suspended in a solution to be coated on a substrate along with reduced metal ions. However, these studies do not mention the characteristics of embedding nor the deposition kinetics. This phenomenal was regarded as a peculiarity until Guglielmi published an article explaining the reaction mechanism [32].

The aim of his study was primarily explaining the deposition steps of inert particles while additionally developing a model for analyzing the reaction kinetics. The relation of current density and particle concentration with deposition rate is also analyzed.

Guglielmi states that codeposition of inert particles can be considered possible as a result of electrophoresis or adsorption. Either of these theories have controversies. Electrophoresis fits as an explanation since the relationship of incorporated volume of particles to current density coincides with electrophoresis.

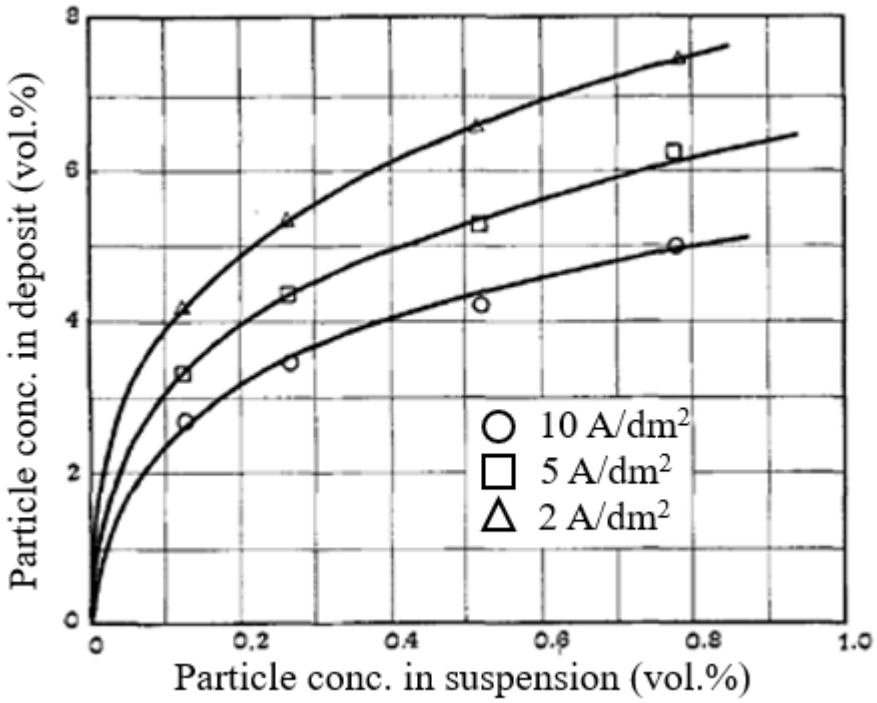

Figure 3.2 : Incorporation of TiO_2 particles by deposition from nickel sulfamate electrolyte [32].

Although the current density – volume relationship coincides with electrophoresis, particle volume dependence of the electrolyte in codeposition is non-linear, therefore contradictions emerge against electrophoresis [33]. Adsorption effect also fits the codeposition process, however it is not enough for explaining the dependence on current density.

To outcome the inability of electrophoresis and adsorption theories to explain codeposition process, adsorption effect is analyzed by dividing it into different stages. Guglielmi states that deposition process of reinforcing phase along with metal ions consists of a two-step mechanism. In first step, particles suspended in the electrolyte become weakly adsorbed on the cathode surface by physical forces while covering a very high amount of the cathode surface. Although particles in the solution are inert, ions encapsulate the inert particles and canalize them to the negative electrode. Along with solution ions, additives may also be in charge of this orientation. In the following

step, by electrochemical forces, strong adsorption occurs for some of the weakly adsorbed particles. Electrical field strips the thin ion film of the particle and thus the field assistance also helps creation of a stronger particle-electrode bonding. The strongly adsorbed particles are then codeposited and become permanently incorporated in the coating. By dividing adsorption into two stages, both contradictions regarding dependences of current density and concentration are solved.

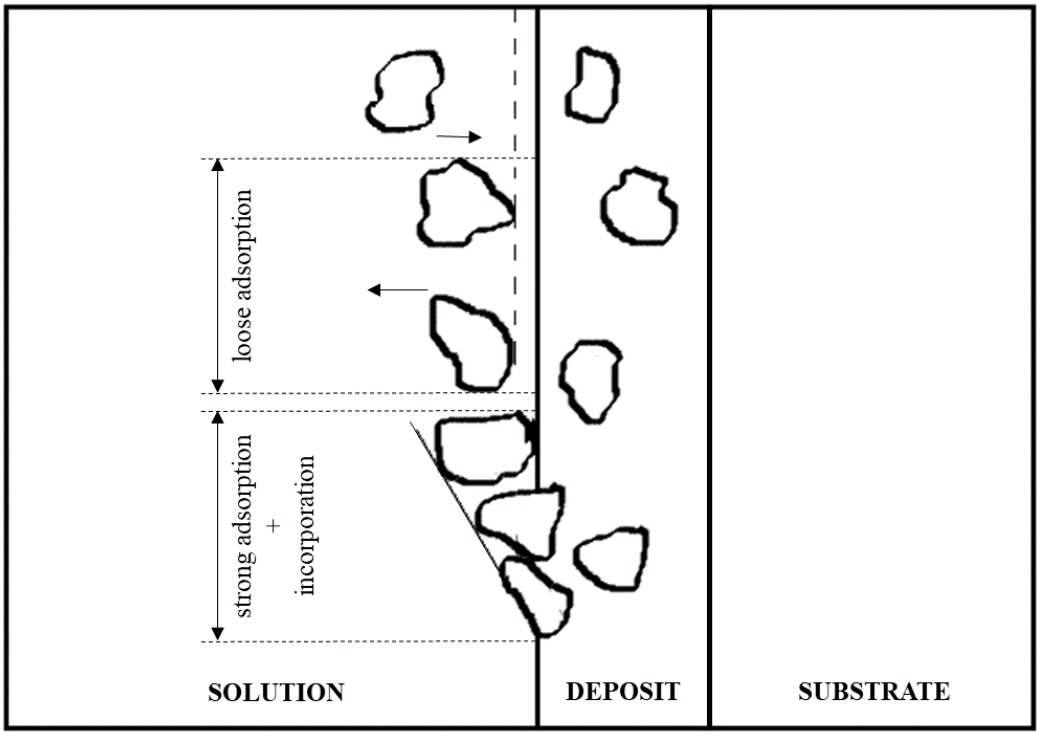

Figure 3.3 : Illustration of a two-step adsorption process [32].

After Guglielmi, scientists continued producing theories regarding codeposition phenomenal, including electrophoresis and adsorption similar to Guglielmi, also different theories about mechanical incorporations like the diffusion theory.

Although codeposition mechanism was not totally understood, studies mainly focused on solving the dilemmas existing in Guglielmi's model. It is decided to be more handful to investigate this circumstance by analyzing each codeposition step individually.

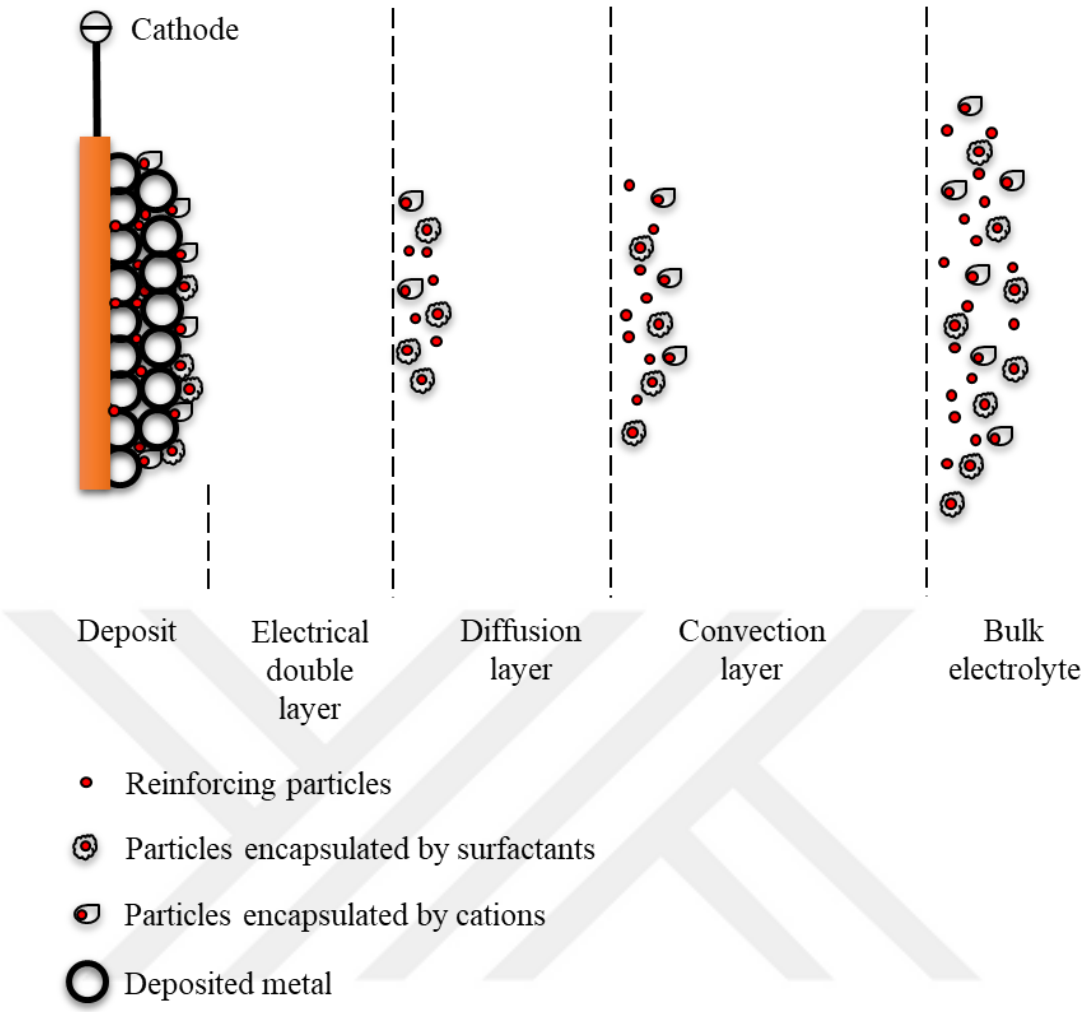

Figure 3.4 : Illustration of codeposition mechanism consisting of various steps [34].

In 1990, Celis explained the mechanism in a wider range. Codeposition mechanism is stated to consist of five stages. At first stage, as Guglielmi mentioned, thin ion films encapsulate the inert particles. These ion films are called surfactants in electrochemistry. This step occurs for particles that are suspended anywhere in the electrolyte. After particles are covered surfactants, they migrate through the convection layer to diffuse into the electrical double layer. Last step is adsorption on cathode surface prior to becoming incorporated in the deposit. Figure 3.4 depicts the mechanism, where the thicknesses of electrical double layer, diffusion layer and convection layer are in nanometer, micrometer and milimeter scales respectively [34].

3.3 Recent Studies

Investigating the pioneering studies, it is seen that the drawback of electrochemical composite plating is the low volume percentage of incorporated phase. In order to achieve the most efficient material properties, some applications may require a reinforcement volume of more than 50%. Obtaining such volume percentages by conventional techniques is not possible. Studies have been conducted by many researchers to improve the incorporation amount by altering the electrodeposition parameters. Although many parameters have been modified to increase incorporation volume above a certain percentage, conventional codeposition techniques are insufficient.

Sediment codeposition technique (SCD) on the other hand is a newly developing technique for composite electroplating where reinforcement incorporation up to 75% is possible.

3.3.1 Conventional codeposition techniques

In 2006 Dongyun aimed to incorporate Al_2O_3 nanoparticles in a copper matrix by electrocodeposition [35]. The used electrocodeposition technique was conventional electrodeposition as it is illustrated in Figure 3.5.

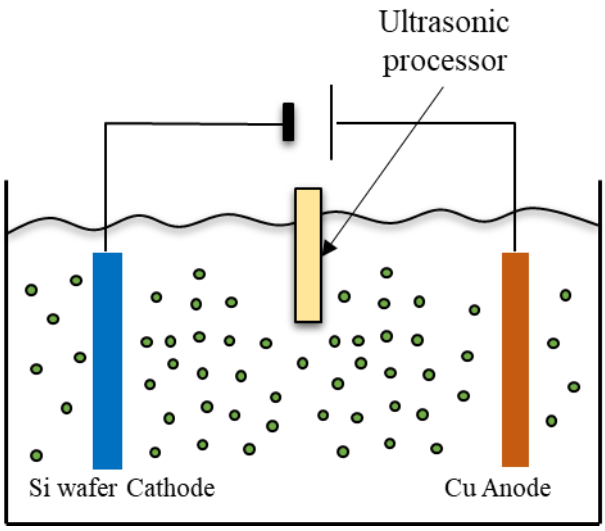

Figure 3.5 : Electrocodeposition cell with an ultrasonic processor.

Silicon wafer cathode was coated with a 5 nm Cr layer for the adhesion of the Au film, 50 nm thick Au film was coated to Cr layer to create conductive layer. Process parameters for electrocodeposition of Cu/Al_2O_3 are given in Table 3.4.

Table 3.4 : Process parameters for the electrocodeposition of Cu/Al_2O_3 [35].

Process parameters	Values
$CuSO_4.5H_2O$	112, 150, 250 g/l
H_2SO_4 (98%)	100 g/l
Temperature	50 °C
Current density	2 A/dm^2
Stirring rate	500 rpm
Ultrasonic irradiation	0, 70, 100, 120 W/cm^2
Al_2O_3 particle conc.	20 g/l
pH	1

In order to increase the volume of incorporated alumina particles, ultrasonic irradiaton is was applied. Table 3.5 shows the change in the volume fraction of Al_2O_3 with the influence of ultrasonic energy. Even though the volume fraction can be increased three times, it still cannot exceed 6.2%.

Table 3.5 : Change in the volume fraction of Al_2O_3 with ultrasonic irradiation [35].

Ultrasonic energy density (W/cm2)	Al_2O_3 conc. in deposit (vol.%)
0	2.4
70	1.5
100	4.1
120	6.2

In 2015, Hamal studied the effect of stirring rate on reinforcement concentration in deposit [36]. Nickel-Silicon Carbide composite was produced by conventional electroplating system. The bath compositions and operating conditions are given in Table 3.6 & 3.7.

Table 3.6 : Electrolyte composition for Ni-SiC composite plating [36].

Constituents	Concentration (g/L)
$Ni(NH_2SO_3)_2$.	300
$NiCl_2$	10
H_3BO_3	40
CTAB	0.2
Saccharine	2
SiC	20

Table 3.7 : Operating conditions for Ni-SiC composite plating [36].

Operating conditions	Value
pH	4
Temperature	50 °C
Current type	Pulse
Duty cycle	0.25
Pulse frequency	100 Hz
Current density	6 A/dm^2
Stirring rate	100, 250, 400 rpm

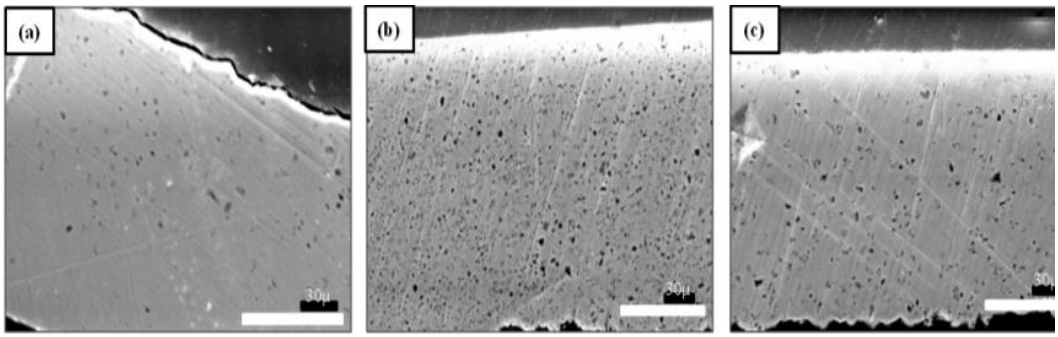

Figure 3.6 : SEM images from cross-sections indicating three different experiments with different stirring rates. In (a), stirring rate is 100 rpm, in (b) 250 rpm, in (c), 400 rpm [36].

Table 3.8 : Effect of stirring rate to the volume fraction of reinforcement [36].

Stirring rate (rpm)	SiC conc. in deposit (vol.%)
100	2.8
250	11.5
400	6.3

The volume fraction of particles increase approximately five times by optimizing the stirring rate. The deposition rate decreases after a certain stirring rate, since the particles do not settle on the cathode due to their excessive velocity. However, even if the volume fraction is increased five times, it still cannot exceed 11.5%.

In 2001 Garcia incorporated SiC particles in nickel matrix by conventional electroplating method for increasing the wear resistance of the material [37]. SiC particles with ranging particle sizes were used. In order to increase the amount of codeposited SiC particles, effect of solution concentration and particle size were analyzed. The plating solution was Watts Bath, electrodeposition parameters are given in Table 3.9.

Table 3.9 : Electrodeposition parameters for Ni-SiC composite plating [37].

Operating conditions	Value
pH	3.8
Temperature	50 °C
Current type	DC
Current density	2 A/dm^2
Deposition time	75 minutes
Cathode	Brass (12 cm^2)
Anode	Nickel (12 cm^2)

SiC with particle sizes 0.3, 0.7 and 5 μm was used. Particle densities and concentrations of particles in solutions are given in Table 3.10.

Table 3.10 : Particle size, density and concentration in solution [37].

Particle size (μm)	Particle density (particle/m^3)	Conc. (g/l)
5	5 x 10^{12}	1.04
5	10^{13}	2.1
5	10^{14}	20.8
5	5 x 10^{14}	104
0.7	5 x 10^{14}	0.28
0.7	10^{15}	0.57
0.7	10^{16}	5.71
0.3	5 x 10^{16}	0.56
0.7	10^{17}	57.1
0.3	5 x 10^{17}	5.62
0.3	5 x 10^{18}	56.2

The effects of particle size and bath concentration on incorporation volume are shown in Figure 3.7 and 3.8. As expected, volume increases with increasing particle size and particle concentration. The highest volume is achieved when the particle size was largest, 5 µm. Particles with a diameter of 0.7 µm were unexpectedly incorporated less than particles with diameter 0.3 µm. The reason for that can be explained by agglomeration of 0.3 µm particles.

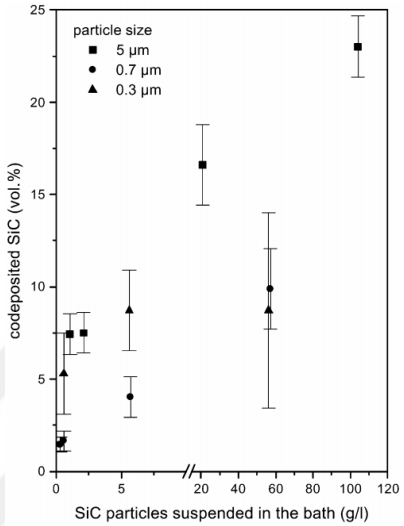

Figure 3.7 : Change in the volume of codeposited SiC particles by various bath concentrations [37].

The study shows that increased amount of particle codeposition has a positive effect on material properties. Wear resistance increases with increasing reinforcement volume.

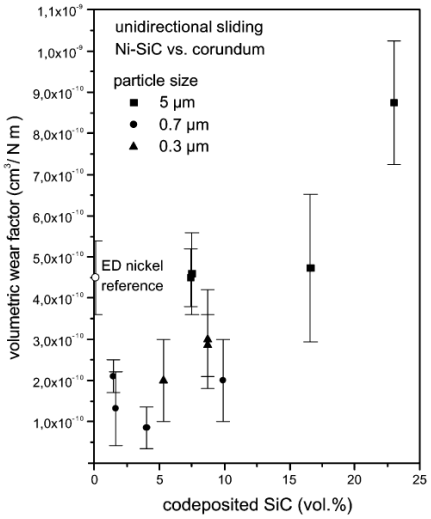

Figure 3.8 : Volumetric wear factor dependence on SiC volume [37].

Low et al., conducted a wide and excellent research on codeposition of secondary particles in 2005, where various materials in nanometer particle range such as alumina, diamond, silicon carbide, zirconia, titania were codeposited with copper and nickel [28]. Effect of the most important parameters such as current type, current density, particle size, bath agitation, surfactant ratio on the volume of incorporated particles were analyzed.

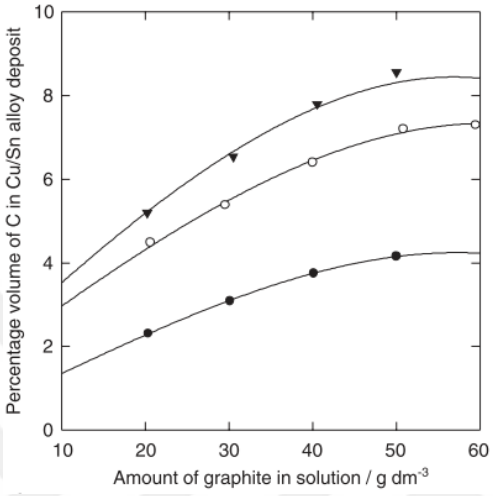

Figure 3.9 : Effects of bath concentration and stirring rate to deposit [28].

10 µm graphite powder was codeposited with copper. (Figure 3.9.) Lines with black dots, white dots and triangles represent magnetic stirring rates which are 50 rpm, 100 rpm, 200 rpm respectively. Similar to Hamal and Garcia, increasing stirring rate and increasing particle concentration lead to an increment in incorporated particle volume. However, the maximum incorporation is only around 8%.

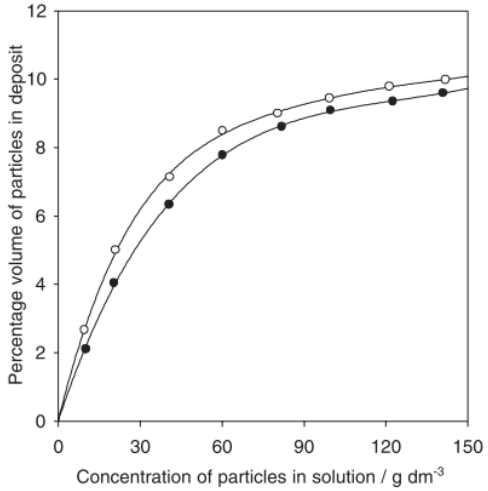

Figure 3.10 : Effects of bath concentration and temperature to deposit [28].

Figure 3.10. indicates the effect of bath conc. and tempreature to deposit properties. 500 nm alumina powder was codeposited with nickel-cobalt alloy. The impact of temperature on incorporated particle volume was investigated. Lines with white dots and black dots stand for experiments conducted at 50 °C and 60 °C respectively. At lower temperature reinforcement incorporation is higher.

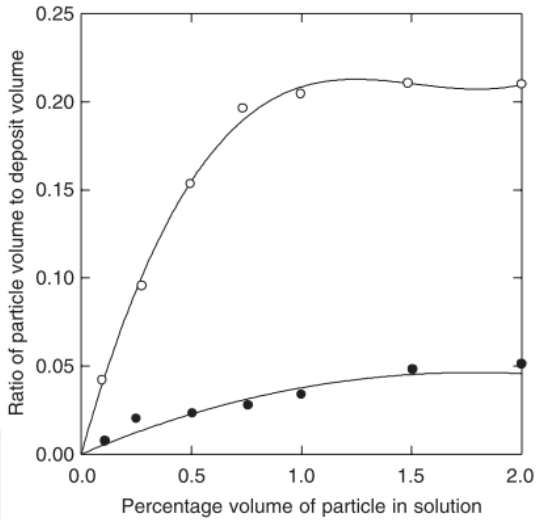

Figure 3.11 : Effect of particle size on the amount of incorporated phase [28].

300 nm alumina powder (white dots) and 50 nm alumina powder (black dots) were codeposited with nickel. Similar to the unexpected result of Garcia, higher particle size resulted in increased incorporation volume. (Figure 3.11.)

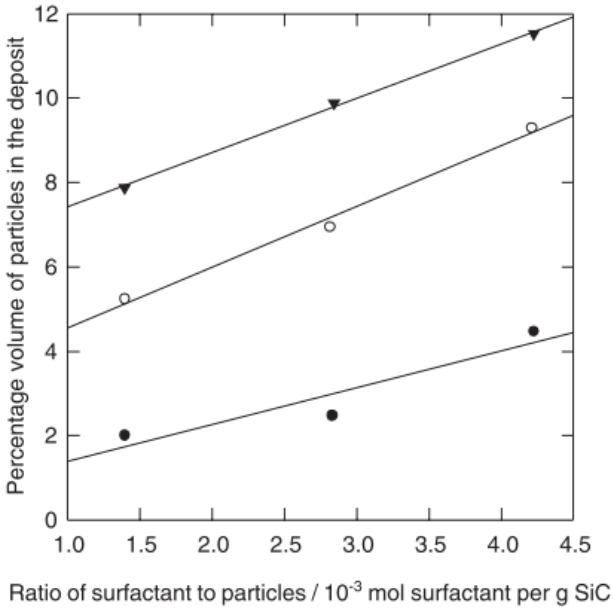

Figure 3.12 : Effect of additives to deposition properties [28].

Silicon carbide particles with an average particle size of 250 nm were codeposited with nickel. Cetyltrimethylammonium bromide (CTAB) is used as surfactant. (Figure 3.12.) Effects of surfactant concentration in the electrolyte and surfactant/particle ratio to incorporation volume were analyzed. Black dots, white dots and triangles represent 1 g/dm^3, 10 g/dm^3, 20g/dm^3 CTAB concentration respectively.

Increasing the surfactant concentration and surfactant/particle ratio both have a positive impact on percentage of incorporated reinforcement, however even at higher surfactant concentration the incorporation volume cannot exceed 12%.

3.3.2 Sediment codeposition technique

Volume of incorporated particles in conventional electroplating systems is limited by the rate of strongly adsorbed particles as Guglielmi modelled. Even loosely adsorbed particles in first step cannot cover the whole surface area of the cathode. The surface coverage drops dramatically when it comes to permanent adsorption. Most of these particles are detached from the surface and only a few percentage is embedded in the deposit.

For increasing the percentage of embedded particles in deposit, as stated, conventional electrodeposition technique has been revised by surfactant additions, changing electrolyte concentration, applying a different current type, using different agitation methods such as ultrasonic irradiation. However, incorporation percentage cannot exceed %12 since it still is mostly dependent on particle adsorption.

In order to increase the volume of reinforcing phase up to higher values, Sediment Co-Deposition (SCD) technique is developed. SCD in principle is very similar to conventional codeposition technique.

The major difference is that in SCD, electrodes are placed horizontal with respect to the ground. Reinforcing particles are settled on the cathode surface.

When current is applied, electrodeposited metal atoms fill the gaps between the settled particles and thereby a metal matrix composite material is produced.

Although SCD technique has gained attention in previous decade, its history extends back to 1972. In 1972, Viswanathan and Doss published the paper where they first developed SCD technique [38]. In 1980, developers of SCD method electrodeposited copper from a copper sulfate bath while incorporating graphite, molybdenum disulfide

and tungsten disulfide particles for tribological applications [38]. The study aimed to observe the effect of important parameters such as bath concentration and current density on embedded particle concentration in the deposit. Same parameters were used for both SCD technique and conventional electrodeposition method.

The highest volume percentages for incorporation are achieved for graphite. As expected, increasing reinforcement concentration in the electrolyte had a positive effect for incorporation in CED, likewise the same effect applies for SCD.

Increased current density also has a positive effect on percentage of embedded particles, however the effect is revealed on current densities above 5 A/dm^2, which is a leading factor for dendritic growth morphology and may cause a dramatic failure for desired applications.

The interesting point of the study is that volume percentage of incorporated particles reaches 25% although only a short amount of time has passed since the discovery of the technique.

In 2004, aluminum particles were codeposited with nickel to be converted into Ni_3Al intermetallic alloy and used as structural material later on [39]. The bath composition and operating conditions are given in Table 3.11 & 3.12.

Table 3.11 : Bath composition for Ni-Al codeposition [39].

Bath composition	Concentration (g/l)
$NiSO_4.6H2O$	270
$NiCl_2.6H_2O$	45
H_3BO_3	40
$CH_3(CH_2)_{10}CH_2OSO_3Na$	0.2
Al particle (3 μm)	5 - 150

Table 3.12 : Operating conditions for Ni-Al codeposition [39].

Operating conditions	Value
Anode	Pure Ni
pH	4
Temperature	25 °C
C.D	2-9 A/dm^2
Off-On Time	10/1200 s
Plating time	3 h

As substrate, a high-performance alloy was used. Both anode and cathode were surface treated for a smooth coating. Electrolyte was periodically stirred to keep the particles suspended and then settle on the substrate surface. After plating, substrate was cut, mounted and polished for characterization. Reinforcement volume up to 37% were successfully achieved in the deposit.

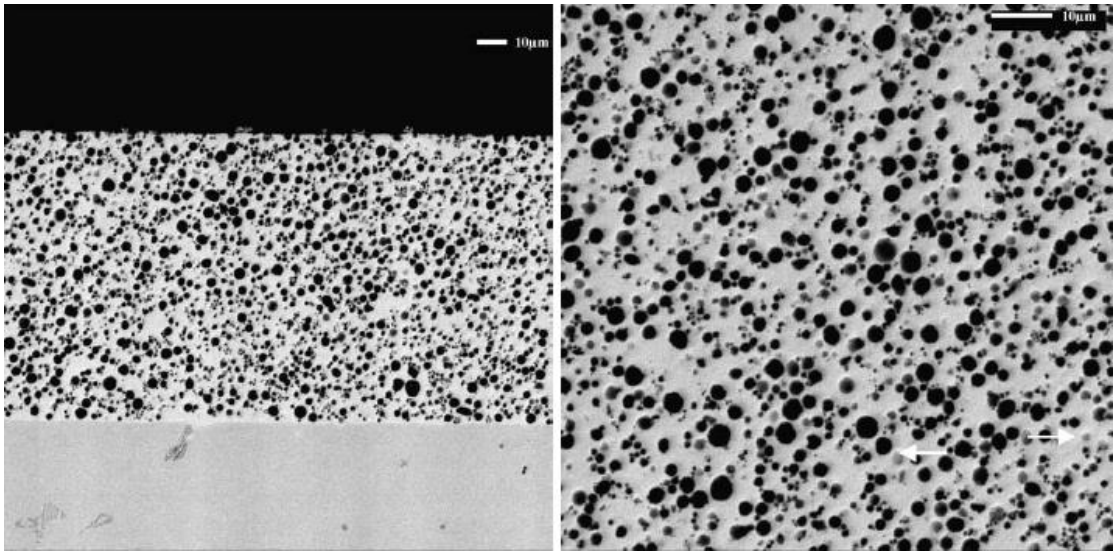

Figure 3.13 : SEM image of Ni-Al composite cross-section with back scattered electrons [39].

In 2014, diamond particles were codeposited with nickel by SCD, where volume of diamond particles in the deposit exceeded 75% [10]. Bath concentration and operation conditions are given in Table 3.13.

Table 3.13 : Bath composition and operating conditions for Ni-Diamond codeposition [10].

Electrolyte/Parameters	Value
$NiSO_4.6H2O$	300 g l^{-1}
$NiCl_2.6H_2O$	45 g l^{-1}
H_3BO_3	45 g l^{-1}
Diamond particles	1, 3 , 5 g l^{-1}
pH	3.2
Temperature	40, 50, 60 °C
CD	2, 4, 6 A/dm^2

Highest incorporation volume was obtained for temperature at 40 °C and current density at 2 A/dm^2 and expectedly at particle concentration of 5 g l^{-1}, with approximately 50% volume percentage.

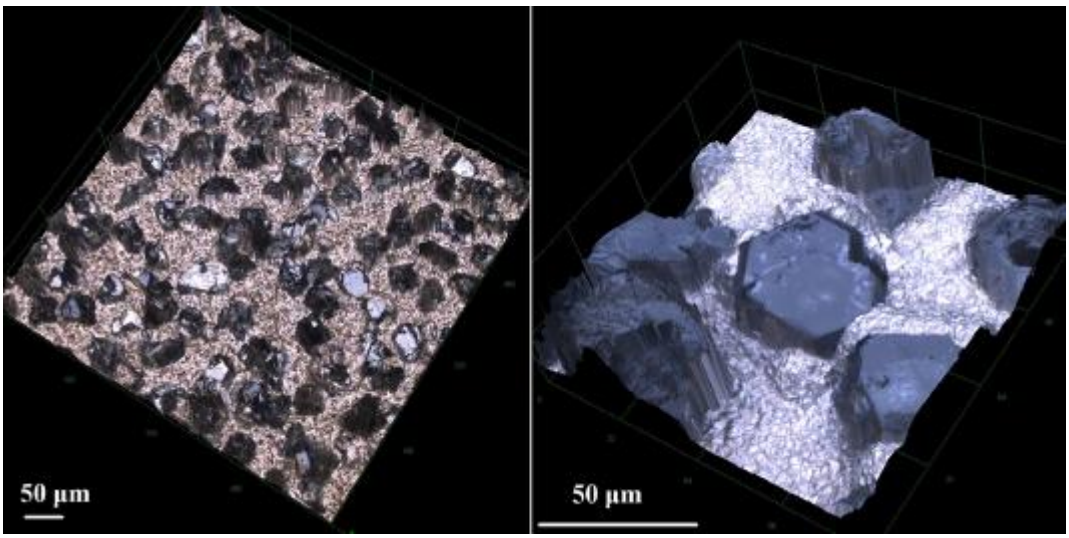

Figure 3.14 : 3D images of electrodeposited Nickel-Diamond composite under parameters of 2 A/dm^2 current density, 50 °C temperature [10].

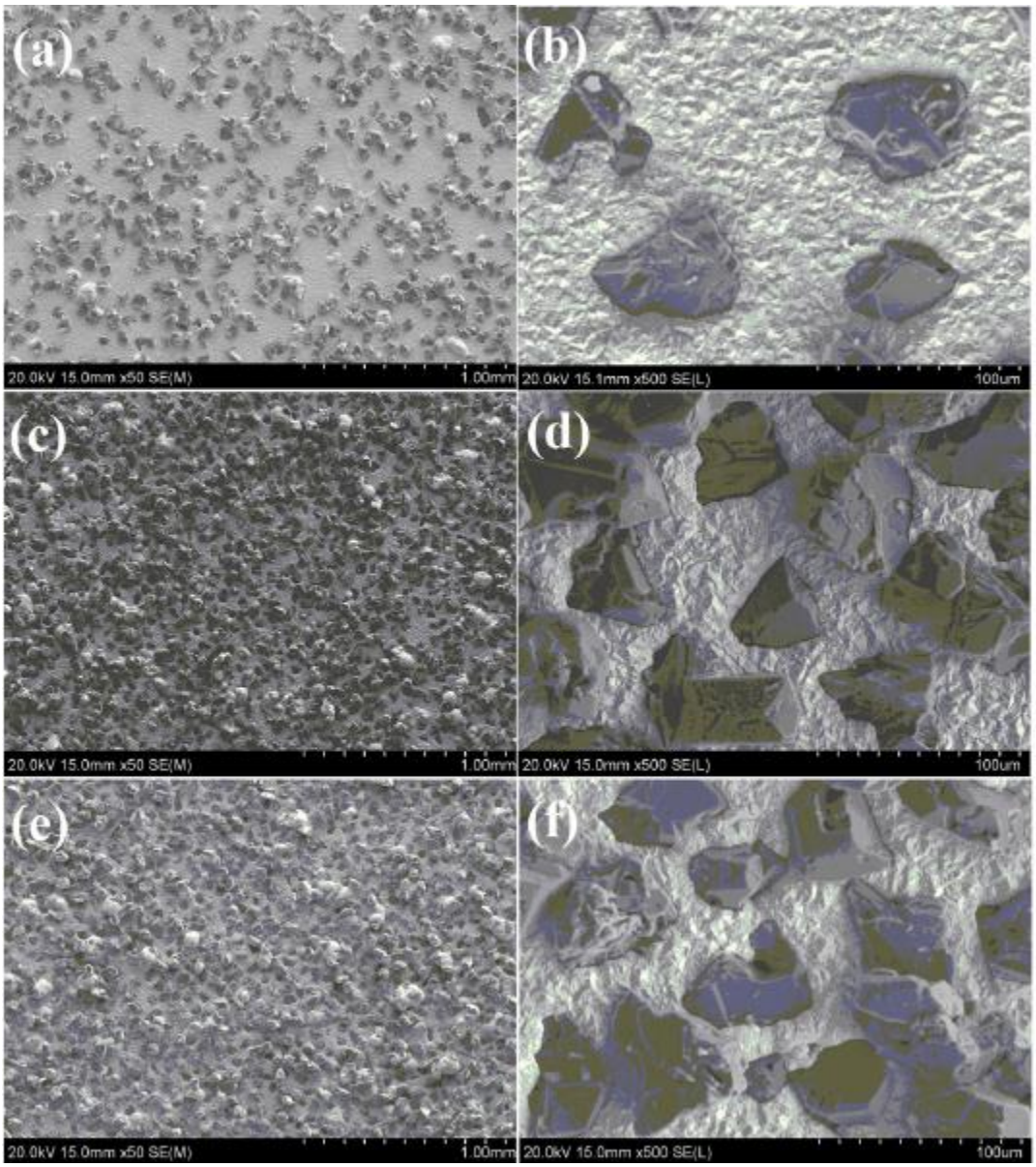

Figure 3.15 : SEM images composites produced by SCD method with steady parameters of 2 A/dm^2 current density and 50 °C temperature and various diamond conc. in electrolyte, (a,b) 1 g/l, (c,d) 3 g/l, (e,f) 5 g/l [10].

It is clearly observed from the coating surface that diamond particles are settled homogeneously and cover a major part of the surface area. However, scanning electron microscopy imaging from the cross-section reveals that the coating mostly consists of only one particle thick coating. Although the substrate surface are coated with reinforcing particles remarkably, the particles are not completely submerged in the deposit throughout the surface area. The coating thickness is stated as 35 ± 5 μm and is not enough to investigate the growth morphology of deposited metal during SCD process.

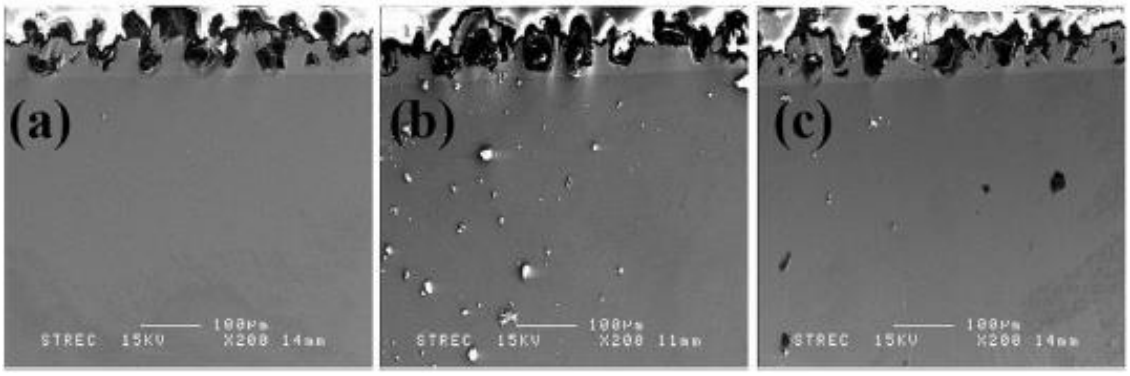

Figure 3.16 : SEM images produced by SCD method from the cross-sections at various current densities, (a) 2 A/dm^2, (b) 4A/dm^2, (c) 6 A/dm^2 [10].

In literature, the lack of a profound visual exhibition of composite materials by electroforming is perceptible. The motivation of this thesis is nevertheless providing concrete display of the manufactured composite together with electron microscopy imaging and macro imaging.

4. EXPERIMENTAL STUDIES

Experimental studies chapter consists of two main sub-sections, including electroforming procedure and results & discussion. Electroforming procedure section mentions the manufacturing process of the composite from raw materials to the final product; containing processes such as electrolyte preparation, electrode surface treatment, electroplating system setup, particle settlement and electrodeposition. Post-treatments applied on composite are also adressed in this chapter.

Analysis of composite properties along with characterizations are given in the results & discussion part. Electron microscopy imaging and x-ray diffraction patterns of as deposited and treated composites are presented.

4.1 Electroforming Procedure and Sample Treatments

Through the literature overview, electrochemical composite coating has proved itself as an alternative for other production techniques [38-47].

Codeposition of silicon carbide with copper is possible with SCD technique and high reinforcement volumes in the deposit are achieved [48-51].

As the first step of the experimental procedure, an acid copper sulfate electrolyte was prepared, Table 4.1 shows the bath constituents of used electrolyte.

Table 4.1 : Concentration of the Cu-SiC codeposition bath.

Constituents	Concentration (g/L)
Copper sulfate	180
Sulfuric acid	30
Hydrochloric acid	0.1
Thiourea	0.05
SiC particles	0 - 5

An experimental setup was designed for composite electroforming. In literature, sediment codeposition is generally conducted with a system consisting of horizontal electrodes and an electrolyte filled with reinforcing particles. Electrolyte is stirred for suspending the particles and then particles settle on the cathode surface.

For producing a composite in which particle dispersion occurs homogenously; additionally for manufacturing a composite with near net shape, a decent electroforming setup needs to be prepared. Near net shape manufacturing in materials engineering is a fabrication technique where the material is produced in the desired shape and can be directly used for its application without requiring a surface finish. Copper-SiC composite with high SiC volume ratio is highly brittle, therefore it cannot be plastically formed into the final shape. It is more favourable to be produced in the final shape. For this purpose, an electroforming setup is designed and built where the composite can simple be stripped from the substrate with the required dimensions.

Important section of the experimental setup is the cathode since the product is formed on cathode surface. For building the cathode, a copper sheet with dimensions presented in Figure 4.1 was bent in an L shape. Afterwards, the sheet was partially coated with a heat shrink tube.

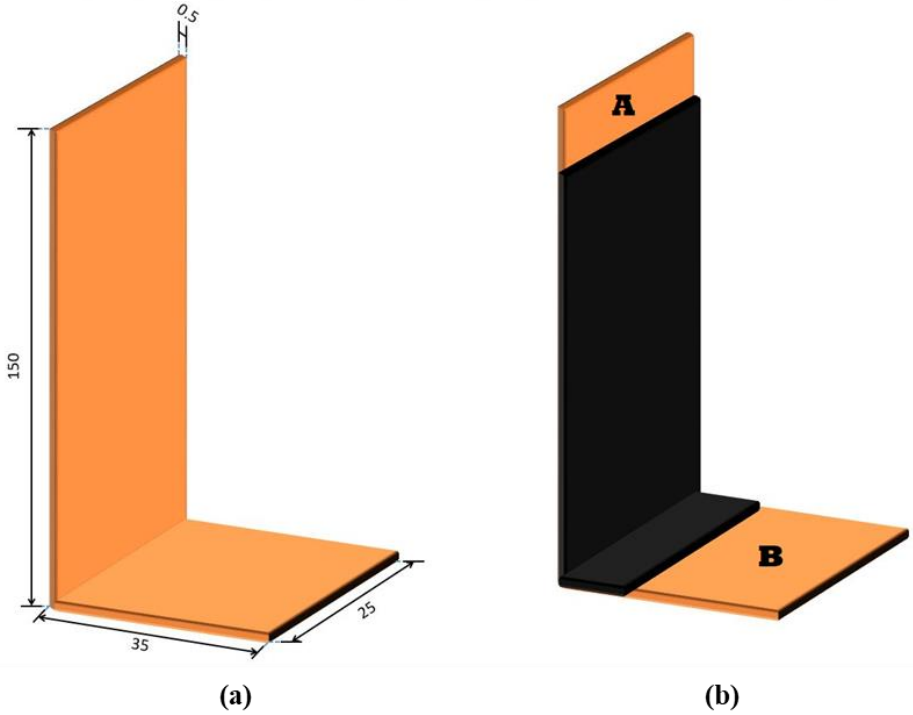

Figure 4.1 : Initial steps of cathode setup preparation, copper is (a) bent in L shape, (b) covered with heat shrink tube.

Copper sheet with a 0.5 mm thickness was bent and cut by regular scissors. Heat shrink tube protects the cathode from interfering with the electrolyte while also preventing reduction of metal ions by isolating the cathode surface.

Isolation of the cathode is crucial since any open sites for reduction affects the current density. Only the parts that are desired to be electroplated must be in contact with the electrolyte.

The area marked by “A” in Figure 4.1 was not covered with heat shrink tube because the cathode was planned to be connected to a power supply from that area by a crocodile clip. The area marked “B” was also uncovered, because another copper plate, which is the substrate, represented in Figure 4.2 was meant to be mounted on that section. The only function of area “B” is conducting the current to the substrate.

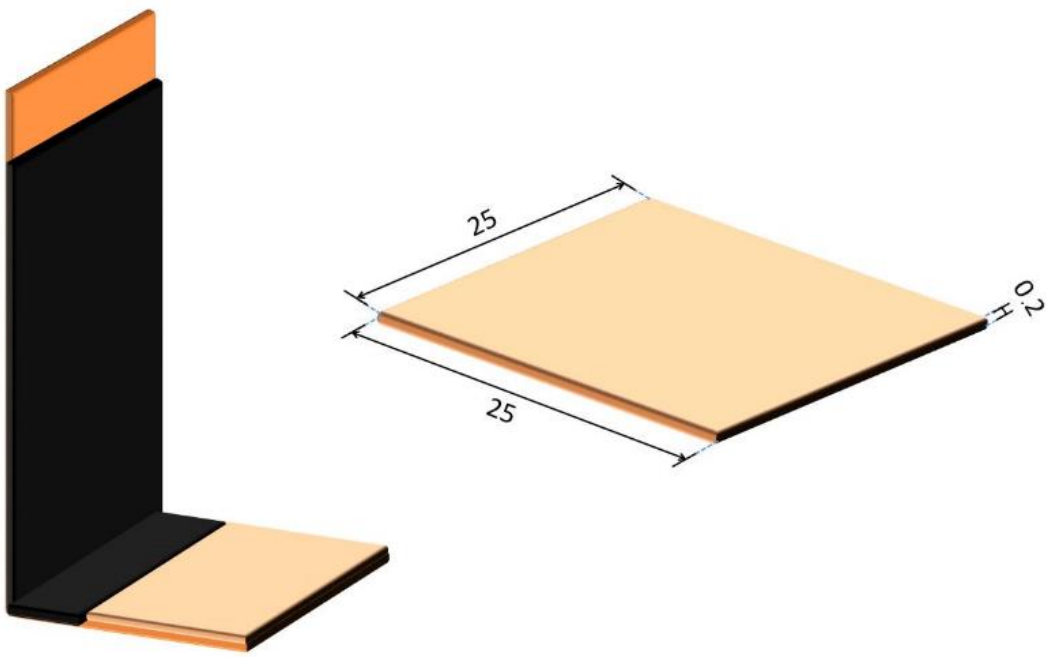

Figure 4.2 : Mounting the substrate with given dimensions on cathode setup.

The substrate was desired to be partially in contact with the electrolyte. In order to strongly clench bent copper with substrate two lids were fabricated from Plexiglas. Forms and dimensions of the Plexiglas lids are represented in Figure 4.3.

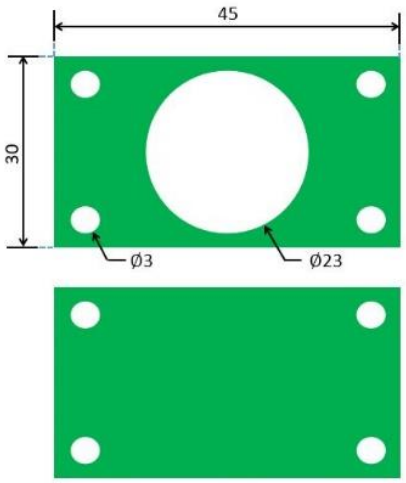

Figure 4.3 : Designed Plexiglas lids with dimensions.

The lid with a 23 mm diameter hole was placed above the substrate and the other lid was placed under the cathode. Bolts were inserted through 3 mm holes for compression. Polymer bolts are used because metal bolts get copper coated in copper sulfate bath by cementation and contaminate the electrolyte with metal ions. For avoiding electrolyte leakage, O-Ring seals were attached to the top lid and a thin silicone sealant film covered the other lid.

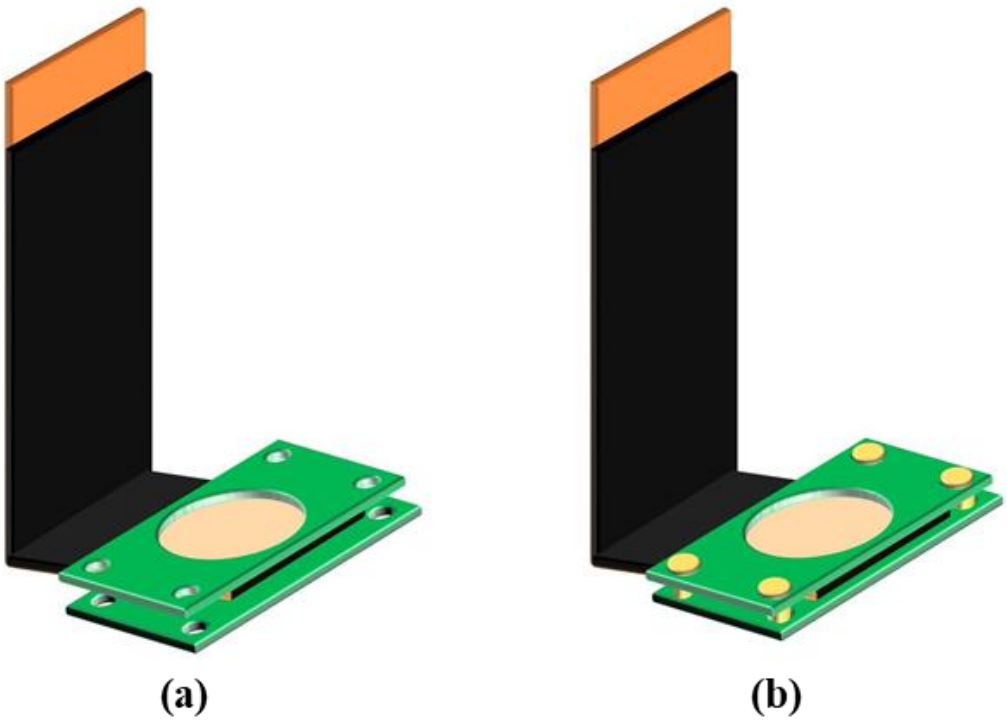

Figure 4.4 : Final shape of cathode system, Plexiglas lids are (a) mounted on substrate, (b) clenched with bolts.

Final design of the cathode-substrate part is represented in Figure 4.4. The only conductive part of the system is the hole with 23 mm diameter. The built design was submerged in a beaker while it was held by a clamp stand. Another copper sheet with same dimensions of cathode was cut from a 1 mm thick copper sheet to be placed as anode. The designed setup under operation is shown in Figure 4.5.

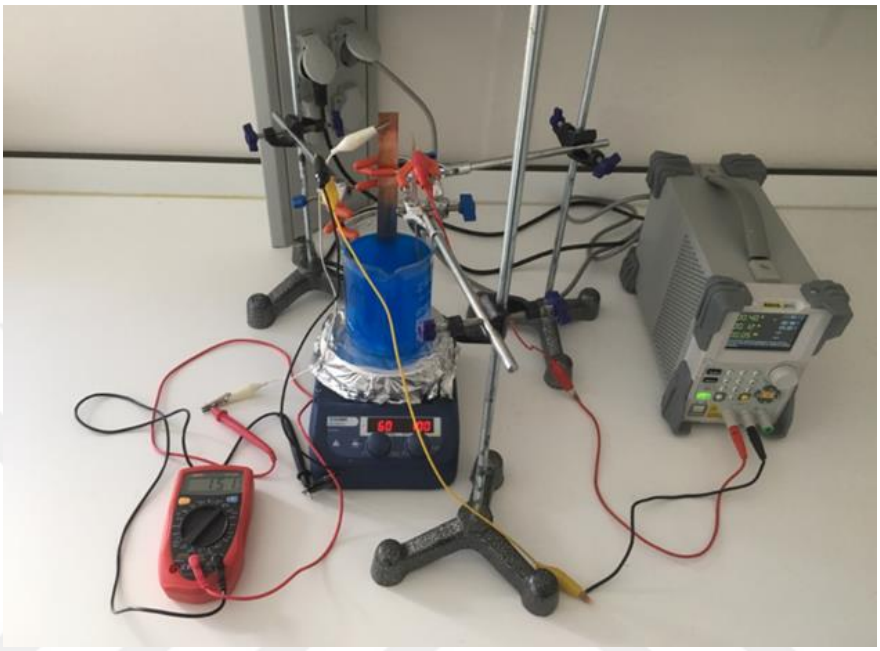

Figure 4.5 : Designed experimental setup for electroforming.

Optimized operating conditions are given in Table 4.2. Benchmarking of parameters such as current density, applied potential and current type are explained in Chapter 4.2.2 (p.52).

Table 4.2 : Operating conditions of the Cu-SiC codeposition bath.

Operating conditions	Value
pH	0.5
Temperature	40 °C
Current type	DC
Applied potential	300 mV
Read potential	160 mV
Current density	1 A/dm^2
Stirring rate	0 - 200 rpm
Particle size	75 - 1000 μm

Prior to electroforming, copper substrate was surface treated by grinding, pickling with %20 HCl for 10 seconds, rinsing with ethanol and drying. Afterwards, it was mounted on the cathode surface and was clenched between Plexiglas lids. Cathode and anode were stabilized by two clamp stands. Electrodes were connected to an external power supply. A copper reference electrode was also connected to a voltmeter along with cathode so that potential difference between cathode and reference electrode was read simultaneously.

A set of experiments were conducted by pouring 5 g/l SiC particles in the electrolyte where particles were settled on the cathode surface through stirring the bath. Another set of experiments were conducted with an electrolyte which did not contain any reinforcing particles in it. Powders were settled by pouring SiC particles into the designed substrate hole. At first, dry, non-treated SiC particles were used in electrodeposition. The surface qualities of the deposits were investigated.

For enhancing particle settlement step, instead of directly using powder from chemical pack, SiC particles were initially wet in a beaker containing copper plating electrolyte by agitating with magnetic stirrer for 10 minutes. Wet SiC particles were taken from the beaker and poured into the substrate hole. For investigating the surface of the composites, scanning electron miscroscopy imaging was performed.

In order to optimize electroforming parameters, polarization curve of the electrolyte was plotted, a set of coatings were fabricated under various current densities. After optimizing the operating conditions and particle settlement, Cu-SiC composites with particle sizes 75 μm and 1000 μm were electroformed for 30 hours.

Deposited composite was manually detached from the substrate by applying pressure. In order to analyze the composite structure, XRD patterns were plotted. For investigating the interface between copper matrix and silicon carbide particles, cross-sections of the samples were investigated by SEM.

For further enhancement of the matrix-particle interface, a set of post treatments were conducted. Samples with different particle sizes were annealed at 650 °C for 2 hours, cold isostatic pressed under 1500 kN and cold isostatic pressed prior to annealing with same parameters. Surfaces and cross-sections of post-treated samples were investigated with SEM to see the results at the interface. XRD patterns of each sample were plotted to analyze the structural changes.

Table 4.3 : Post-treatments applied to deposits with various particle sizes.

Sample number	Particle size (μm)	Treatment
1	75	No treatment
2	75	CIP
3	75	Annealing
4	75	CIP + Annealing
5	1000	No treatment
6	1000	CIP
7	1000	Annealing
8	1000	CIP + Annealing

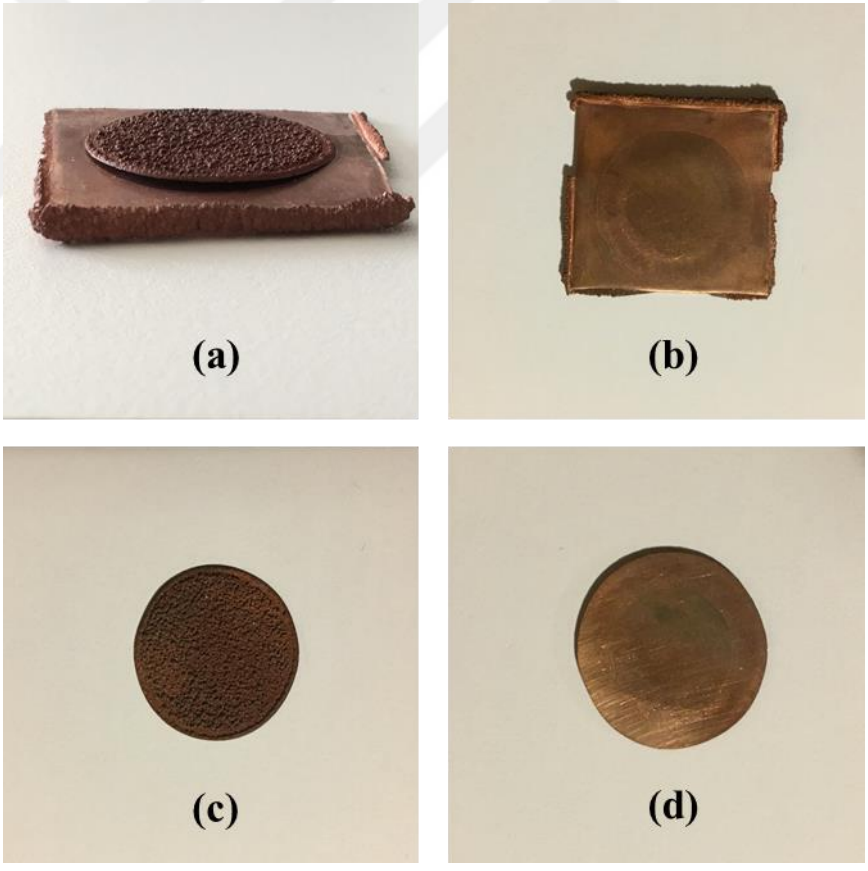

Figure 4.6 : Fabricated composite with optimized conditions. (a) Deposit is almost detached from from substrate, (b) substrate after detachment, (c) front view of detached deposit, (d) back view of the detached deposit.

Finally, in order to support the comments obtained by SEM imaging and XRD patterns and to analyze the behavior of composites under plastic deformation, flexural strengths of a different set of composites were measured by three-point flexural test. For this purpose, two samples were electroformed, first sample was not post-treated (as deposited), the latter was annealed at 650 °C for 2 hours.

Figure 4.7 : Devices used for post-treatment: (a) Vacuum furnace, (b) CIP

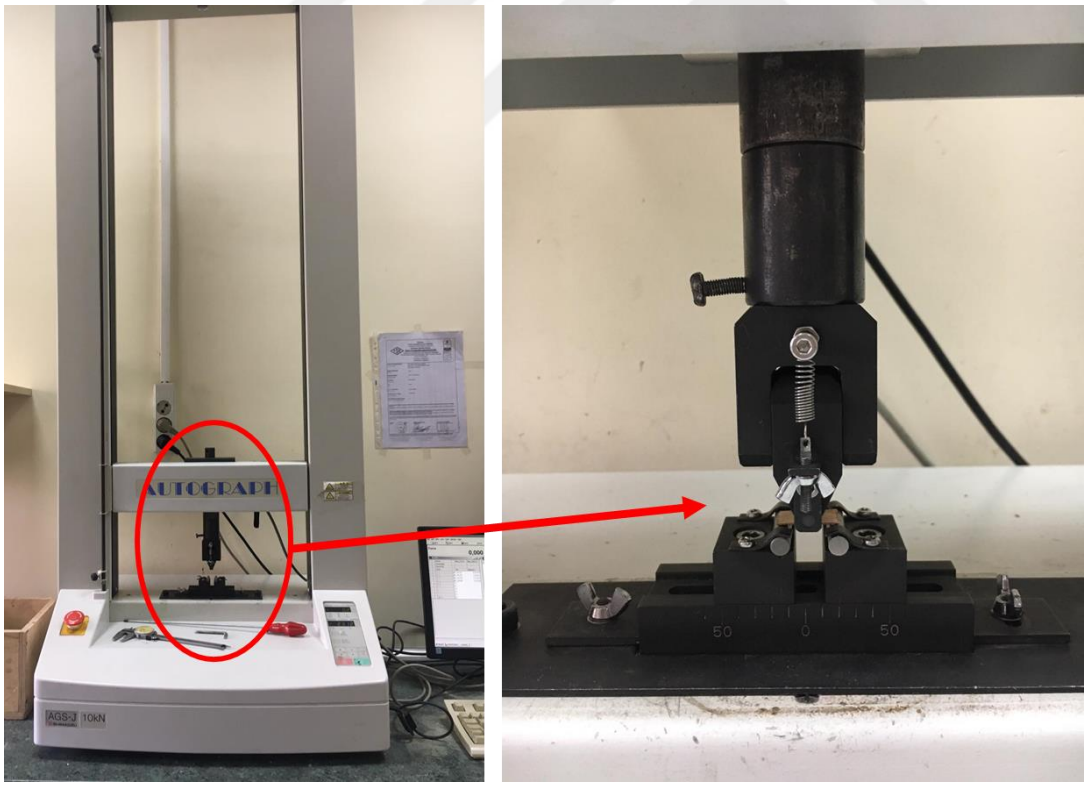

Figure 4.8 : Three-point bend test for calculating the flexural strength.

4.2 Results and Discussion

4.2.1 Optimization of particle settlement

In literature, SCD technique is done by adding particles to the electrolyte and then suspending the particles by stirring. During stirring, some of the suspended particles settle and stay on the horizontal cathode surface. Afterwards, electroforming process begins and reduced metal ions fill the gaps between the settled particles.

Although this is a practical method for particle settlement, it is hard to control the settlement process regarding the amount of settled particles. Additionally, it is also inconvenient for obtaining a homogenous particle distribution above the cathode surface. Considering the drawbacks of stirring induced settlement, another method is developed.

As the first step, 0,35 g SiC particles with a particle size of 75 μm were taken. The particles were carefully placed on the cathode surface within the hole of the plexiglas lid. Afterwards, the cathode setup was submerged in the bath and copper was deposited for 6 hours at 40 °C, 3 A/dm^2.

Figure 4.9 : Unsuccesful deposit fabricated by unwetted SiC particles.

The outcome of directly placing the particles from pack on substrate was a failure. Reduced metal ions did not fill the gaps between particles, instead built a thin copper film above the particles as seen in Figure 4.9. Considering the reasons behind this

circumstance, it was supposedly caused by agglomeration of unwetted particles. Once the particles agglomerated, they formed a sediment layer between substrate and electrolyte, which prevented the electrolyte to wet the interfaces between particles. Therefore, metal ions could only be reduced at random nucleation sites and from there a copper film above the particles was formed.

As a solution, SiC particles were initially wet in a solution containing the same copper electroforming electrolyte as used in deposition by magnetic stirring in a 25 ml beaker for 10 minutes. Afterwards, the particles were taken from the beaker and carefully placed on the substrate within the hole. An experiment with same operating conditions was conducted.

Figure 4.10 : Deposit fabricated by wetted SiC particles.

This time, electrolyte could reach the substrate through the settled particles owing to the capillary forces. Silicon carbide particles were hereby successfully incorporated in the copper matrix. However, as it is seen from Figure 4.10, deposit has a dentritic morphology along the composite surface. To closely investigate the deposit morphology, scanning electron microscopy images are taken from the surface and the cross-section of the sample. (Figure 4.11 & 4.12)

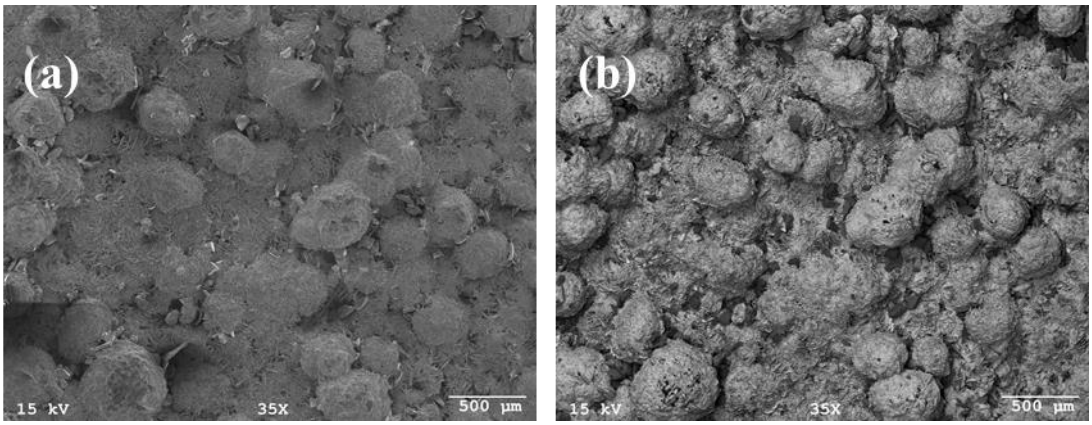

Figure 4.11 : SEM image of sample surface with; (a) secondary electrons (SE) at 35X mag, (b) back-scattered electrons (BSE) at 35X mag.

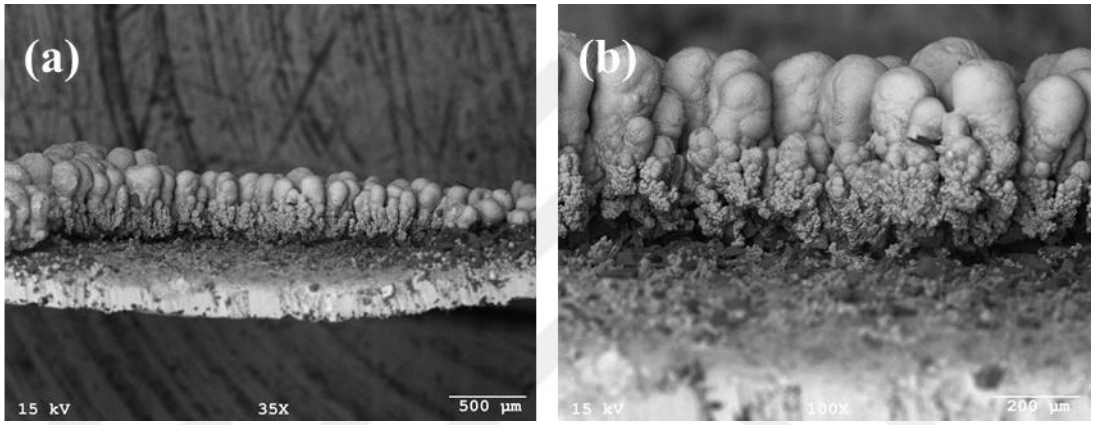

Figure 4.12 : SEM image of sample cross-section with back-scattered electrons, (a) with 35X mag, (b) with 100X mag.

Although it is observed from the electron microscope images taken from the cross-section of the sample that copper was deposited around SiC particles, there is not a concrete interface between matrix and reinforcement. In fact, copper just grew in a needleshape without interacting with silicon carbide. It is desired for copper to reduce in a way that it covers reinforcing particles smoothly, while also building a pore-free strong matrix-reinforcement interface. Therefore, dendritic growth is not acceptable.

4.2.2 Benchmark of current density

The most important parameter affecting the growth morphology is overpotential and the current density [22]. Another troubling issue with composite electroforming is calculation of the current density. As mentioned, during electroforming process, substrate surface is covered with reinforcing particles and due to the nonconductive settled particles, cathode surface is not completely conductive. For that reason alone, current density cannot be precisely calculated. However, the potential region of "good"

electrodeposition with respect to a reference electrode can be obtained from the cathodic polarization curve. In order to measure the change of cathodic current density by increasing the voltage, potentiostatic curve was plotted. The used electrolyte was the electroforming electrolyte and had the same composition as Table 4.1. Since the electrodes in composite electroforming setup are both pure copper, a copper reference electrode can be used.

Figure 4.13 : Setup for plotting polarization curve in used electrolyte.

The curve was plotted at a scan rate of 2 mV/s and in a voltage range of 0 to – 1V. Anode and cathode were polarized by applying a potential. Meanwhile, the reference electrode was neutral. Potentiostat also measured and recorded the potential difference between cathode and reference electrode. The plotted curve in Figure 4.14 shows the polarization curve. The y-axis shows the potential difference between cathode and copper reference electrode. The reason copper was used as a reference electrode is that a copper foil can simple be immersed in electrolyte without any drawback and it makes the experimental procedure very practical. During electroforming, a copper sheet can easily be connected to a voltmeter along with cathode. The applied potential to the setup can easily be arranged to the desired value by stabilizing the voltage read from the voltmeter.

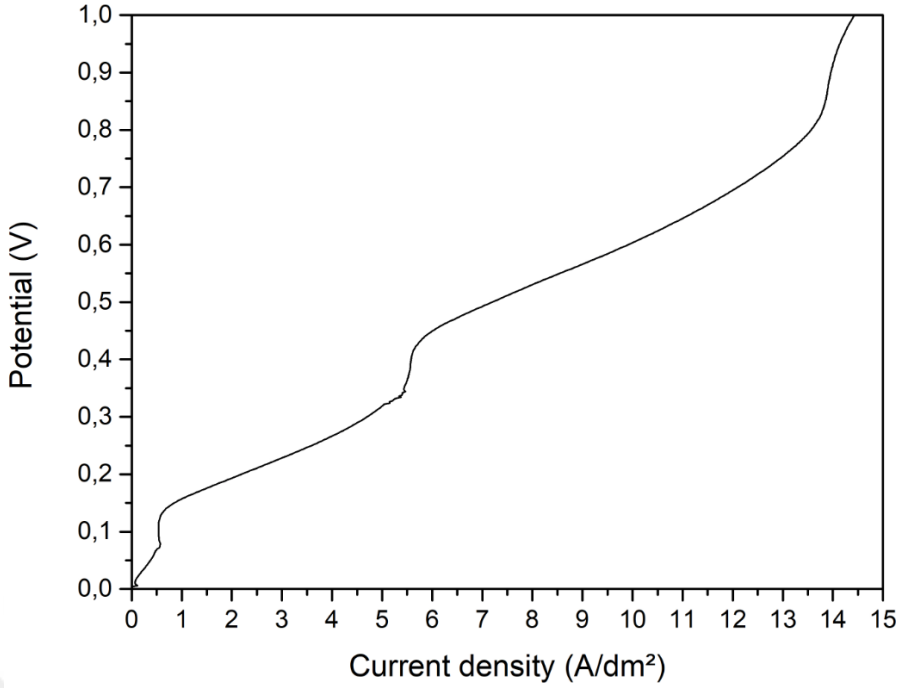

Figure 4.14 : Polarization curve plotted in copper electroforming electrolyte.

Operating current density depends on the function of the deposit. For composite fabrication, filling the gaps between particles is a necessity. Therefore, deposit morphology must be arranged in a way the electrolyte must be capable of filling micro voids. This demand is similar in micro electronic component production, where copper has been deposited for filling micrometer thick diameters. In literature, cathodic current density for the mentioned purpose ranges between 0,8 - 2 A/dm^2 [54,55].

In order to optimize the cathodic current densities, a set of experiments were conducted with current density as a parameter. Applied current densities and their corresponding potential differences of cathode/reference electrode are taken from the polarization curve values and are given in Table 4.4.

Table 4.4 : Cathodic current densities and corresponding potential differences.

Cathodic current density (A/dm2)	Potential difference (mV)
1,074	160
1,620	180
2,249	202

Going through the previous studies, polarization is both done current controlled and potential controlled, however statement for selection is unavailable. Considering the mechanism of SCD, at the initial point, surface area of the substrate is covered with particles. In time, metal deposition takes place and gaps between the particles are filled. A change of cathode area is present. Therefore, process cannot be done by a current controlled system. Once there is a change in cathode area, if the same current is applied, there will be a change in the current density.

Current density, as mentioned, is one of the most important parameters for electroforming. Current density must be steady throughout the entire process. Therefore, system should be potential controlled. Assuming the cathode area increases during process, there will be a larger conductive site and current will pass more easily. In that case, passing current will increase along with area and current density will kept steady. Assuming cathode area decreases during electroforming, there will be a decrement in conductive sites and electrical resistance will be higher. Passing current will decrease while area is also decreasing, current density is kept steady in this situation as well.

Three samples were fabricated with current densities 1,04, 1,62, 2,25 A/dm^2. Other operating parameters were fixed as it is in Table 4.2.

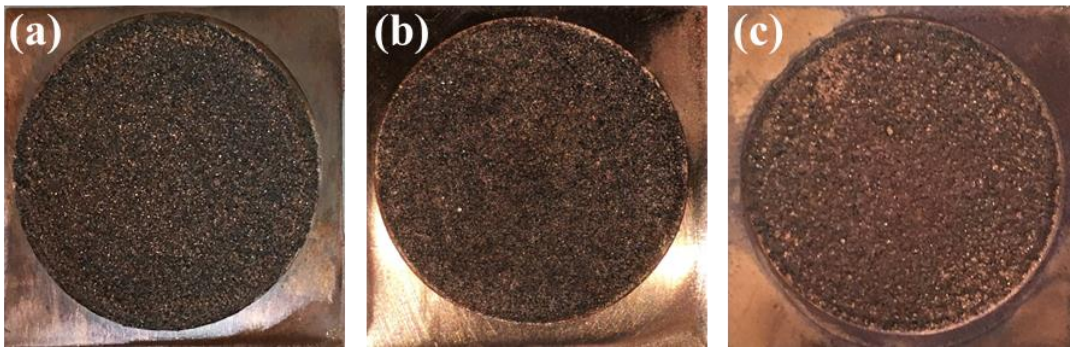

Figure 4.15 : Cu-SiC composites fabricated at different current densities; (a) 1,04 A/dm^2, (b) 1,62 A/dm^2, (c) 2,25 A/dm^2.

As seen in Figure 4.15, SiC particles were homogeneously dispersed at the surface. For a profound investigation of surface morphology, SEM characterization was conducted for each sample.

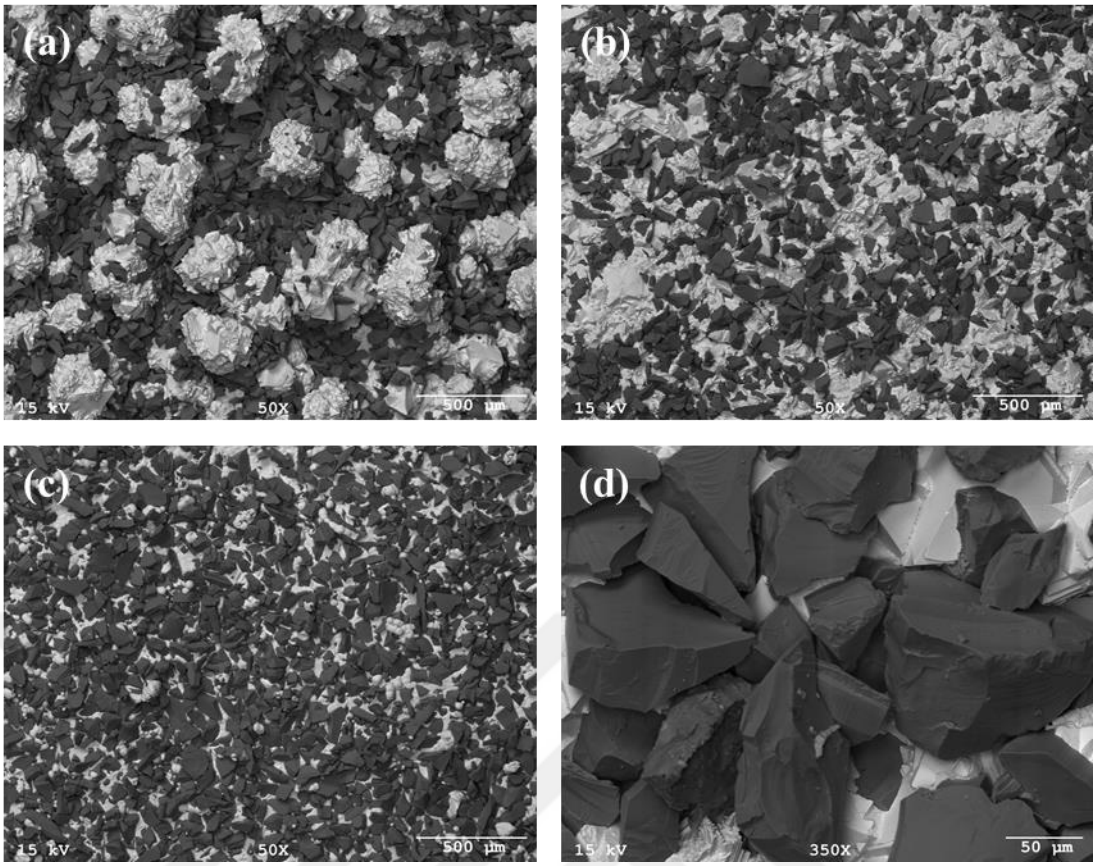

Figure 4.16 : SEM images of sample surfaces with backscattered electrons with different current densities: (a) 2,25 A/dm^2, (b) 1,62 A/dm^2, (c) 1,04 A/dm^2 at 50X magnification. (d) shows particle distribution for deposit fabricated with 1,62 A/dm^2 current density at 350X magnification.

From surface images represented in Figure 4.16, as current density is increased, dentritic formation takes place at specific sites. This is clearly observed for sample produced at current density 2,25 A/dm^2. The sample produced with 1,04 A/dm^2 current density showed an excellent particle distrubition regarding homogenity and smoothness of deposited copper, silicon carbide particles cover 85% of the surface. From image with 350X magnification it is seen that deposited copper wraps the silicon carbide particles as desired. Comparing surface morphologies of (a), (b) and (c), operating current density is selected as 1 A/dm^2 for the following fabrications.

Maintaining the current density at 1 A/dm^2 is arranged by working potential controlled. By connecting a voltmeter to the working electrode (cathode) and to a copper sheet immersed in electrolyte as a reference electrode, the potential difference of them is measured. According to the polarization curve represented in Figure 4.10, current density is 1 A/dm^2 when the difference in potential is 160 mV. 160 mV potential difference between WE/RE is satisfied when 300 mV of potential is applied from the

power supply to WE/CE. After the current density was optimized, 4 samples were fabricated at same parameters given in Table 4.2, for controlling the reproducibility of the composite. Samples produced under same operating conditions are presented in Figure 4.17.

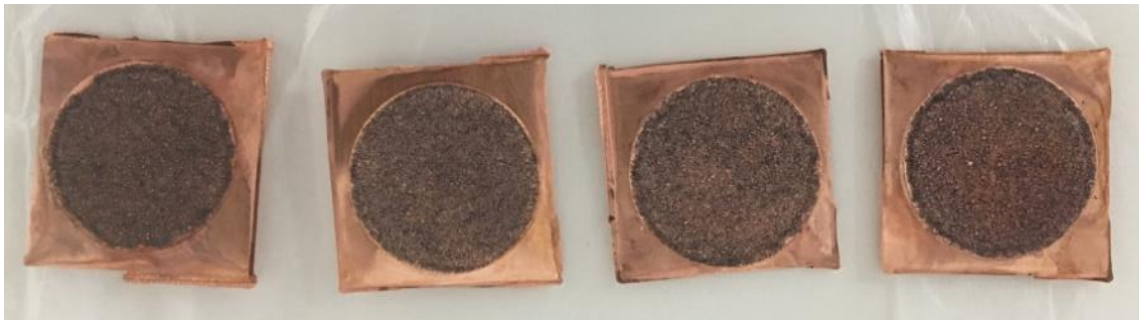

Figure 4.17 : Samples fabricated under same conditions for controlling the reproducibility

Considering the macroscopic analysis of samples, under potential controlled system, desired surface morphologies were achieved and the process is reproducible.

4.2.3 Incorporation of particles

After optimizing the operating conditions and homogeneously emplacing reinforcing particles at substrate surface, the next step is continuing the deposition process long enough, that each particle surface is compeletely coated with copper, thereby become incorporated in the deposition. In order the achieve this, deposition time was increased from 6 hours to 30 hours.

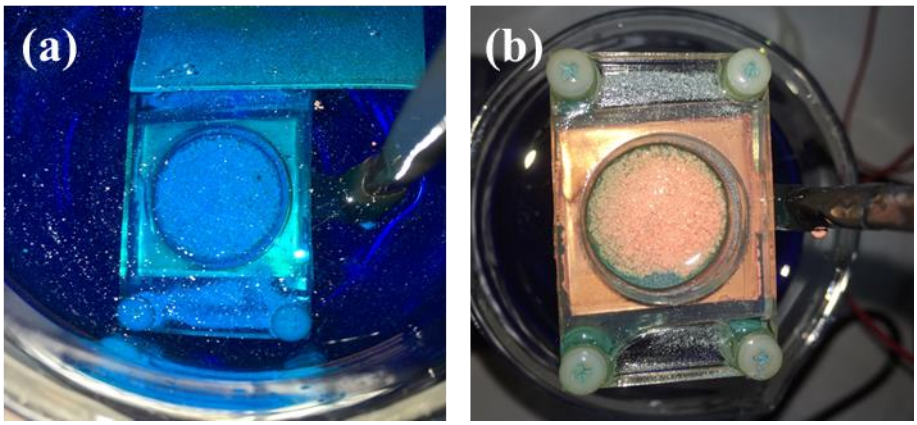

Figure 4.18 : Deposition after 30 hours, (a) deposition takes place; (b) the substrate is ready to be extracted.

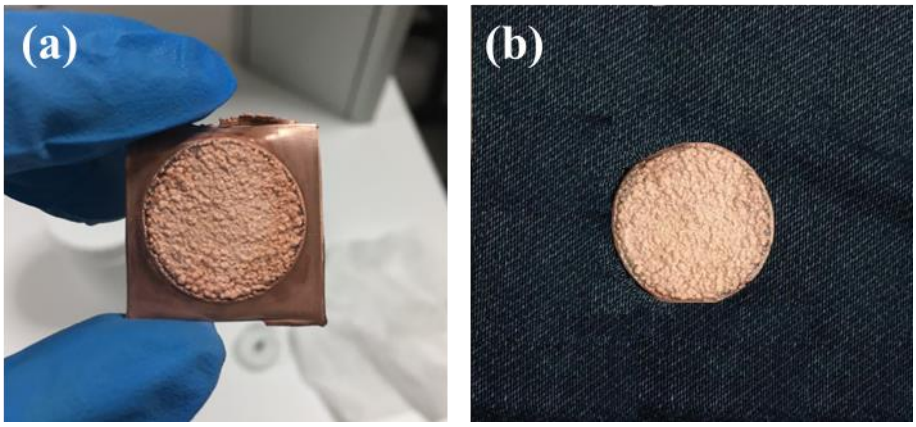

Figure 4.19 : Fabricated composit after 30 hours; (a) deposit is grown on substrate, (b) deposit is stripped from substrate

As seen in Figure 4.19, a bright deposit was achieved and surface of the particles was covered with copper. Unexpectedly, deposit was able to be easily detached from the substrate without any deformation. SEM imaging from both surfaces and cross-section were conducted to analyse the surface quality, particle incorporation and copper-silicon carbide interfaces.

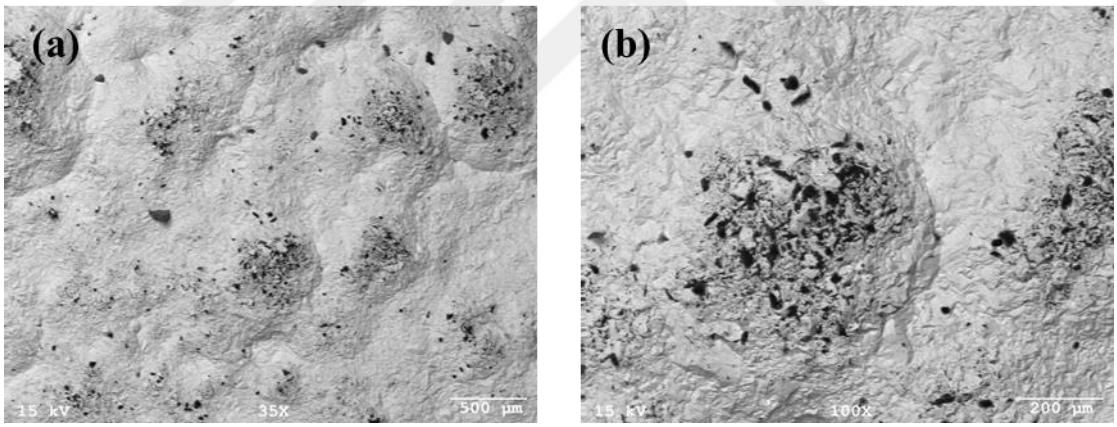

Figure 4.20 : SEM image of top surface with backscattered electrons, (a) at 50X magnification, (b) at 100X magnification.

Top surface imaging presented in 4.20 shows that surface of silicon carbide particles were covered with deposited copper and the morphology is smooth and bright. However, the images revealed that there were particles with an average particle size of 10 µm. In order to see if these particles were over-grinded SiC particles or an impurity, elemental analysis was conducted by Energy Dispersive X-Ray Spectroscopy (EDS) method. Result of the analysis is given in Figure 4.21.

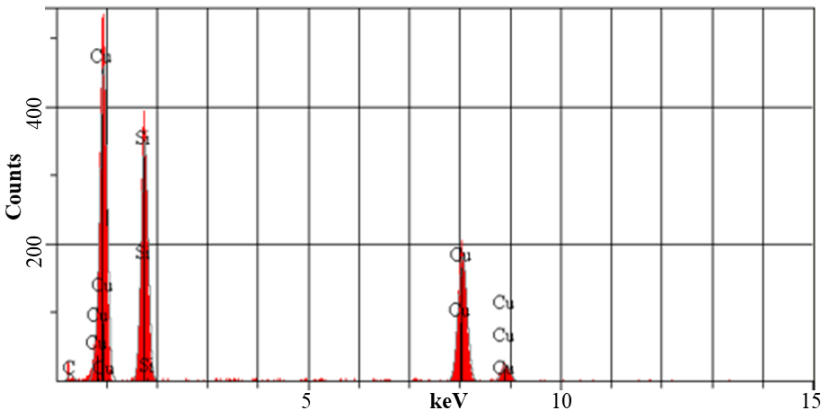

Figure 4.21 : Elemental analysis of the particles located on sample surface.

With EDS analysis it is seen that the undefined particles are SiC particles which are over-grinded, but they are not impurities. Bottom surface of the deposit, where it is in touch with substrate, was also analyzed with SEM. Images of the bottom surface are given in Figure 4.22. Prior to imaging, sample was cut in two sections for cross-section analysis by first sawing a thin line and then breaking.

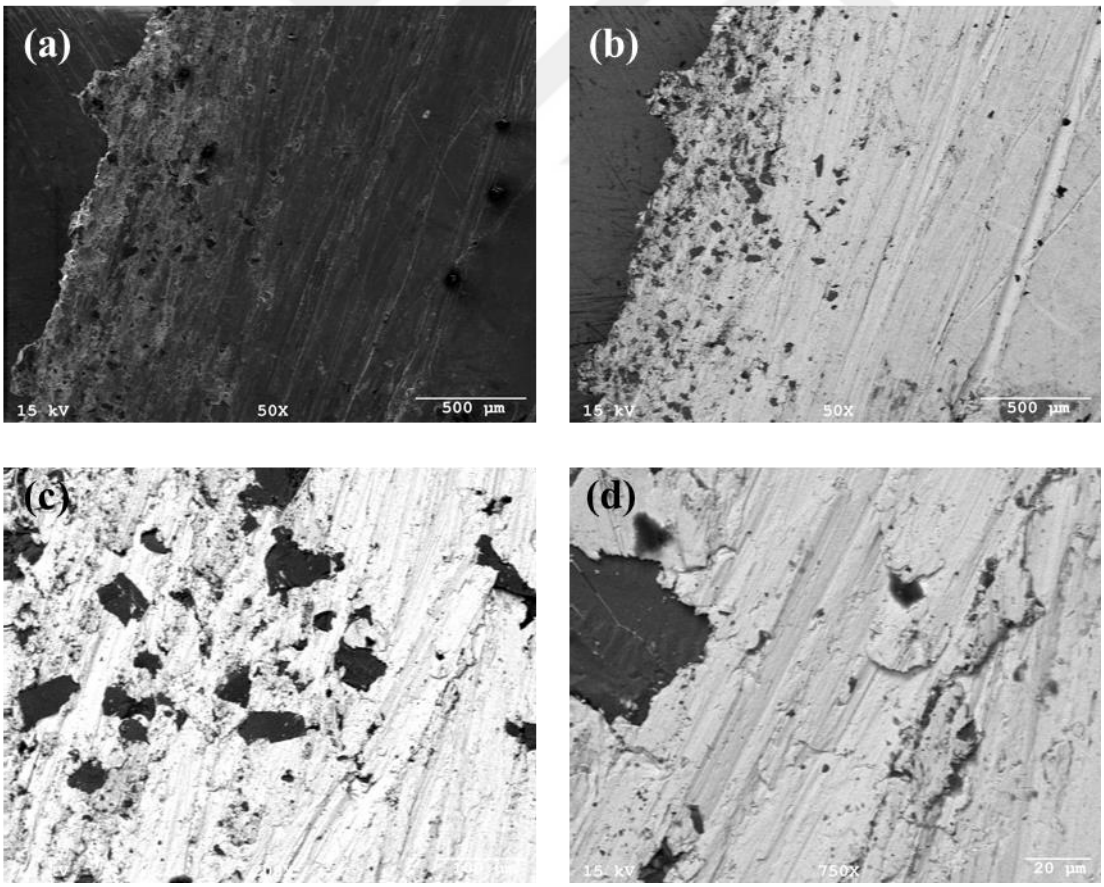

Figure 4.22 : SEM images of bottom surface with (a) SE at 50X mag. (b) BSE at 50X mag. (c) BSE at 200X mag. (d) BSE at 750X mag.

There is a zone with a high concentration of silicon carbide particles at the left edge of bottom surface shown in Figure 4.22. Normally, the bottom surface of the sample was almost completely copper. Silicon carbide particles are seen at that area because sample was sawed to indent a thin line to provide an easy sectioning. Sawing functioned as grinding and removed the copper layer at the bottom surface, which revealed the first-incorporated silicon carbide particles. These particles are the first particles settled on the substrate surface.

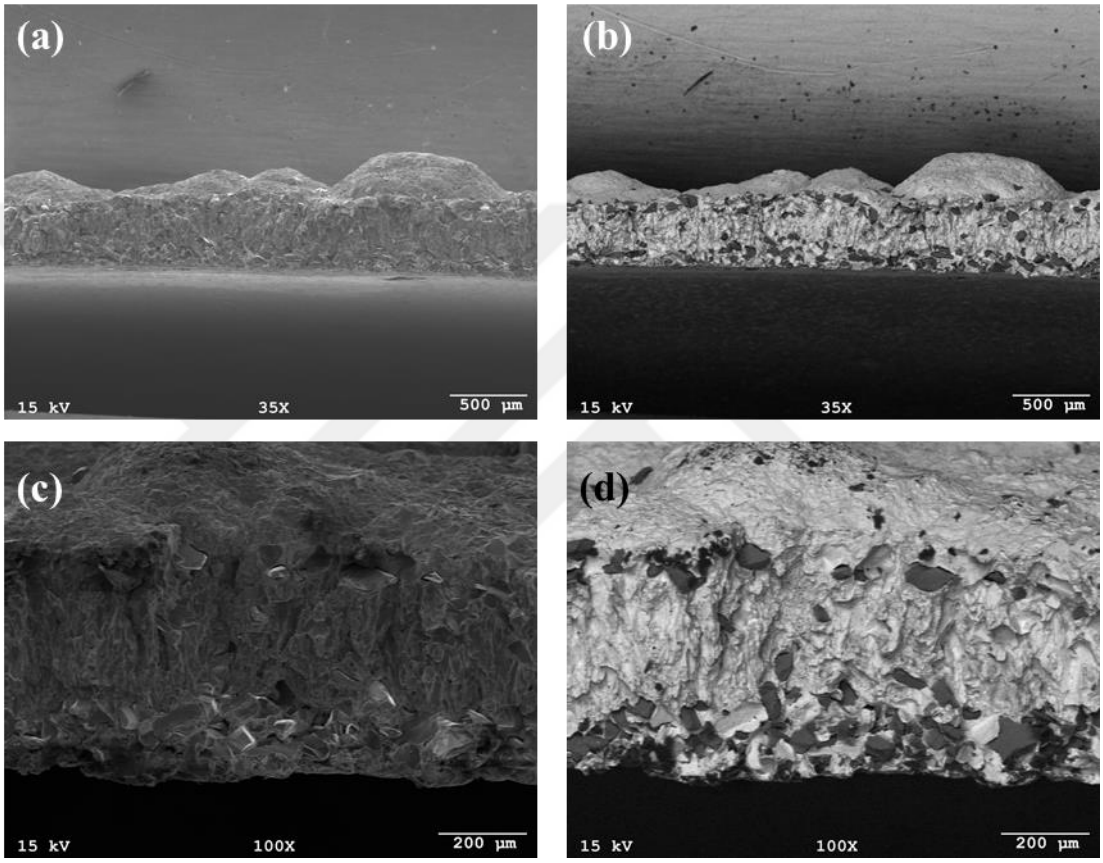

Figure 4.23 : SEM images of 30h deposited samples cross-section, (a) with SE at 35X mag. (b) with BSE at 35X mag. (c) with SE at 100X mag, (d) with BSE at 100X mag.

Images from the cross-section revealed that at lower regions particle distribution and incorporation are remarkable. However, in the middle, there is a region lacking SiC particles. Investigation under higher magnifications revealed that these spaces actually contained SiC particles as well. (Figure 4.24.)

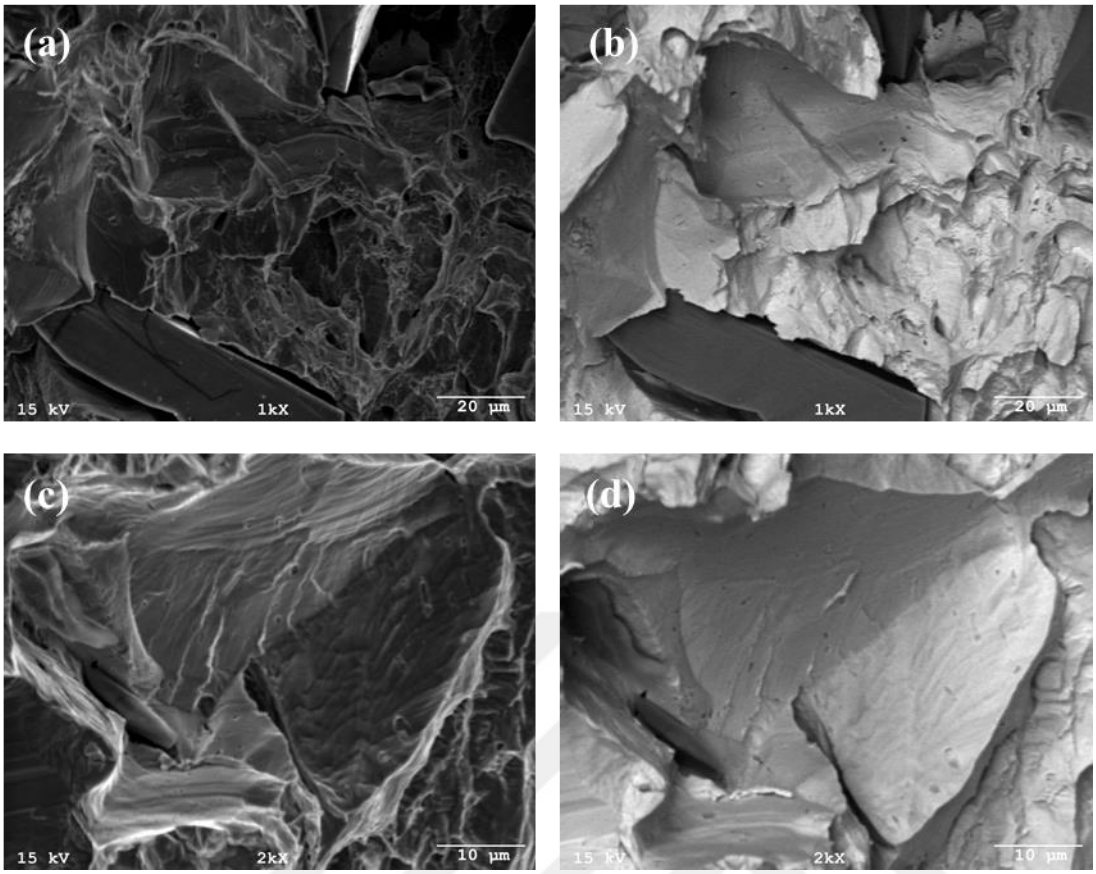

Figure 4.24 : Examination of spots caused by detached particles, (a) with SE at 1000X mag. (b) with BSE at 1000X mag, (c) with SE at 2000X mag, (d) with BSE at 2000X mag.

Some SiC particles were detached during sample sectioning. Additionally, some particles were left on the negative piece of the sample. Therefore, during volume fraction calculation of incorporated particles, the holes emerged from detached particles must also be taken into account.

Cross-section imaging also revealed the matrix-reinforcement interface. The spots of detached particles have the exact shape of the particles. This means particles are smoothly coated with copper and become strongly incorporated. However, it is also seen from Figure 4.24, that there are slight voids at the interface.

The voids either emerge during sample sectioning or they form while deposition. In order to enhance the interface strength, samples were subjected to post treatments, including annealing, cold isostatic pressing (CIP) and annealing prior to CIP. Additionally, along with 75 µm particles, samples with 1000 µm particle size were also fabricated and post treated for a better understanding of the structure and copper-silicon carbide interface.

4.2.4 Post-treatments

4.2.4.1 Annealing

Samples were post-treated as reported in Table 4.3. A sample was annealed at 650 °C for 2 hours. By annealing it was expected that the residual stresses emerged during deposition will be removed. Additionally, it is expected that voids at matrix-reinforcement interface will be diminished. After annealing, SEM imaging from surface and cross-section is conducted.

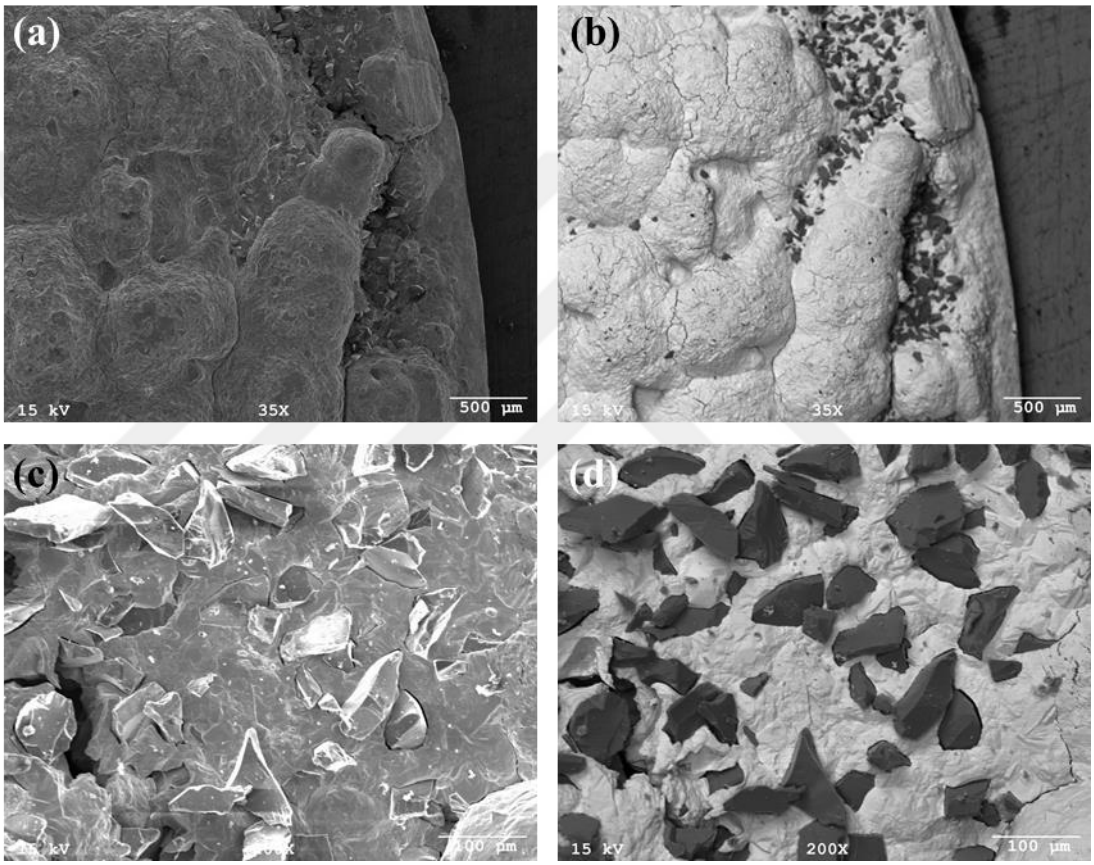

Figure 4.25 : SEM image of annealed samples from surface, (a) with SE at 35X mag. (b) with BSE at 35X mag. (c) with SE at 100X mag, (d) with BSE at 100X mag.

Annealing caused formation of micro-cracks at the surface where there is pure copper. However, cracks did not occur at places with high SiC ratio. This indicates that there is a difference in thermal expansion coefficients for pure copper and Cu-SiC composite. Pure copper zone expanded and cracked while composite section remained its form. Images from the cross-sections also validate this theory and confirms that CTE of copper-silicon carbide composite is lower than copper as desired.

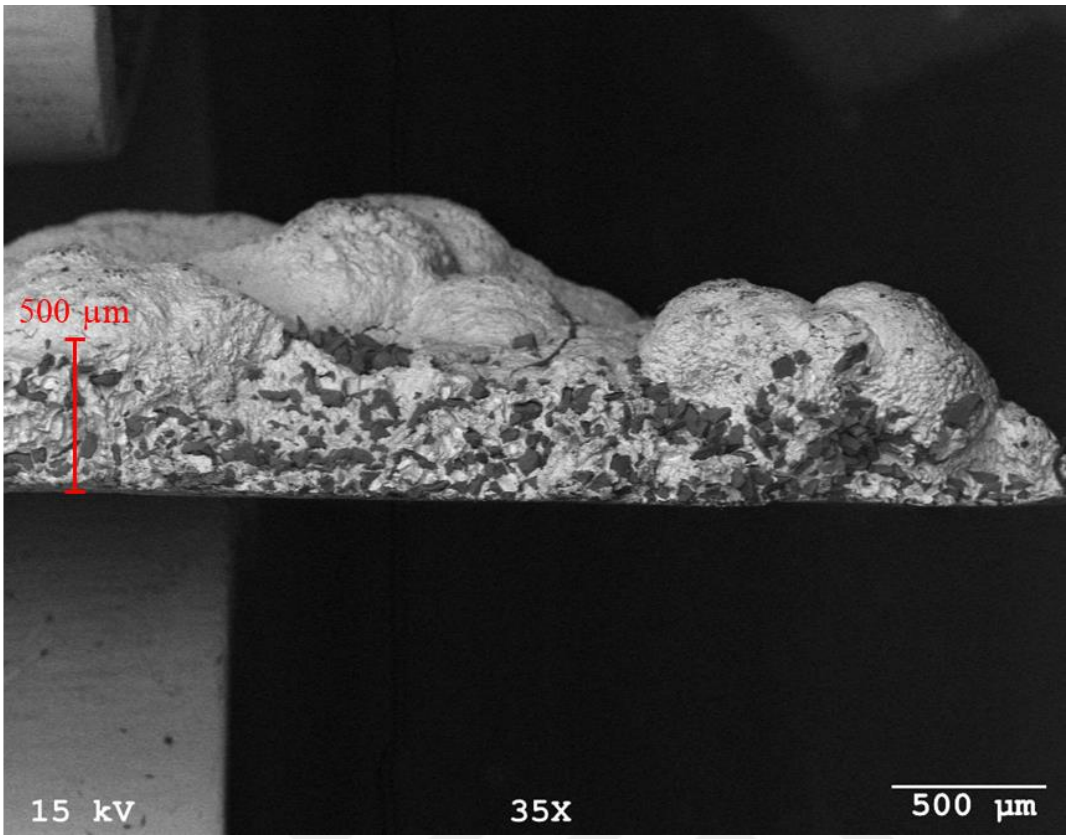

Figure 4.26 : SEM image of annealed cross-section with BSE at 35X magnification.

Cross-section of the annealed sample contains less detached particles compared to the non-treated sample. However, this is not due to annealing. Samples were already sectioned before annealing.

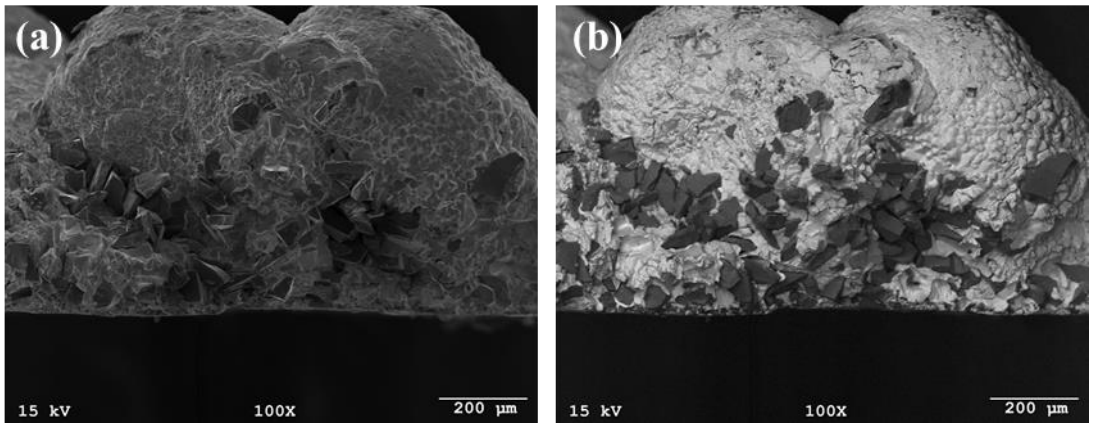

Figure 4.27 : SEM image of the annealed cross-section at 100X magnification, (a) with SE, (b) with BSE.

In order to see the effect of annealing on matrix-reinforcement interface, cross-section was observed with higher magnification. Figure 4.28 reveals that there is not an encountered void between particle and matrix. SiC particles after annealing are strongly attached to copper and hereby the interface is enchanced by means of strength.

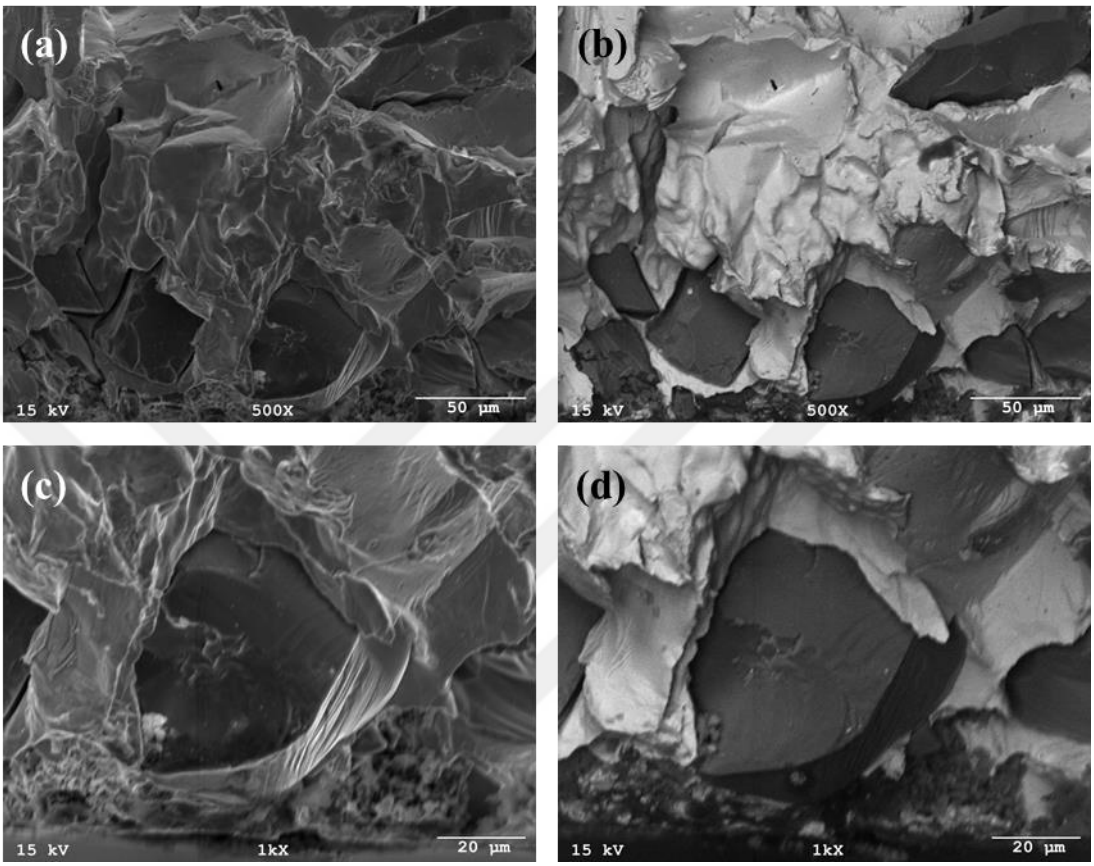

Figure 4.28 : SEM image of the annealed cross-section, (a) with SE at 500X mag. (b) with BSE at 500X mag. (c) with SE at 1000X mag. (d) with BSE at 1000X mag.

4.2.4.2 Cold isostatic pressing

Another way of diminishing the pores at the interface is densification by pressing the sample and producing a more compact structure. Compaction was done by cold isostatic pressing the sample under 1500 kN for 10 minutes. Even though sample was pressed isostaticly, surfaces with almost pure copper surfaces will be pushed into the sample center. Since the hardness of silicon carbide particles are much harder than copper, it will flow around settled silicon carbide particles. After compaction, sample was analyzed with SEM from the surface and cross-section for again observing the matrix-reinforcement interfaces. Thereby, sample will be densificated.

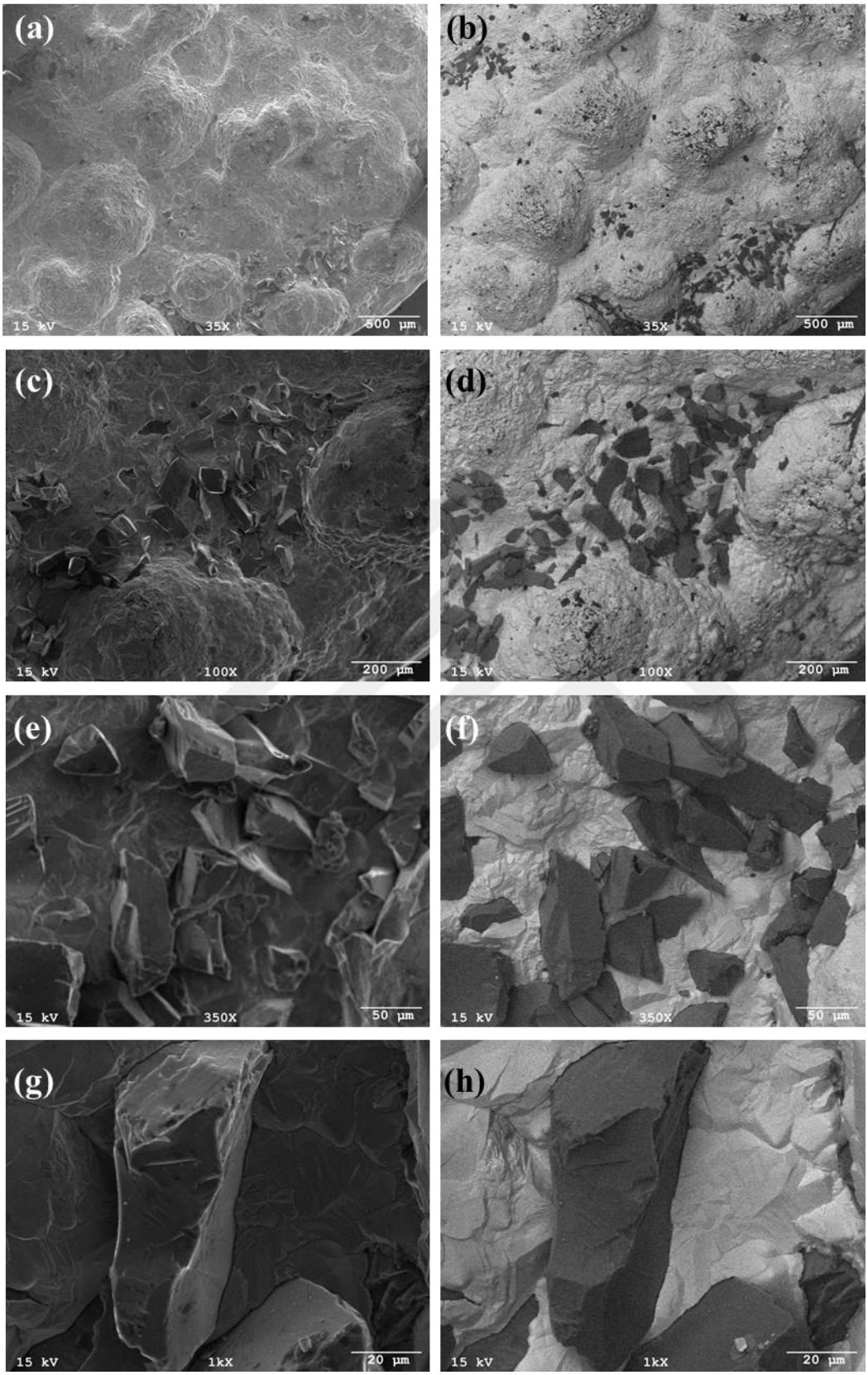

Figure 4.29 : SEM images of CIP'd sample surface with (a) SE at 35X, (b) BSE at 35X, (c) SE at 100X, (d) BSE at 100X, (e) SE at 350X, (f) BSE at 350X, (g) SE at 1000X, (h) BSE at 1000X.

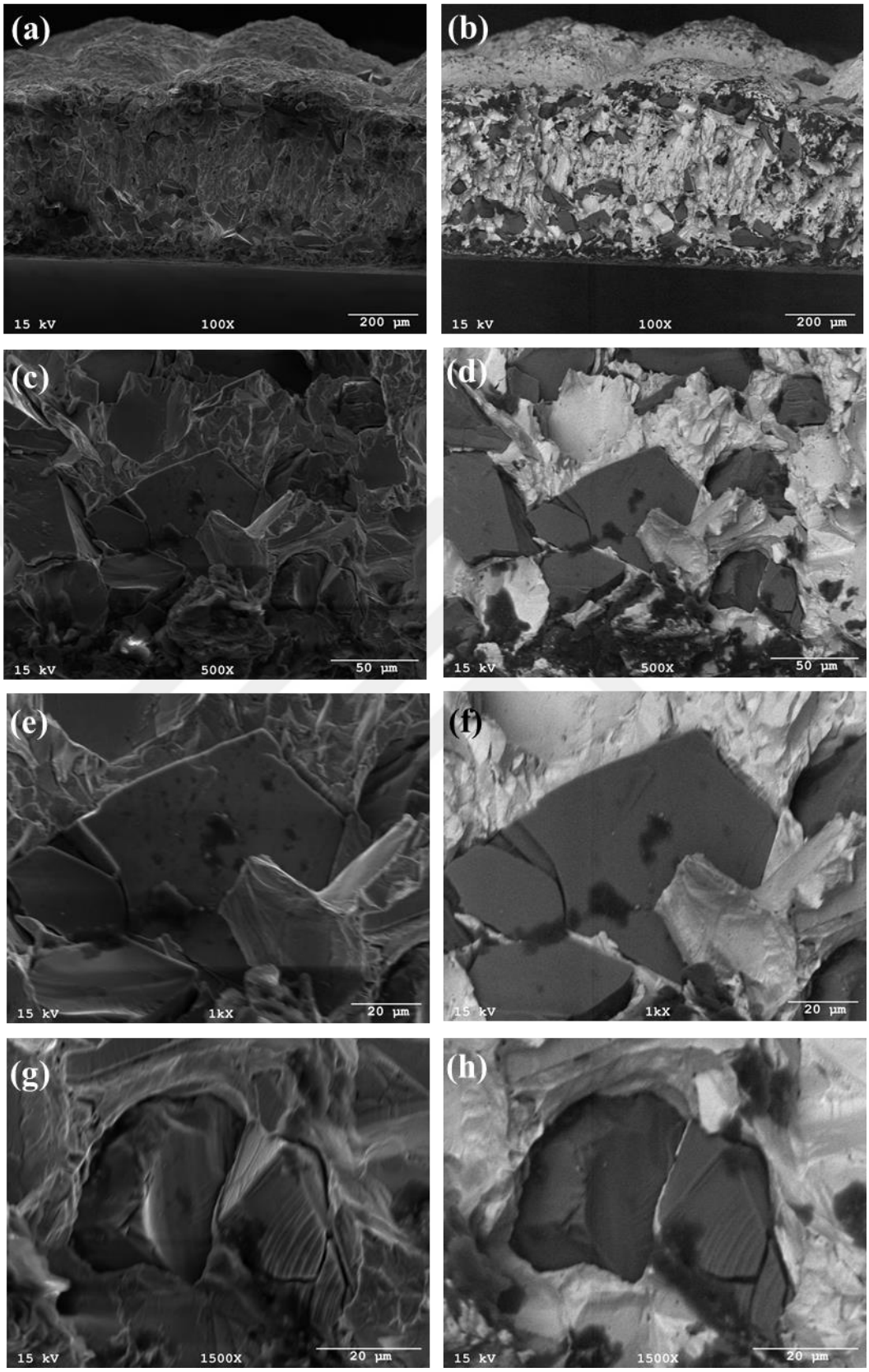

Figure 4.30 : SEM images of CIP'd sample cross-section with (a) SE at 100X, (b) BSE at 100X, (c) SE at 500X, (d) BSE at 500X, (e) SE at 1000X, (f) BSE at 1000X, (g) SE at 1500X, (h) BSE at 1500X.

As seen in Figure 4.29, particles are held by the copper matrix without a presence of any voids. Cross-sections are also investigated and shared in Figure 4.30, images of the cross-section validate this theory as well.

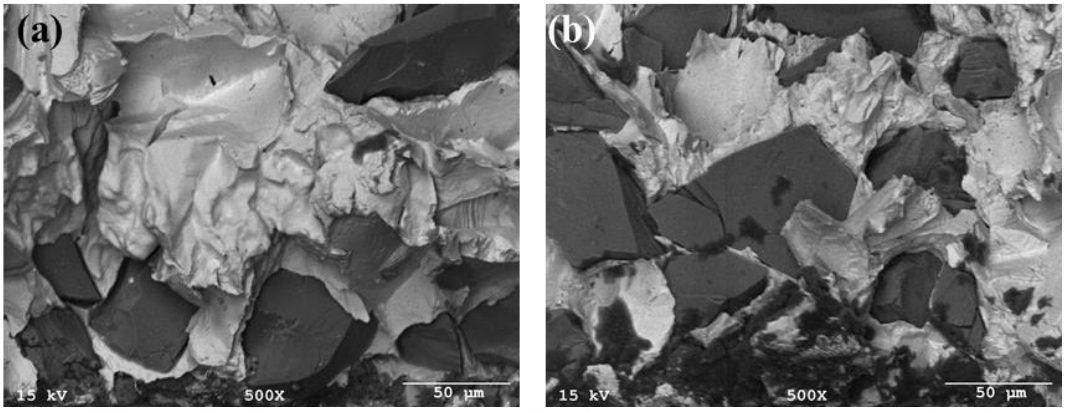

Figure 4.31 : Comparison of matrix morphology between (a) annealed and (b) cold isostatic pressed samples.

Figure 4.31 clearly shows the efffect of CIP to copper, when pressure is applied, extensively from surfaces, copper was compressed into the sample center. During compression, voids are closed, however it is seen that morphology of copper changes into a need-like and cornered form, where morphology is much smoother for annealed sample. Another visual confirming this theory is seen in Figure 4.30 (f), (g), and (h) where SiC particles were cracked due to pressure. Although this is a drawback for CIP, it can be solved by optimizing the applied pressure. However, cold pressing inevitably induces compression stress. Increased dislocation density during CIP strengthtenes the material while decrasing its ductility. Brittleness is undesired for the usage application for the composite since it may require a final plastic deformation, additionally, lattice defects and grain boundary energy highly affects the thermal conductivity of SiC [5]. Therefore CIP'd samples must be annealed prior to application for enhanced mechanical properties.

4.2.4.3 Annealing the cold isostatic pressed sample

For dissipiating the internal energy and increasing ductility, CIP'd sample was annealed at 650 °C for 2 hours. SEM imaging was performed from the surface and cross-section.

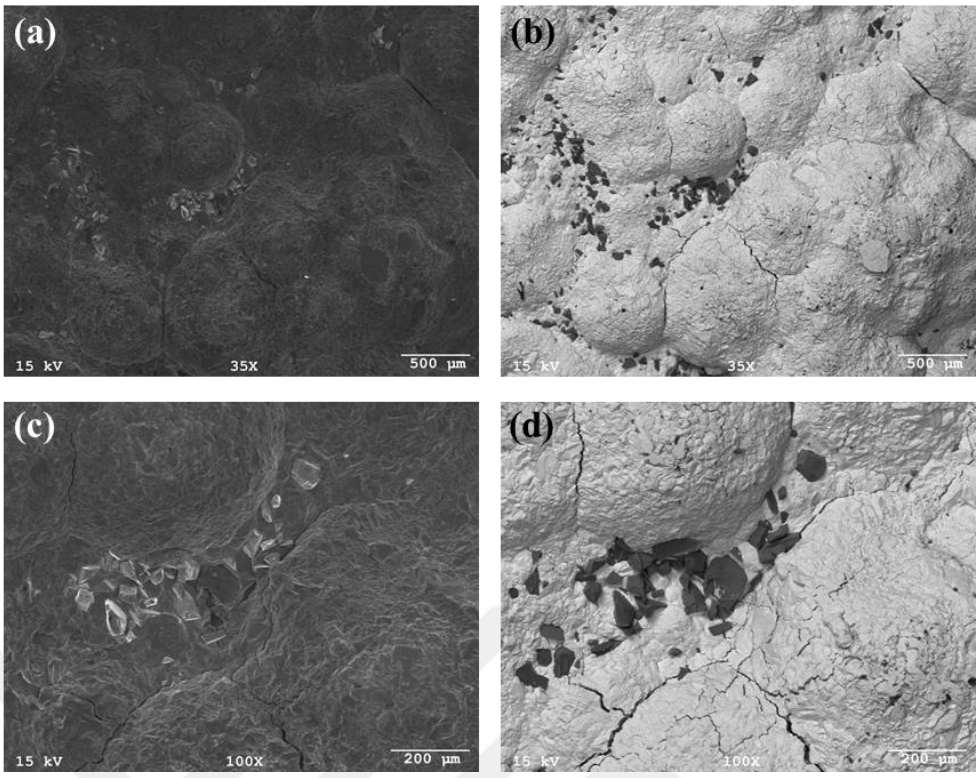

Figure 4.32 : SEM image of CIP'd then annealed samples from surface, (a) with SE at 35X mag. (b) with BSE at 35X mag. (c) with SE at 100X mag, (d) with BSE at 100X mag.

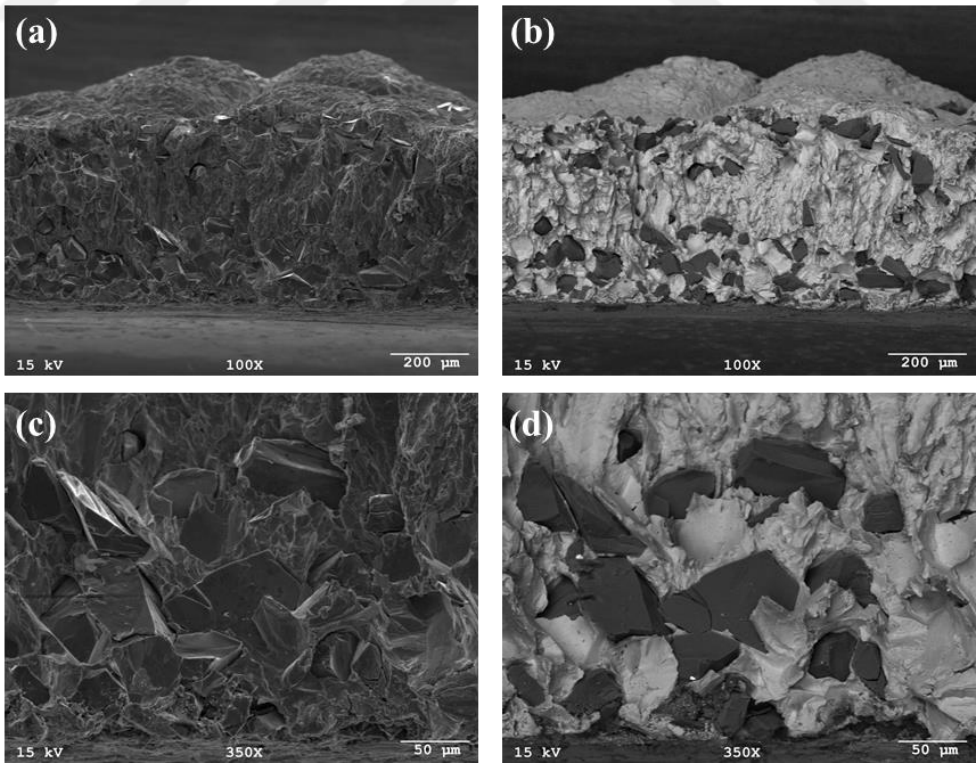

Figure 4.33 : SEM image of CIP'd then annealed samples from cross-section, (a) with SE at 100X mag. (b) with BSE at 100X mag. (c) with SE at 350X mag, (d) with BSE at 350X mag.

Annealing caused formation of micro-cracks at locations consisting of pure copper again. Cross-section, as seen in 4.33, does not possess any cracks. It validates the previous theory claiming that CTE value of silicon-carbide region was lower than the value of pure copper region. Voids are mostly annihilated as expected. Angular morphology which is formed after cold isostatic pressing is remained after annealing.

4.2.4.4 Samples with 1 mm reinforcement size

In order to investigate the interfaces and effects of post-treatments in another perspective and observing how particle size affects the process, samples with 1000 μm particles were fabricated and post treated under same parameters.

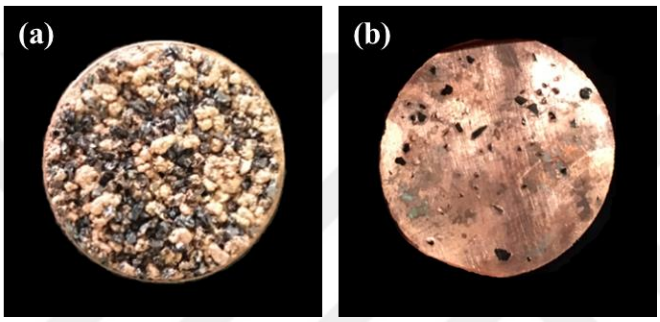

Figure 4.34 : Fabricated Cu-SiC composites with 1000 μm SiC particle size, (a) top surface, (b) bottom surface.

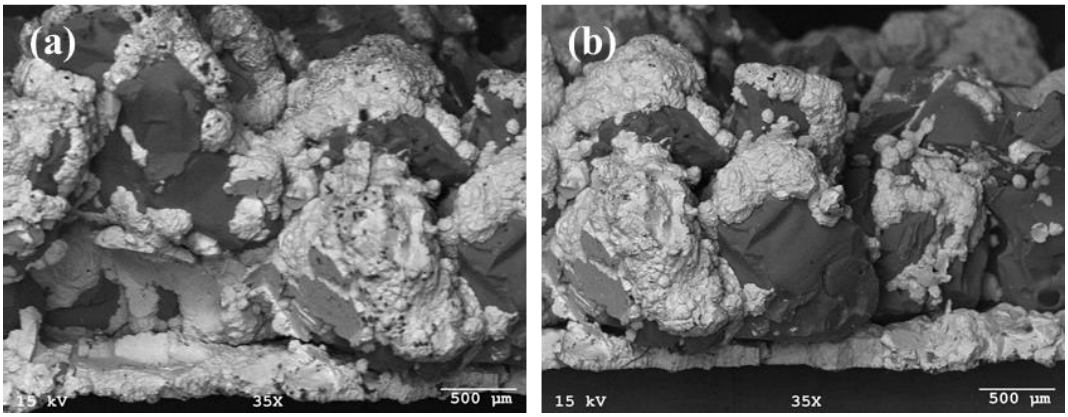

Figure 4.35 : SEM image of sample with 1000 μm SiC particle size at 35X magnification with BSE, (a) as deposited, (b) as annealed

Comparison of as deposited and as annealed samples with 1000 μm by analizing the cross-section image taken from same region does not indicate any severe changes. Only appering difference is that over-grinded SiC particles were detached during annealing.

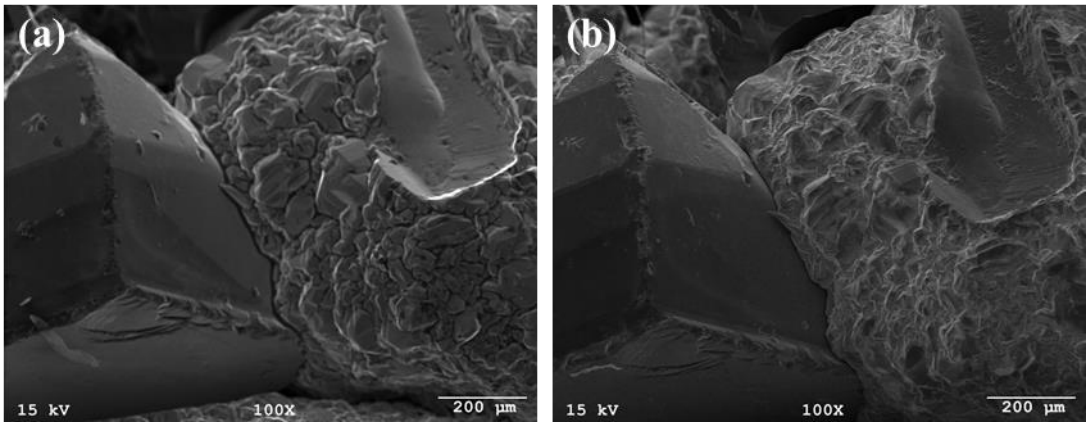

Figure 4.36 : SEM image of sample with 1000 µm SiC particle size at 100X magnification with SE, (a) as CIP'd, (b) CIP'd and annealed.

4.2.5 Structural investigation

In order to analyze why deposited samples could be detached from the substrate and for analyzing the structural changes induced by post treatments, XRD patterns of samples were plotted after each treatment. Figure 4.37 represents the XRD patterns of sample with 75µm particle size, plotted in gonio mode.

XRD pattern reveals that (111), (200) and (220) peaks of copper slightly shift to smaller angles compared to Cu reference pattern. This indicates that compression stress forms during deposition.

It is mentioned in literature that presence of incorporated particles during composite electroplating can force the deposit to compressive stresses [56].

Formation of compression stresses during composite electroforming can be associated with compression stress formation by hydrogen embrittlement. As hydrogen atoms forms hydrogen molecules in the deposit, compressive stress forms in the deposit [22]. Similarly, incorporated particles can apply a pressure in the deposit like hydrogen molecules and cause compressive stresses. It also explains why the deposit can easily be stripped from the substrate. Although this circumstance makes the process more practical by enhancing the product with a trait of being self-standing without requiring any finishing, induced stress affect thermal and mechanical properties and has an adverse effect for the application area.

Residual stresses induced during deposition can be revoked by annealing. During annealing, grain growth occurs and grain boundaries are reduced. As grains grow, strain development takes place [57]. Annealing can even initiate tensile stress [58].

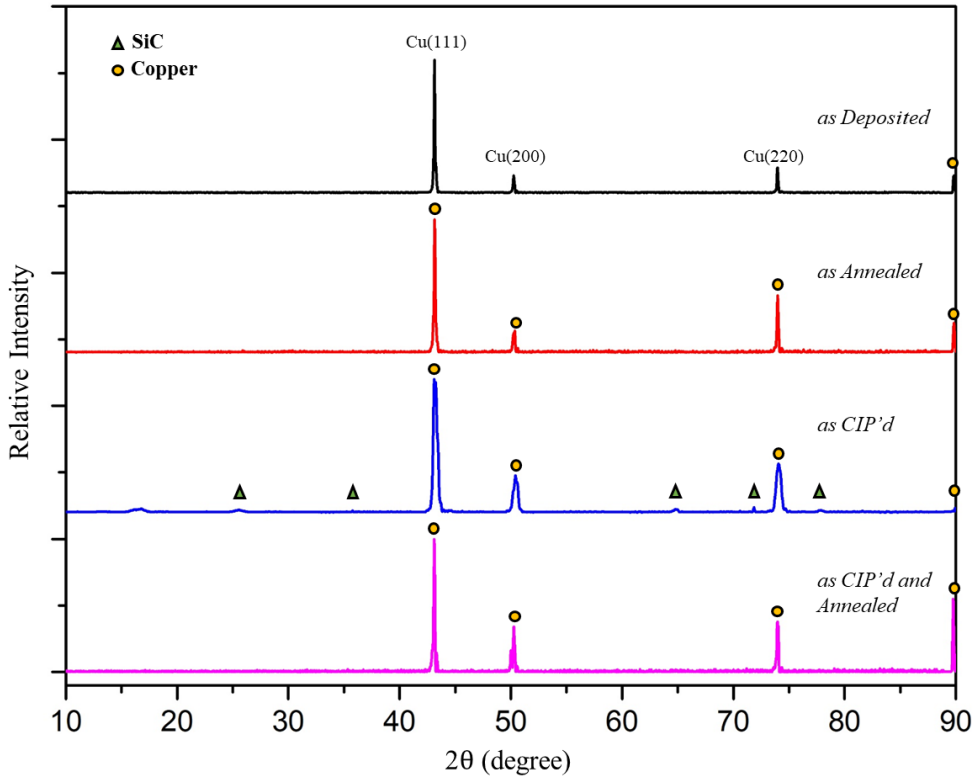

Figure 4.37 : XRD patterns of as deposited, as annealed, as Cold Isostatic Pressed (CIP'd) and as CIP'd and annealed composites with SiC particle size of 75 µm, plotted in gonio mode.

Thus, stress at opposite direction takes place. After anealling (111), and (200) peaks of copper shift to larger angles. Since copper and silicon carbide have different thermal expansion coefficients, it is also possible that lattice distortion takes places during annealing and internal stress is formed [59]. Regardless, there is not a significant structural change, confirming that composite can withstand 650 °C annealing temperature. More importantly, a chemical reaction does not take place between copper and silicon carbide.

Surface of the samples are covered with a pure copper layer, therefore silicon carbide peaks are not expected to be seen on XRD patterns. Interestingly, these peaks are seen in the pattern of cold isostatic pressed sample. This is however fairly understandable considering the mechanism of CIP. As it was explained with Figure 4.31 in p.70, cold isostatic pressing highly affects the copper morphology, copper is compressed from both surfaces into the center while SiC particles remain their positions due to their increased hardness. In other words, copper flows between the SiC particles into the center. This causes a needle-like, sharp cornered morphology for copper matrix. Another effect of this situation is on positions of SiC particles. While SiC particles

mostly remain their position but copper is compressed, SiC particles become closer to the surface. Therefore SiC peaks can be obtained for as cold isostatic pressed sample.

Cold isostatic pressed sample has also a broad peak width compared to as deposited and as annealed samples. This is expected since cold isostatic pressing induces high amount of stress to the material and dislocation density is increased through plastic deformations. Due to the generated defects, lattices have various lattice parameters and a repeating long range order is reduced. As a result, crystallinity of the sample is decreased and broad peaks came out.

Annealing at 650 °C removed these defects and initiated recrystallization. Additionally, grain growth occurred and crystallinity is increased. Therefore, annealed samples have sharper peaks.

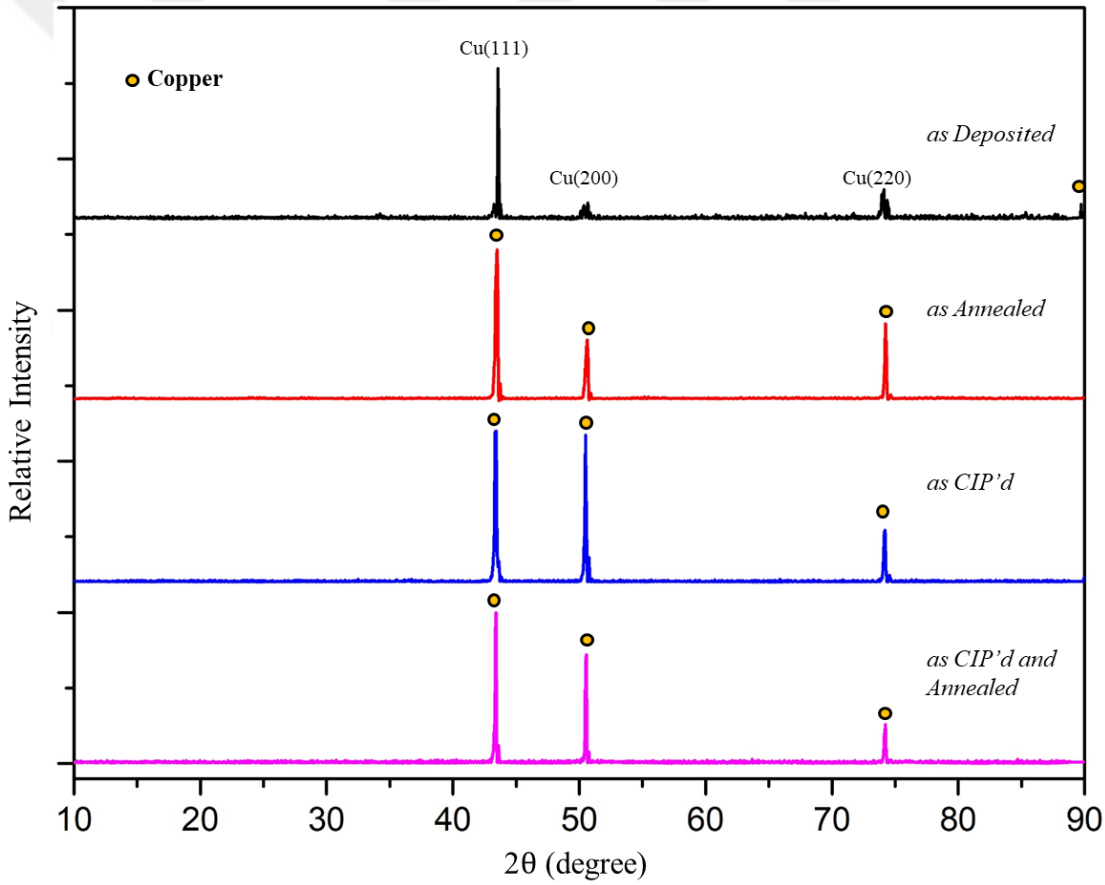

Figure 4.38 : XRD patterns of as deposited, as annealed, as Cold Isostatic Pressed (CIP'd) and as CIP'd and annealed composites with SiC particle size of 1 mm, plotted in gonio mode.

XRD patterns of composites with 1 mm SiC particle size, as shown in Figure 4.38, show less structural differences compared to composites with 75 μm particle size. The

reason for that is; patterns of samples with 1 mm particle size were plotted by diffracting X-Rays from the bottom surface of the sample. Similar to the samples with smaller particle size, annealed sample shows higher crystallinity than cold isostatic pressed sample. Annealing the cold isostatic pressed sample again removes the defects and increases crystallinity. Figure 4.38 confirms that annealing shifted the peaks to larger angles compared to as CIP'd sample, implying that tensile stress is formed during annealing, while as CIP'd sample show formation of compressive stress.

4.2.6 Flexural strength analysis

In order to analyze the formability of the composite, as deposited and annealed samples were subjected to 3 point bending test. The ductilities and flexural strengths of samples were compared. Results of 3 point bend test are given in Figure 4.39. Applied load values during test are converted to stress by using equation 4.1.

$$\sigma = \frac{3FL}{2bd^2} \tag{4.1}$$

Where σ is stress, F is applied load, L is sample length, b is sample width and d is sample thickness. The test results are curve fitted by using software Origin.

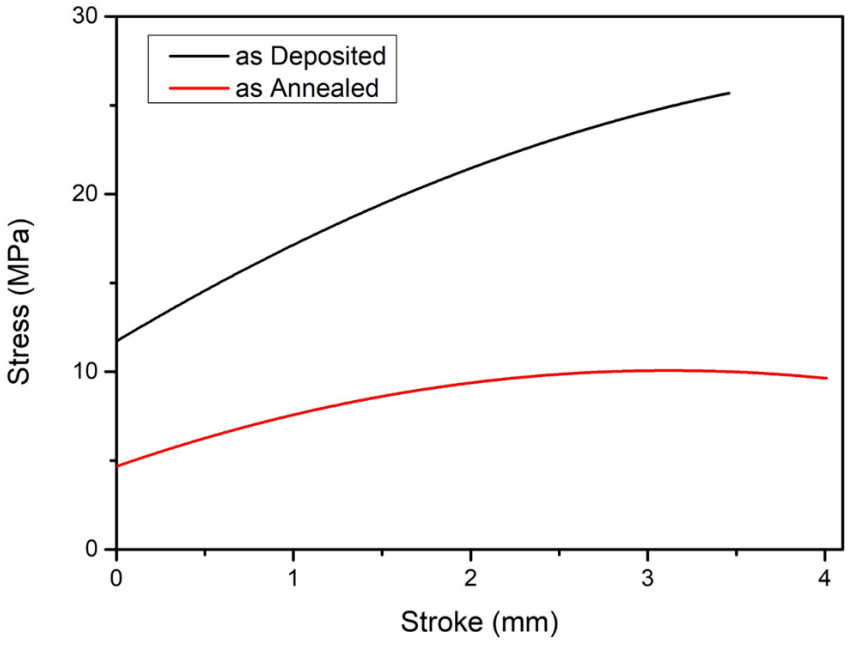

Figure 4.39 : Stress-stroke diagram of as deposited and annealed samples

As seen from the stress-stroke curve, annealed sample is deformed under smaller stress values. This is because grain growth occurs during annealing and strength of material

decreases, additionally, compression residual stress induced by deposition is revoked during annealing and thus thoughness of material is increased.

Flexural strength quantifies resistance of material to bending. It is calculated by measuring the stress value at which the sample started bending. In this case it is the y-axis intercept. Flexural strength of as deposited sample is measured 11,72 MPa while the flexural strength of as annealed sample is measured 4,67 MPa. Flexural strength of as deposited sample is 2,5 times higher than as annealed sample however, flexural strength is inproportionate with formability.

As a result of annealing, formability of the composite is increased and it can be applied to sample depending on the application area.

5. CONCLUSION

Silicon carbide particles are settled on cathode surface by placing them manually. By this manner control of the deposited particle thickness and homogeneous settlement are gained. Silicon carbide particles must be wet prior to settlement for incorporation, otherwise deposited metal atoms do not fill the gaps between reinforcing particles. Plating electrolyte is suitable for wetting reinforcing particles.

Current density calculation in composite electroforming is troubling due to the difficulties in calculation of conductive area. Therefore, polarization curve of the electrolyte is plotted while the potential between copper cathode and a copper reference electrode was measured. Throughout the experiments, a copper reference electrode is used and applied potential is set by adjusting the potential between cathode and reference electrode. Benchmarked current density is 1 A/dm^2 and at that current density the potential between cathode-copper reference electrode is 160 mV while potential applied from the external power supply is 300 mV.

Operating potential controlled is more suitiable for composite electroforming since the current density can be maintained at the same amount.

After 30 hours of electroforming, copper-silicon carbide composite is fabricated with an average thickness of 500 μm and reinforcement concentration volume above 65%. Sample can easily be detached from the substrate by applying pressure.

SEM images of as deposited sample from cross-section reveal that matrix-reinforcement interfaces are already very strong and contain very low amounts of voids.

Post treatments including annealing, cold isostatic pressing and annealing prior to cold isostatic pressing densificated the composite, almost no voids are present at the post-treated interfaces.

XRD patterns of samples show that compression residual stress is induced by deposition, residual stresses are revoked by annealing. Annealing also increases the

crystallinity by grain growth. Cold isostatic pressing causes various stress distribution at the sample surface and therefore have broad peak widths at XRD patterns.

XRD patterns prove that a chemical reaction does not take place between copper and silicon carbide. Additionally, there is not a significant structural change occurring through post-treatments which could affect the material negatively. Effects of the treatments on samples are as expected.

Three point bending test results show that the flexural strength of as deposited sample is 11.72 MPa and flexural strength of annealed sample is 4.67 MPa. Annnealed sample has higher formability. The strength of annealed sample is reduced through recovery of residual stresses while its ductility is increased, annealed sample is suitable for plastic deformation.

Depending on the application area, fabricated copper–silicon carbide composite is suitable to be directly used as a product right after deposition without requiring any post-treatments. It can also be cold isostatic pressed, annealed or cold isostatic pressed prior to annealing for complicated applications.

REFERENCES

[1] **Çengel, Y. A.** (2007). *Heat & Mass Transfer: A Practical Approach*. McGraw-Hill Education (India) Pvt Limited.

[2] **Shu, K. M., & Tu, G. C.** (2001). Fabrication and characterization of Cu-SiCp composites for electrical discharge machining applications. *Materials and Manufacturing Processes*, *16*(4), 483–502.

[3] **Kang, Q., He, X., Ren, S., Qu, X.** (2013). Preparation of copper-diamond composites with chromium carbide coatings on diamond particles for heat sink applications. *Applied Thermal Engineering*, *60*(1–2), 423–429.

[4] **Miura, S., & Honma, H.** (2003). Advanced copper electroplating for application of electronics. *Surface and Coatings Technology*, *169–170*, 91–95.

[5] **Román-Manso, B., Chevillotte, Y., Osendi, M. I., Miranzo, P.** (2016). Thermal conductivity of silicon carbide composites with highly oriented graphene nanoplatelets. *Journal of the European Ceramic Society*, *36*(16), 3987–3993.

[6] **Yih, P., & Chung, D. D. L.** (1996). Silicon carbide whisker copper-matrix composites fabricated by hot pressing copper coated whiskers. *Journal of Materials Science*, *31*(2), 399–406.

[7] **Pappacena, K. E., Johnson, M. T., Xie, S., & Faber, K. T.** (2010). Processing of wood-derived copper-silicon carbide composites via electrodeposition. *Composites Science and Technology*, *70*(3), 485–491.

[8] **Blucher, J. T.** (1992). Discussion of a liquid metal pressure infiltration process to produce metal matrix composites. *Journal of Materials Processing Tech.*, *30*(3), 381–390.

[9] **Narasimman, P., Pushpavanam, M., & Periasamy, V. M.** (2011). Synthesis, characterization and comparison of sediment electro-codeposited nickel-micro and nano SiC composites. *Applied Surface Science*, *258*(1), 590–598.

[10] **Limpanart, S., Thueploy, A., Zhang, X., Liu, R.** (2014). The high concentration and uniform distribution of diamond particles in Ni-diamond composite coatings by sediment co-deposition. *Surface and Interface Analysis*, *47*(3), 331–339.

[11] **Arpaci, V. S., Kao, S. H., & Selamet, A.** (1999). *Introduction to Heat Transfer*. Prentice Hall.

[12] **Omar, M.** (1994). *Elementary Solid State Physics: Principals and Applications*.

[13] **Callister, W. D., & Rethwisch, D. G.** (2012). *Fundamentals of Materials Science and Engineering: An Integrated Approach*.

[14] **Grinyaev, K. V., Ditenberg, I. A., Smirnov, I. V., Sallamand, P.** (2013). ASM Ready Reference: Thermal Properties of Metals. *Journal of Nuclear Materials*, *573*(1–3), 439–441.

[15] **Jiang, G., Diao, L., & Kuang, K.** (2012). *Advanced Thermal Management Materials*. Springer New York.

[16] **Donald Askeland**. (1996). *The Science and Engineering of Materials*. Springer.

[17] **Al-mangour, B., & Angeles, L.** (2015). Stainless Steel: State-of-the-Art, Challanges, and Development. *Stainl. Steel.*, 37–80.
[18] **Upadhyaya, G. S.** (2002). *Aluminium powder metallurgy technology*. 1–157.
[19] **Bollina, R.** (2008). *Thermal Management and Packaging with Diamond Composites*.
[20] **Motta, F. V., Balestra, R. M., Ribeiro, S., & Taguchi, S. P.** (2004). Wetting behaviour of SiC ceramics: Part I. E2O3/Al2O3additive system. *Materials Letters*, *58*(22–23), 2805–2809.
[21] **Conway, B. E.** (1995). *Modern Aspects of Electrochemistry* (Vol. 38). Springer US.
[22] **Kanani, N.** (2005). *Electroplating: Basic Principles, Processes and Practice*. Elsevier Science.
[23] **Schlesinger, M., & Paunovic, M.** (2010). Modern Electroplating. In *Journal of The Electrochemical Society* (Vol. 121).
[24] **Olevsky, E. A., Wang, X., Ma, J., Stern, M. B.** (2007). Sequential deposition and electroforming of metal–ceramic composites for thermal management applications. *Surface Engineering*, *23*(1), 12–17.
[25] **Sancakoglu, O.** (2016). A New Approach — In-Situ Codeposition of Composite Coatings. *Electrodeposition of Composite Materials*.
[26] **Walsh, F. C., & Ponce de Leon, C.** (2014). A review of the electrodeposition of metal matrix composite coatings by inclusion of particles in a metal layer: an established and diversifying technology. *Transactions of the IMF*, *92*(2), 83–98.
[27] **Abro, D. M. K., Dable, P., Cortez-salazar, F., Girault, H.** (2016). Design and Characterization of a Horizontal Double Impinging Jet Cell : Determination of Flow Modes at the Surface of a Flat Electrode. *Journal of Materials Science and Chemical Engineering*, *4*, 18–28.
[28] **Low, C. T. J., Wills, R. G. A., & Walsh, F. C.** (2006). Electrodeposition of composite coatings containing nanoparticles in a metal deposit. *Surface and Coatings Technology*, *201*(1–2), 371–383.
[29] **Amadi, S. A.** (1990). *Agitation for the electrodeposition of printed circuit boards.* Loughborough University of Technology.
[30] **Sautter, F. K.** (1962). *Electrodeposition of Dispersion-Hardened NickeI-AI20 Alloys*. *110*(6), 557–560.
[31] **Williams, R. V., & Martin, P. W.** (2017). Electrodeposited Composite Coatings. *Transactions of the IMF*, *42*(1), 182–188.
[32] **Guglielmi, N.** (1971). Kinetics of deposition of inert particles from electrolytic baths. *J. Electrochem. Soc.*, *119*, 1009–1012.
[33] **Lanki, M., Nourmohammadi, A., & Feiz, M. H.** (2013). Electrophoretic growth of PbTiO3 Nanotubes. *Ferroelectrics*, *448*(1), 134–144.
[34] **Celis, J. P.** (2006). A Mathematical Model for the Electrolytic Codeposition of Particles with a Metallic Matrix. *Journal of The Electrochemical Society*, *134*(6), 1402.
[35] **Lee, D., Gan, Y. X., Chen, X., & Kysar, J. W.** (2007). Influence of ultrasonic irradiation on the microstructure of Cu/Al2O3, CeO2 nanocomposite thin films during electrocodeposition. *Materials Science and Engineering A*, *447*(1–2), 209–216.
[36] **Hamal, K., Rajbhandari, A., Gyawali, G., & Lee, S. W.** (2015). Effect of stirring rate on electrochemical codeposition of Ni-SiC composite. *Scientific World*, (12), 30–33.

[37] **Garcia, I., Fransaer, J., & Celis, J. P.** (2001). Electrodeposition and sliding wear resistance of nickel composite coatings containing micron and submicron SiC particles. *Surface and Coatings Technology*, *148*(2–3), 171–178.

[38] **M. Ghouse, M. V. and E. G. R.** (1980). *Electrodeposited Composites of Graphite, Molybdenum Disulfide and Tungsten Disulfide with Copper for Tribological Applications*.

[39] **Liu, H., & Chen, W.** (2005). Electrodeposited Ni-Al composite coatings with high Al content by sediment co-deposition. *Surface and Coatings Technology*, *191*(2–3), 341–350.

[40] **Zhu, J., Liu, L., Zhao, H., Hu, W.** (2007). Microstructure and performance of electroformed Cu/nano-SiC composite. *Materials and Design*, *28*(6), 1958–1962.

[41] **Verelst, M., Bonino, J. P., & Rousset, A.** (1991). Electroforming of metal matrix composite: dispersoid grain size dependence of thermostructural and mechanical properties. *Materials Science and Engineering A*, *135*(C), 51–57.

[42] **Erler, F., Jakob, C., Romanus, H., Steinhäuser, S.** (2003). Interface behaviour in nickel composite coatings with nano-particles of oxidic ceramic. *Electrochimica Acta*, *48*(20–22), 3063–3070.

[43] **Brendel, A., Popescu, C., Leyens, C., Bolt, H.** (2004). SiC-fibre reinforced copper as heat sink material for fusion applications. *Journal of Nuclear Materials*, *329–333*, 804–808.

[44] **Gómez, E., Pané, S., & Vallés, E.** (2005). Magnetic composites CoNi-barium ferrite prepared by electrodeposition. *Electrochemistry Communications*, *7*(12), 1225–1231.

[45] **Pradhan, A. K., & Das, S.** (2014). Pulse-reverse electrodeposition of Cu-SiC nanocomposite coating: Effect of concentration of SiC in the electrolyte. *Journal of Alloys and Compounds*, *590*, 294–302.

[46] **Abro, D. M. K., Dable, P. J. M. R., Amstutz, V., Girault, H.** (2017). Forced Electrocodeposition of Silica Particles into Nickel Matrix by Horizontal Impinging Jet Cell. *Journal of Materials Science and Chemical Engineering*, *05*(02), 51–63.

[47] **Farrokhzad, M. A., Saha, G. C., & Khan, T. I.** (2014). Three-body wear performance of co-electrodeposited cermet coatings. *Wear*, *313*(1–2), 34–42.

[48] **Hovestad, A., & Janssen, L. J. J.** (1995). Electrochemical codeposition of inert particles in a metallic matrix. *Journal of Applied Electrochemistry*, *25*(6), 519–527.

[49] **Narasimman, P., Pushpavanama, M., & Periasamy, V. M.** (2012). Effect of Surfactants on the Electrodeposition of Ni-SiC Composites. *Portugaliae Electrochimica Acta*, *30*(1), 1–14.

[50] **Asnavandi, M., Ghorbani, M., & Kahram, M.** (2013). Production of Cu-Sn-graphite-SiC composite coatings by electrodeposition. *Surface and Coatings Technology*, *216*, 207–214.

[51] **Stojak, J. L., & Talbot, J. B.** (2001). Effect of particles on polarization during electrocodeposition using a rotating cylinder electrode. *Journal of Applied Electrochemistry*, *31*(5), 559–564.

[52] **R.Balaji, Maiathy Pushpavanarm, K. Y. K. K. S.** (2006). *Electrodeposition of Copper-Tin-PTFE composite coatings*. *3*(3), 381–387.

[53] **Ghorbani, M., Mazaheri, M., Khangholi, K., & Kharazi, Y.** (2001). Electrodeposition of graphite-brass composite coatings and characterization of the tribological properties. *Surface and Coatings Technology*, *148*(1), 71–76.

[54] **Jung, D. H., Sharma, A., Kim, K. H., Jung, J. P.** (2015). Effect of Current Density and Plating Time on Cu Electroplating in TSV and Low Alpha Solder Bumping. *Journal of Materials Engineering and Performance*, *24*(3), 1107–1115.

[55] **Gau, W. C., Chang, T. C., Lin, Y. S., Cheng, C. L.** (2000). Copper electroplating for future ultralarge scale integration interconnection. *Journal of Vacuum Science & Technology A: Vacuum, Surfaces, and Films*, *18*(2), 656.

[56] **Saraloğlu Güler, E., Karakaya, İ., & Konca, E.** (2014). Effects of current density, coating thickness, temperature, pH and particle concentration on internal stress during Ni–MoS 2 electrocodeposition. *Surface Engineering*, *30*(2), 109–114.

[57] **Kao, L. C., Hsu, L. H., Brahma, S., Lo, K. Y.** (2016). Stabilized copper plating method by programmed electroplated current: Accumulation of densely packed copper grains in the interconnect. *Applied Surface Science*, *388*, 228–233.

[58] **Volinsky, A. A., Hauschildt, M., Vella, J. B., Gerberich, W. W.** (2011). Residual Stress and Microstructure of Electroplated Cu Film on Different Barrier Layers. *MRS Proceedings*, *695*(1), 1–6.

[59] **Xiao, Z., Geng, H., Sun, C., Luo, H.** (2015). Effect of yttrium on properties of copper prepared by powder metallurgy. *Advanced Powder Technology*, *26*(4), 1079–1086.

CURRICULUM VITAE

Name Surname **:** Burak Evren

Place and Date of Birth **:** Şişli, 22.05.1994

E-Mail **:** burak.evren@tau.edu.tr

EDUCATION **:**

- **B.Sc.** **:** 2017, Istanbul Technical University, Faculty of Chemistary and Metallurgy, Metallurgical and Materials Engineering
- **Highschool** **:** 2013, İstanbul Alman Lisesi

PROFESSIONAL EXPERIENCE AND REWARDS:

- 2018, Research Assistant, Turkish-German University, Department of Materials Science and Technologies
- 2016, Eregli Iron and Steel Industry, Eregli Zonguldak, Product Internship
- 2016, Mercedes Benz Turk, Esenyurt Istanbul, Management Internship
- 2015, Yomser Packaging Industry, Gebze Kocaeli, Atelier Internship